AL/OE-TR-1993-0096

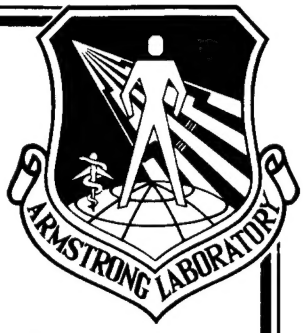

ARMSTRONG LABORATORY

FLOW THROUGH A COMPLIANT STENOTIC ARTERY: A PARAMETRIC EVALUATION

J. Micah Downing

OCCUPATIONAL AND
ENVIRONMENTAL HEALTH DIRECTORATE
BIOENVIRONMENTAL ENGINEERING DIVISION
WRIGHT-PATTERSON AFB OH 45433-7901

MARCH 1993

FINAL REPORT FOR THE PERIOD DECEMBER 1991 - MARCH 1993

AIR FORCE MATERIEL COMMAND
WRIGHT-PATTERSON AIR FORCE BASE, OHIO 45433-6573

NOTICES

When US Government drawings, specifications, or other data are used for any purpose other than a definitely related Government procurement operation, the Government thereby incurs no responsibility nor any obligation whatsoever, and the fact that the Government may have formulated, furnished, or in any way supplied the said drawings, specifications, or other data, is not to be regarded by implication or otherwise, as in any manner, licensing the holder or any other person or corporation, or conveying any rights or permission to manufacture, use or sell any patented invention that may in any way be related thereto.

Please do not request copies of this report from the Armstrong Laboratory. Additional copies may be purchased from:

National Technical Information Service
5285 Port Royal Road
Springfield VA 22161

Federal Government agencies and their contractors registered with Defense Technical Information Center should direct requests for copies of this report to:

Defense Technical Information Center
Cameron Station
Alexandria VA 22314

TECHNICAL REVIEW AND APPROVAL

AL/OE-TR-1993-0096

This report has been reviewed by the Office of Public Affairs (PA) and is releasable to the National Technical Information Service (NTIS). At NTIS, it will be available to the general public, including foreign nations.

This technical report has been reviewed and is approved for publication.

Thomas J. Moore

THOMAS J. MOORE, PhD
Chief
Biodynamics and Biocommunications Division
Armstrong Laboratory

REPORT DOCUMENTATION PAGE

Form Approved
OMB No. 0704-0188

1. AGENCY USE ONLY *(Leave blank)*	2. REPORT DATE	3. REPORT TYPE AND DATES COVERED
	March 1993	Final report December 1991-March 1993

4. TITLE AND SUBTITLE
Flow throught a Complaint Stenotic Artery: A Parametric Evaluation

5. FUNDING NUMBERS
PR: ILIR
TA: ILIROB
WU: ILIROB2A

6. AUTHOR(S)
J. Micah Downing

7. PERFORMING ORGANIZATION NAME(S) AND ADDRESS(ES)
Armstrong Laboratory
Occupational and Environmental Health Directorate
Bioenvironmental Engineering Division
Human Systems Center
Air Force Materiel Command
Wright-Patterson AFB OH 45433-7901

8. PERFORMING ORGANIZATION REPORT NUMBER
AL/OE-TR-1993-0096

9. SPONSORING/MONITORING AGENCY NAME(S) AND ADDRESS(ES)

10. SPONSORING/MONITORING AGENCY REPORT NUMBER

11. SUPPLEMENTARY NOTES

12a. DISTRIBUTION/AVAILABILITY STATEMENT
Approved for public release; distribution is unlimited

12b. DISTRIBUTION CODE

13. ABSTRACT *(Maximum 200 words)*

Hardening of the arteries from atherosclerosis can produce high grade stenoses which lead to morbid symptoms of heart attack and stroke. Blood flow through the stenosis produces a low pressure zone at the throat which may cause the elastic artery to collapse. A one-dimensional model of collapsible tube flow through a smooth, compliant stenoses was developed to evaluate the realtive effects of several physiologic parameters. These variables included changes in percent stenosis, distal resistance, viscous separation losses, unsteady effects, stiffness variations, and non-linear tube law shapes. The range of variation attempted to bracket the conditions expected for diseased carotid and coronary arteries. The time-dependent equations were solved using MacCormack's method.

Collapsed flow was more likely to be achieved with soft stenoses greater than 80% by diameter, low downstream resistances, and high external pressures. Collapsed flow was less likely to occur with stiff stenoses of less than 80% (dia) with a high distal resistance, large viscous losses, and a low external pressure. Pulsatile conditions resulted in situations where flow could alternate between supercritical and subcritical flow during the cycle. The results demonstrate that collapse of high grade stenotic arteries can occur under physiological conditions.

14. SUBJECT TERMS
Atherosclerosis
Fluid Mechanics
Collapsible Tube
Computational Fluid Dynamnics

15. NUMBER OF PAGES
153

16. PRICE CODE

17. SECURITY CLASSIFICATION OF REPORT	18. SECURITY CLASSIFICATION OF THIS PAGE	19. SECURITY CLASSIFICATION OF ABSTRACT	20. LIMITATION OF ABSTRACT
UNCLASSIFIED	UNCLASSIFIED	UNCLASSIFIED	UNLIMITED

SUMMARY

Hardening of the arteries from atherosclerosis can produce high grade stenoses which often lead to morbid symptoms of heart attack and stroke. Blood flow through the stenosis produces a low pressure zone at the throat which may cause the elatic artery to collapse in this region. Flows through collapsible tubes can exhibit transitions to supercritical flow and elatic jumps back to subcritical conditions. The hemodynamic behavior of flow through these compliant stenoses in the carotid and coronary arteries can be modelled using the collapsible tube theory of Shapiro.

A one-dimensional model of collapsible tube flow through a smooth, compliant stenoses was developed to include the effects of viscous friction losses. The hyperbolic system of time-dependent equations were solved using MacCormack's method. The boundary conditions and tube laws were varied parametrically to investigate the relative importance of several physical parameters which are present in the *in vivo* environment. These variables included changes in percent stenosis, distal resistance, viscous separation losses, unsteady effects, tube stiffness variations along the length of the stenosis, and non-linear tube law shapes. The range of variation attempted to bracket the conditions expected for diseased carotid and coronary arteries. The results were then compared to existing experimental measurements obtained by others.

The numerical solutions for flow through a high grade, compliant stenosis quantified the conditions for supercritical flow in the throat region with downstream elastic jumps. A binary-type behavior between subcritical and supercritical flow was found to occur for slight changes in the assumed conditions. Critical flow was more likely to be achieved with stenoses greater than 80% by diameter, low downstream resistances, and high external pressures. Factors which were of secondary importance included viscous losses, changes in the local tube stiffness, mean arterial pressure, and artery diameter. Pulsatile conditions resulted in a situation where flow could alternate between supercritical flow during systole and subcritical flow during diastole.

The results demonstrate that collapse of high grade stenotic arteries can occur under physiological conditions, even eith viscous losses and increasing stiffness of the plaque. Supercritical flow would be confined to a small region just downstream of the throat. Collapse would be augmented in a lipid-laden plaque by lowering the distal resistance, resulting in choked flow. Conversely, collapse would be hindered by calcification of the plaque which may be a beneficial adaptive response by the artery.

ACKNOWLEDGEMENTS

This report describes the research effort which was partially funded by the Independent Laboratory Inhouse Research Program of the Armstrong Laboratory of the United States Air Force (WU ILIROB2A).

The author would like to thank the people who provided encouragement, support, and motivation during this work. First, I would like to thank my advisor, Dr. David Ku, for his guidance and support. Second, I would like to thank my boss, Mr. Jerry Speakman, who provided me the time and resources to complete this work. Third, I would like to thank my committee, Dr. Robert Nerem, Dr. N.L. Sankar, Dr. Alan Lumsden, and Dr. P.V. Desai for their input and assistance. I also appreciate the technical advice and knowledge of Dr. William Hankey of Wright State Univ. and Dr. Roger Kamm of MIT, and the editorial advice of Mr. Jeffery Donnell.

Next, I would like to thank my fellow workers at Georgia Tech: Barbara, Chris, Jimmy, and John, and at Wright-Pat: Bob, McBob, Craig and Maj Bob, for their friendship. I would like to thank Ms. Jackie Brennaman and Ms. Bea Heflin for their assistance in preparing the manuscript for publishing. Finally, I would like to acknowledge the love and support of my wife, Lisa, and my father and mother, Charles and LaVerne Downing.

Table of Contents

LIST OF FIGURES

LIST OF TABLES

List of Symbols

A	cross-sectional area
A_o	nominal area variation
A_{oo}	nominal area
A_{in}	dynamic inlet area
A_{min}	minimum area
A_{th}	throat area
c	area wave speed
c_o	nominal area wave speed
D_o	nominal diameter
De	hydraulic diameter
DS	dynamic stiffness
E	Young's modolus
f	frequency of pulsatile pressure variation
f	friction factor
f_L	viscous friction factor
F'_{frict}	friction loss term in momentum equation
F'_{sep}	separation loss term in momentum equation
h	channel height
h_w	wall thickness
Kp	local tube stiffness
Kp_o	nominal tube stiffness variation
Kp_{oo}	nominal tube stiffness
K_{Sep}	separation coefficient
$n1$	tube law parameter governing positive pressure response
$n2$	tube law parameter governing negative pressure response
$P-P_e$	transmural pressure
P_1	inlet, perfusion, or upstream pressure
P_2	outlet, distal, or downstream pressure
P_e	external pressure
P_{min}	minimum pressure

Q_c	critical flow rate
R	tube radius
R_{dis}	distal resistance
Re_D	Reynolds number
S	speed index
S_{max}	maximum speed index
U	cross-sectionally averaged velocity
u	non-dimensional velocity
t, x	independent time and space variables
α	non-dimensional area ratio
β	artifical viscosity coefficient
Γ	integral of Π with respect to α
$\Delta\tau$	time step
$\Delta\xi$	spatial grid step
η	computational safety factor
λ_{A_o}	nominal area reduction amplitude
$\lambda_A(x)$	nominal area reduction curve
λ_{Kp_o}	stiffness variation amplitude
$\lambda_{Kp}(x)$	stiffness variation curve
μ	fluid viscosity
ν	Poisson's ratio
ξ	non-dimensional x
Π	non-dimensional pressure
ρ	density
σ_{11}	normal stress component
τ	non-dimensional time
τ_w	wall shear stress
ϕ	elastic jump variable
$\mathcal{A}, \mathcal{B}, C$	matrice for system of equations

BACKGROUND OF STENOTIC ARTERIAL FLOW

Clinical Motivation

Atherosclerosis progresses by building localized plaques on the interior wall of the artery. The plaque consists of a thickening of the intima surmounted by a fibrous cap. The thickened intima contains atheroma which is composed in varying degrees of collagen, elastin, cell debris, and lipids. Atheroma is separated from the lumen by a fibrous cap. Arterial plaques vary in the relative quantity and spatial organization of their component parts. Some plaques, which contain calcium, are characterized as hard. These hard plaques tend to form concentric stenoses (1). These types of plaques are usually found in the arteries of the lower limbs. Other plaques are characterized as soft. Soft plaques are composed of fatty cells and predominantly form eccentric stenoses with a portion of the normal arterial wall exposed to the lumen. Fatty plaques are typically found in the internal carotid arteries. Plaques within the coronary arteries can be of either type. These two different types of stenosis shapes are shown in Figure 1.

As the disease progresses, the plaque will encroach on the lumen and produce a stenosis to the flow of blood. The stenosis can restrict both the flow rate and the distal perfusion pressure to major distal vital vascular beds such as the brain, the lower libs, and the heart. In the early stages of the disease, the arteries appear to compensate for the stenosis by dilating the arterial wall. This dilation maintains a constant lumen size and the flow rates for stenoses up to 40% by diameter (2). However, as the plaque increases in size and encircles the lumen, the artery is no longer able to expand sufficiently to maintain proper flow and perfusion pressure. Clinical symptoms usually start when stenoses have advanced to 75% to 90% of the lumen diameter or until the plaque is disrupted by structural changes (3). At this stage of the disease, plaque disruption can occur, and this disruption is associated with clinical complications in the following vascular locations: coronary arteries, carotid artery, lower limb arteries, and infrarenal aorta.

Fracture or fissure of the atherosclerotic plaque is the disrupting mechanism leading to the episodic and/or terminal clinical symptoms (4-13). Myocardial infarction, (MI), transient ischemic attacks, (TIA), and strokes are associated with complications of plaque disruption (14). The onset of MI, TIA, and strokes is acute, and this acuteness suggests a process within the arteries causes sudden changes to the plaque which produce an obstruction to the flow of blood to the distal vascular beds. Embolism and thrombosis, both of which are signs of plaque disruption, are suggested causes of MI, TIA and strokes (5, 15). The sudden transition of a plaque from a stable to an unstable configuration has been identified as fracture or fissure of the atherosclerotic plaque. Thrombi can form over a fractured plaque. As a thrombus grows, the already restricted lumen becomes occluded resulting in flow cessation. Several researchers have found in 90% of MI cases thrombi covering plaque fissures (4, 5, 6, 9, 10, 16). Emboli are generated by pieces of plaques which have been fractured and moved downstream. As the emboli propagate downstream, they can occlude smaller arteries and stop the blood flow to the distal beds supplied by that vessel. This process leads to strokes or other symptoms (17). Also, uclerated plaques have been associated with TIA and amaurosis fugax (18, 19).

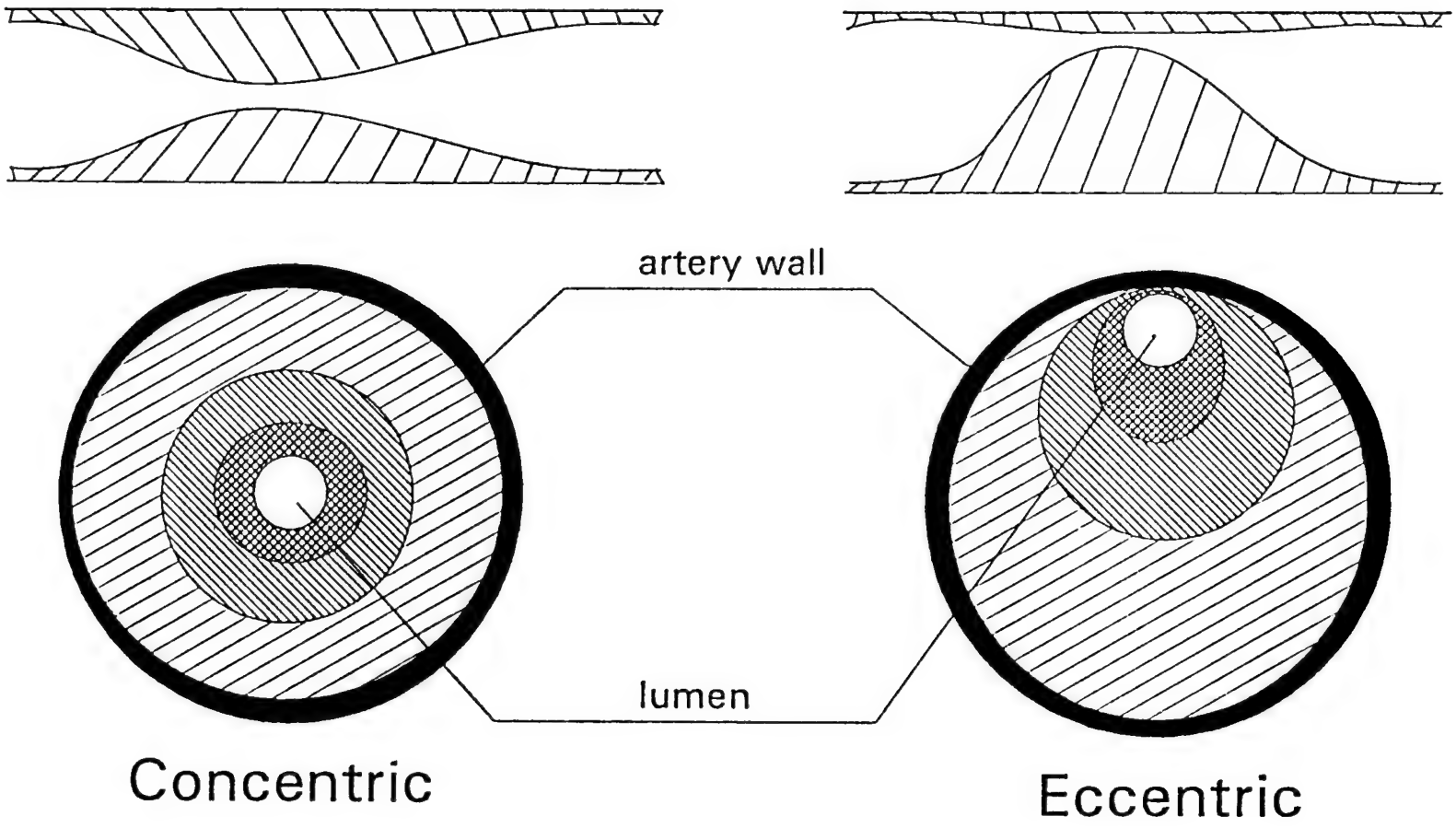

Figure 1 Concentric versus Eccentric Stenoses

Most disrupted plaques contain 'soft' centers. (5) These soft centers permit the plaque itself to be altered and distorted. This alteration and distortion can result in plaque instabilities by forming cleavage planes at the interfaces of plaque components which differ in compliance. Soft plaques have been identified to have a greater tendency towards clinical symptoms when compared to hard plaques (20). In a study of 297 carotid arteries examined by β-mode ultrasonography, soft high grade stenoses (>75% by diameter) had a 95% incidence rate of neurological events in previously asymptomatic patients, whereas hard or calcified plaques with less severe stenoses (<75% by diameter) had no neurological events. Another finding by Davies and Thomas showed a very strong correlation between plaque fissure and thrombus formation. They found plaque fissuring and coronary thrombosis in 103 of 115 cases of fatal MI (5). Fuster (16) also notes that soft plaques are symptomatic and lead the more severe stenoses in terms of clinical observations. Fuster further implicated plaque fissure as the underlying event to acute coronary symptom, and he stated that there needs to be a fuller understanding of the importance of the role of blood flow in plaque disruption.

While many investigators have studied the genesis and propagation of atherosclerotic plaques, few have studied the conditions which cause plaque fracture and fissure. The above references demonstrate a good understanding of the transition of plaque fracture and fissure to clinical complications such as MI, TIA and strokes. However, the cause of plaque fracture is not understood. Suggested causes for fracture are hypertension, pulsatile circumferential stretching of the arterial wall, blood turbulence, intraplaque hemorrhage, metabolic or nutritional and chemical factors, auto-immune injury, calcification, and molecular changes which make the plaque more fragile (8). Understanding the end stage of this disease process is important in identifying susceptible arterial plaques before clinical symptoms become critical and result in mortality and morbidity.

These findings suggest that mechanical forces may be an important factor in initiating plaque fissure. A look at the physical forces involved in stenotic arterial flow highlight a possible mechanism for plaque fracture and fissure. As the blood flows through a high grade stenosis, a low pressure zone is generated at the throat of the stenosis. If the throat pressure drops below the external pressure, the artery and plaque can collapse which applies bending and compressive stresses to the plaque. Although the collapse is not a complete buckling of the artery, the collapse may apply sufficient stresses to fracture a soft or friable plaque. Thus, the mechanism behind plaque fracture may be the collapsing stresses induced by a coupling of the hemodynamics and the compliancy of the artery and arterial plaque.

Recent Research of Collapsible Tubes

Vessel collapse is a topic of great interest in biomechanical engineering (21), since most of the fluid conducting vessels in the body are elastic in nature. The collapse of a vessel occurs when the transmural pressure, defined as the difference between the intraluminal pressure and the external tube pressure, falls below a certain value. Some examples of physiological vessels which can experience collapse are systemic veins above the heart; intramyocardial coronary vessels during systole; arteries compressed by a sphygmomanometer cuff; pulmonary vessels of the upper lungs; and major airways

during coughing and/or forced expiration. These examples demonstrate that the phenomena of collapsible tube does exist in the human body. Many researchers have used collapsible tube models successfully to describe physiological flows.

Experiments in collapsible tubes have typically used a Starling resistor arrangement as shown in figure 2. A Starling resistor consists of a compliant tube segment mounted between two rigid tubes and enclosed in a pressure chamber. This arrangement allows the following variables to be controlled and measured: the upstream pressure (P_1), the downstream pressure (P_2), the external pressure (P_e), and the flow rate (Q). Experimenters have shown that for steady flow the system can be characterized by two pressure differences and the flow rate. The experimental relationships depend on which variables are controlled and which are measured. Four experimental approaches can be performed with the Starling resistor arrangement. In the first approach, the pressure difference, P_1-P_e, is held constant while the driving pressure gradient, P_1-P_2, is increased. As P_1-P_2 is increased by lowering P_2, the flow rate at first increases until it reaches a choked value where it remains constant regardless of any further decrease in P_2. This approach was utilized by Powell (22) to determine the critical choked flow rates in a model of a stenotic artery.

In a second approach, the pressure difference P_2-P_e is held constant while the flow rate is increased. P_1-P_2 is the measured quantity. At low flow rates the tube is collapsed, and the flow resistance is high, but as Q is increased, the tube opens from the upstream end. This opening of the tube lowers the resistance to the flow. As Q is increased further, it reaches a critical value where the pressure difference P_1-P_2 levels off and becomes limited. This approach has been utilized and investigated by several researchers (23-26).

In a third approach, P_1-P_2 is held constant while P_2-P_e is decreased. At the start, P_2-P_e is positive, and the tube is fully distended with steady flow rate. As P_2-P_e is decreased, the tube contracts, and the flow will slowly start to decrease. When P_2-P_e becomes sufficiently negative, the tube collapses, the flow resistance increases, and the flow rate has a large decrease. The collapsed section at first is localized at the downstream end. As P_2-P_e is decreased past the onset of collapse, the collapsed section lengthens toward the upstream end.

In a fourth approach, Conrad (27) modified the Starling resistor arrangement by including a flow resistor between the compliant section and the downstream pressure measurement site. In his experiments, the distal resistance and P_e are held constant, and P_1 and P_2 are measured as the flow rate is varied. He constructed many curves which relate P_1-P_2 with the flow rate. The curves highlight the relationships between these two variables for many flow conditions. At high flow rates, the tube is expanded, and the resistance is low. As flow is reduced below a critical value, collapse of the compliant segment starts and P_1-P_2 increases. As the flow approaches zero, the tube becomes severely collapsed, and P_1-P_2 starts to decrease again. He also noted that when P_2 was lowered while P_1 and P_e were lheld constant, collapse of the tube coincided with the choking of flow.

Unsteady flow experiments involving collapsible tube flows fall into two categories: 1) The input parameters are held fixed, but steady flow is not established due to unstable oscillations, and 2) The input parameters are varied with time, and the output parameters vary in a deterministic manner. Recent experiments by Bertram (28) have described in great detail the different parameter regimes in which oscillations

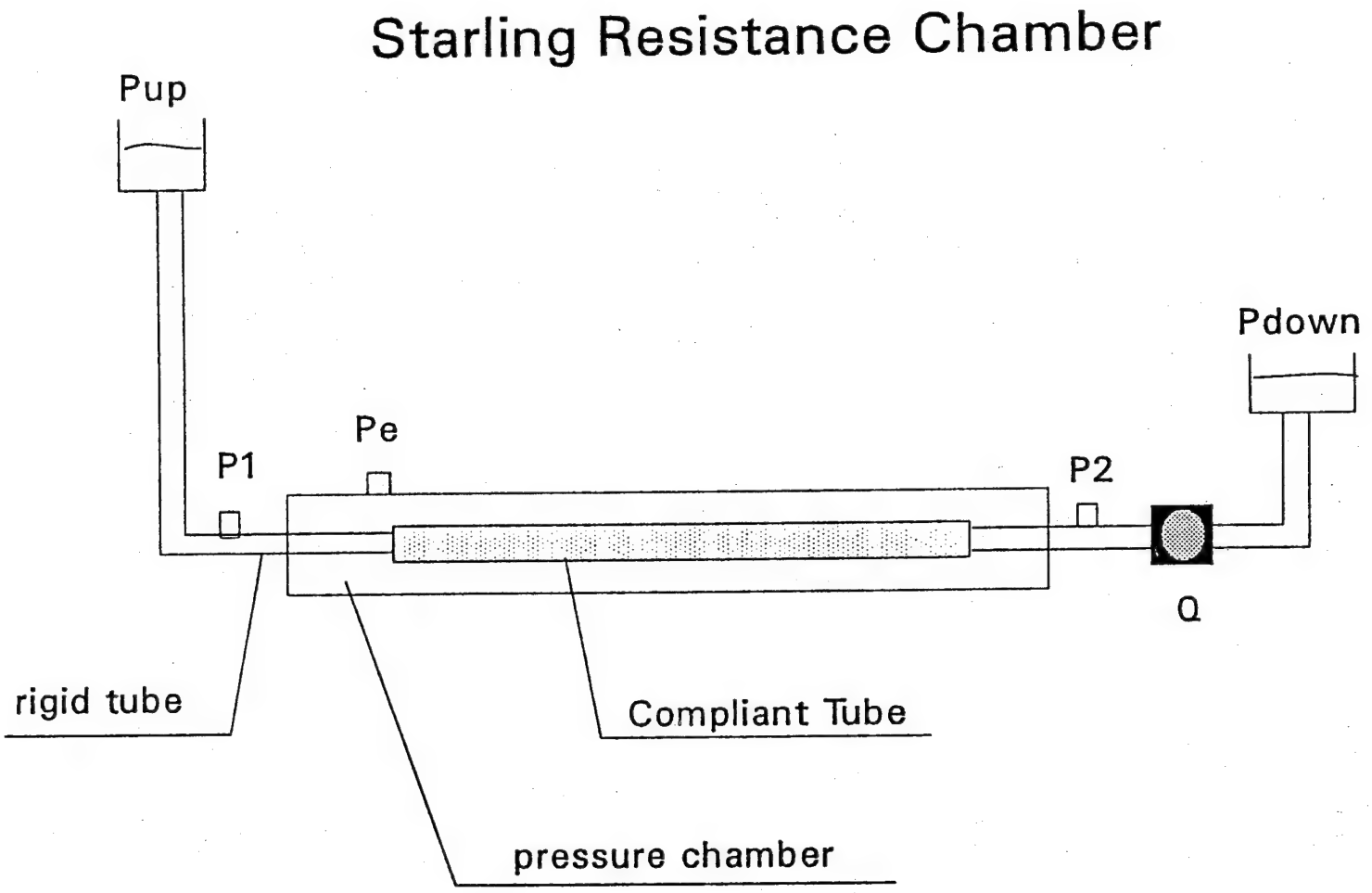

Figure 2 Diagram of Starling Resistor Chamber

occur. The other type of unsteady experiment, as performed by Binns and Ku (29), is directly relevant to stenotic artery flow being investigated by this study. In their experiment, a rigid stenosis was implanted in the compliant tube segment, and the upstream pressure was varied in a periodic manner with the downstream pressure held fixed. As the external pressure was increased, the behavior of the tube was characterized in terms of flow rate, wall motion, and collapse. Their findings demonstrated that some physiological conditions exist in which a stenosis will produce distal wall collapse in an elastic tube. Their conclusions point out that further research is needed to determine the effects that stenoses have on distal collapse of a compliant tube (29).

Theoretical modelling of flow through a compliant tube has evolved parallel to experimental developments. The first models (27, 30) used a lumped parameter approach in which the geometry of the compliant tube was characterized by a single time dependent variable of the minimum cross-sectional area of collapse. Although these models were limited, they demonstrated the behavior of the collapsible segments coupling with other conditions within the flow system.

Early experiments (31) in collapsible tube flow demonstrated that when a section of the compliant tube was pinched, a stable high speed flow was established just distal to the pinch followed by an abrupt deceleration and expansion occurring downstream of the high speed region. This abrupt deceleration was termed an "elastic jump" which had analogies to gas dynamics and free channel flows. Oates (32) and Shapiro (33) developed more detailed models. These models involved one-dimensional steady flow which incorporated fluid continuity and momentum equations with a "tube law". This tube law couples the fluid intraluminal pressure to the structural characteristics of the tube by relating the transmural pressure to the cross-sectional area through the stiffness of the tube wall. Shapiro provided a thorough discussion of the different types of phenomena that occur in steady collapsible tube flow and related them to analogous phenomena in gas dynamic and free surface channel flows. These investigations describe flow choking conditions which result when the fluid velocity is accelerated to a speed equal to the speed of a small amplitude, long wavelength area wave propagated along the tube. The possibility of supercritical flow was demonstrated and the conditions which lead to a smooth transition from subcritical to supercritical flows were derived. Also, the phenomena of an abrupt deceleration from supercritical to subcritical flow in a compliant tube was noted. This abrupt deceleration was termed an elastic jump for collapsible tube flows and is directly analogous to a shock in compressible flow and a hydraulic jump in free channel flow.

In a two part companion study by Kececioglu et al (34) and McClurken et al (35), experimental observations and theoretical studies were done on a steady elastic jump in a compliant tube. This study showed that longitudinal tension is important in characterizing the complex structure of the elastic jumps. Their experimental observations noted that the elastic jump consisted of precursor standing waves upstream which spread the jump region over one to two diameters of a non-stenotic compliant tube. In their analysis, they applied longitudinal tension only on the precursor standing waves and neglected tension downstream of the jump because of singularities in their tension term as the tube expanded to a circular cross-section.

Deterministic unsteady one dimensional flow models have also been analyzed (36, 37, 38) and unsteady self excited flows have been calculated with a model which incorporated longitudinal tension (39). Intrinsically two dimensional models have been developed to incorporate phenomena such as flutter and flow separation to understand the origins of unstable wall oscillations (45, 46). These models can also incorporate a variety of additional factors such as longitudinal and bending tension, wall inertia, and viscoelasticity. However, one dimensional models of unsteady flow should demonstrate the global behavior of flows under physiological conditions without being overly complex mathematically. Moreover, Elad and Kamm (37) have been successful in applying one dimensional flow in a model describing the lung during forced expiration. Although a one dimensional model may simplify the physical description of flow in a compliant tube, it is robust enough to model the complex system without overbearing computational demands.

Ziegler (42) and Ku et al (43) developed a steady one dimensional inviscid model to investigate flow through a stenotic compliant tube. Their model demonstrated that collapse can occur in a stenotic artery under certain physiological conditions. Further analysis is needed to determine more clearly the effects that stenosis, tube stiffness, pressure gradient, unsteadiness, and frictional losses have on stenotic arterial flow. Thus, as an expansion of their approach, this study develops an unsteady one-dimensional flow model which includes frictional losses to evaluate in greater detail the parametric and physiological conditions which have the greatest effect on stenotic artery wall collapse.

Theoretical Analysis: Collapsible Tube Theory

The actual fluid mechanics involved in collapsible tube flow is complex because of the three-dimensionality of the deformable tube, the coupling of the fluid and the tube structure, and the presence of elastic jumps. Modeling these complexities with rigorous theoretical techniques might obscure the physical behaviors since complex mathematics would necessarily be involved in solving the governing system of equations. On the other hand, a simple approximate theoretical model can provide insights into the dominant physical features which control or influence flow through a compliant tube. Since the goal of this investigation is to examine the effect that the physical parameters have on the flow, the developed computer model will solve the one-dimensional equations of motion. This one-dimensional model includes frictional losses and unsteady effects in its description of stenotic artery flow, but neglects the effects of longitudinal tension and tethering on the artery.

Basic Equations of Motion

The field variables defining the collapsible tube flow are transmural pressure, $P-P_e$, the cross-sectionally averaged velocity, U, and the cross-sectional area, A. Shapiro (33) showed that the physical differential equations describing collapsible tube flow are analogous to flows in gas dynamics and open channel free surface flows. The basic equations are the conversation of linear momentum, continuity, and a state equation.

Linear Momentum. First, the equation describing the conservation of linear momentum for one-dimensional unsteady, frictionless flow is

$$\frac{\partial U}{\partial t} + U\frac{\partial U}{\partial x} = -\frac{\partial}{\partial x}\left(\frac{P}{\rho}\right). \tag{1}$$

This equation is the same for each of the above physical cases where ρ is the fluid density, P is the static pressure of the fluid, U is the cross-sectionally averaged fluid velocity, t is time, and x is the longitudinal distance.

Continuity. The equations of continuity for each of the cases are

$$\begin{aligned}
&i) \quad \frac{\partial A}{\partial t} + \frac{\partial (AU)}{\partial x} = 0 \qquad \textit{Collapsible Tube} \\
&ii) \quad \frac{\partial \rho}{\partial t} + \frac{\partial (\rho U)}{\partial x} = 0 \qquad \textit{Compressible} \\
&iii) \quad \frac{\partial h}{\partial t} + \frac{\partial (hU)}{\partial x} = 0 \qquad \textit{Channel}
\end{aligned} \tag{2}$$

where for case (i) A is the cross-sectional area, and for case (iii) h is the height of the free surface above the channel bottom. From these equations, it can be seen that A, ρ, and h have corresponding roles.

Tube Law. Next, an equation of state is needed to complete the system of equations. The state equation relates the pressure to either A in case (i), ρ in case (ii), or h in case (iii). The form of the equations of state for these three cases are

$$\begin{aligned}
&i) \quad A = f(P - P_e) \qquad \textit{Collapsible Tube} \\
&ii) \quad \rho = \rho(P) \qquad \textit{Compressible} \\
&iii) \quad h = (P - P_{atm})/\rho g. \qquad \textit{Channel}
\end{aligned} \tag{3}$$

Equation 3 (ii) is the pressure/density relationship of the gas. Equation 3 (iii) is the hydrostatic law of variations of pressure with depth. Equation 3 (i) relates the tube cross-sectional area with the transmural tube pressure and is referred to as the tube law (33).

While the continuity and the linear momentum equation are well formulated, the tube law is less familiar. The tube law describes the relationship between the transmural pressure and the cross-sectional area of the tube. The tube law is usually expressed in a non dimensional form with the pressure normalized with respect to the tube stiffness and with the area normalized with respect to the nominal tube area at zero transmural pressure. The tube stiffness has been defined by Fung (44) as

$$Kp = \frac{Eh_w^3}{12(1-\nu^2)R^3}, \quad (4)$$

where E is Young's Modulus of the vessel, h_w is the vessel wall thickness, ν is Poisson's ration, and R is the mean tube radius. Thus, the tube law is expressed in the following form:

$$\frac{P-P_e}{Kp} = f(\alpha), \quad (5)$$

where α is the normalized area ratio, which is defined as the actual area divided by the nominal area, $\alpha = \frac{A}{A_o}$.

It is difficult to determine an exact analytical relationship which fits the pressure/area curve over a wide range of pressures such as those present for the physiological case. For positive transmural pressures, the tube has a circular cross-section, but as the transmural pressure reduces to near zero, the tube cross-section becomes elliptical. Further reductions in the pressure results in the cross-sectional area becoming dumbbell shaped. These different stages of the pressure/area curve are highlighted in figure 3.

Flaherty (45) has shown for a mathematical model that the tube law had the following form for $\alpha < 0.27$:

$$\Pi = \alpha^{-n} \quad ; \quad n = 3/2, \quad (6)$$

where Π is the normalized transmural pressure, $\frac{P-Pe}{Kp}$. This expression is very limited in its application due to the restriction on α.

Shapiro (33) approximated the tube law relationship for negative pressures with the following analytical function:

$$\Pi = 1-\alpha^{-n}; \qquad n = 3/2. \quad (7)$$

This expression is still limited since it does not model positive pressure ranges. Elad and Kamm (37) expanded this analytical function to include the positive pressure variations also with the following expression:

$$\Pi = \alpha^{n1} - \alpha^{-n2}; \qquad n1 = 20, \quad n2 = 3/2. \quad (8)$$

This equation has the advantage of allowing one equation to model the pressure/area relationship for α approaching zero to values much greater than 1. In this equation, the *n1* term governs the positive pressure region, and the *n2* term governs the negative regions. This analytical form of the tube law has been used by Elad and Kamm (37) in their model of the lung during forced expiration and by Ziegler (42) and Ku et al (43) in their model of a stenotic artery. These values for *n1* and *n2* correspond to the

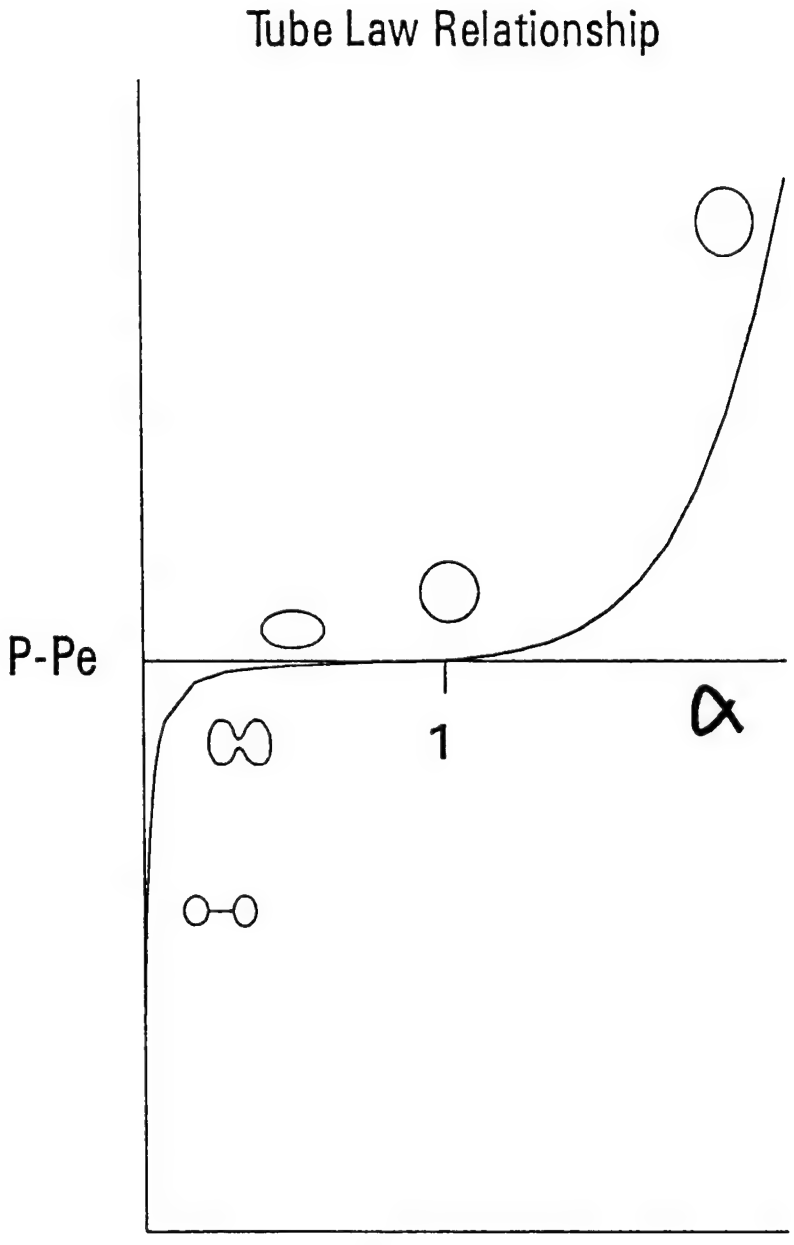

Figure 3 Tube Law: Relationship between Pressure and Cross-sectional Area

pressure/area curves of a Penrose drain tubing, which has been widely used in experiments to represent arteries. The form of the tube law as expressed in equation 8 is implemented in the model being developed for this study. However, *n1* and *n2* will be varied to model high, moderate, and low compliancy tubes.

A closer look at the tube law reveals the origin of the term collapsible tube. At transmural pressures close to zero, the slope of the curve decreases as α approaches 1.0. Thus, small changes in the pressure can result in large changes in the cross-sectional area of the tube. Fung (44) related this flat region of the curve to the buckling of an Euler column. This analogy relates the large area changes to the sudden large deformation of a column, which results from small fluctuations in the applied pressure, but this analogy can mislead one to think of tube collapse as a catastrophic buckling of the tube. When compared to buckling of a column, tube collapse is a smooth recoverable process. Tube collapse refers to the large area changes which can occur because of small changes in the transmural pressure in the flat region of the pressure/area curve. Therefore, tube collapse may be defined as the point when the tube area becomes reduced from its normal condition.

System of Equations. The system of equations for collapsible tube flow is compromised of equations 1, 2(i), and 3(i) and can be written in the following form:

$$\begin{Bmatrix} A \\ U \end{Bmatrix}_t + \begin{Bmatrix} AU \\ \frac{1}{2}U^2 + \frac{P - P_e}{\rho} \end{Bmatrix}_x = \begin{Bmatrix} 0 \\ 0 \end{Bmatrix} \tag{9}$$

with

$$A = f^{-1}(P - P_e),$$

where the subscripts, t and x denote partial differentiation. This system of equations is hyperbolic, which is shown in appendix A. A hyperbolic system allows discontinuous solutions and the propagation of disturbances in the form of characteristics. For collapsible tube, disturbances in the tube propagate along the tube as area waves. The wave speeds for the three cases are

$$\begin{aligned} &i) \quad c^2 = \frac{A}{\rho}\frac{dP}{dA} = \frac{A}{\rho}\frac{d(P - P_e)}{dA} && \textit{Collapsible Tube} \\ &ii) \quad c^2 = \frac{\rho}{\rho}\frac{dP}{d\rho} = \left(\frac{dP}{d\rho}\right)_{entropy} && \textit{Compressible} \\ &iii) \quad c^2 = \frac{h}{\rho}\frac{dP}{dh} = gh. && \textit{Channel} \end{aligned} \tag{10}$$

where P_e is a constant external pressure applied along the tube.

Expected Phenomena: Shapiro

By using the physical analogies (33), phenomena which are anticipated to occur in collapsible tube flow are the following:

i) wave propagation, as a domain mechanism of unsteady flow
ii) "speed index" analogous to the Mach number
iii) opposite effects for super- and sub-critical flows
iv) flow limitation when speed index reaches unity
v) smooth transition from sub- to super-critical flows
vi) abrupt transitions from super to sub critical flows--elastic jumps

Since the system of equations are hyperbolic for collapsible tube flow, disturbances propagate through the domain at characteristic velocities. These characteristic velocities are U+c and U-c, as shown in Appendix A. For collapsible tube flow, the ratio of U to c is referred to as the speed index, S=U/c, where S is directly analogous to the Mach number in compressible flow. When S is less than 1.0, the flow is referred to as subcritical, and disturbances may propagate both upstream at a speed of U-c and downstream at a speed of U+c. When S is greater than 1.0, the flow is called supercritical, and disturbances can not propagate upstream. Between these two flow regimes, a parameter will have opposite effects on the flow (33). For example, a converging area accelerates a subcritical velocity but decelerates a supercritical velocity. When S equals 1.0, the flow is at the critical point and becomes limited or choked. Once the flow is choked, it cannot be increased without changes in the inlet conditions or exit conditions which can unchoke the flow. Thus, the limited flow rate is the maximum flow rate possible for the given inlet conditions.

Collapsible tube flow can transition smoothly between the two regimes once the critical point is reached. The flow may also transition from supercritical to subcritical by an abrupt transition such as a normal shock in compressible flow. For collapsible tube flow this abrupt transition is referred to as an elastic jump (33). The elastic jump can be characterized as a sudden expansion of the tube area over a very short distance with a substantial deceleration of the fluid velocity. Upstream of the elastic jump, the velocity is supercritical with a low fluid pressure and a decreased tube area. Through the elastic jump, the velocity is greatly decelerated and becomes subcritical with a higher fluid pressure downstream of the jump.

Elastic Jump

Once the flow goes supercritical, the flow may transition abruptly to the subcritical state through an elastic jump so that the flow can meet the subcritical outlet boundary conditions, or frictional losses may allow a smooth transition back through S=1 to subcritical. In the region of the elastic jump, the one-dimensional approximation breaks down due to the complex nature of the structure of the elastic jump. To overcome this difficulty, Oates (32) and Cowley (46) derived relationships between the dependent variables immediately up- and down-stream of the elastic jump. Oates and Cowley derived these relations about a control volume that completely surrounded the elastic jump region by combining the tube law with the equations of continuity and momentum to obtain the following:

$$Q = UA \tag{11a}$$

$$\phi(A) = \frac{Q^2}{A} + \int \frac{A}{\rho} \frac{d(P - Pe)}{dA} dA. \tag{11b}$$

Equations 11 a and b are referred to as the elastic jump relationships.

The quantities, Q and ϕ, are conserved across the jump. These relations maintain a constant flow rate and account for dissipated mechanical energy due to the work performed on the elastic tube during the expansion. Cowley (46) stated that this energy loss probably appears in the form of turbulent separation within the jump region. These losses are confined to the jump region since the flow velocity is greatly decelerated by the jump. The magnitude of these elastic jump losses have been observed in the experimental results of Kececuogli et al (34). They noted that the losses incorporated in the elastic jump relationships accounted for the measured pressure losses in their collapsible tube experiment.

Kimmel et al (38) incorporated the jump relations into the governing system of equations by modifying the momentum equation. This modification involves multiplying the continuity equation (eqn. 2i) by U and the momentum equation (eqn. 1) by A and then adding these two equations to obtain

$$\frac{\partial(AU)}{\partial t} + \frac{\partial(AU^2)}{\partial x} + \frac{A}{\rho}\frac{\partial(P - Pe)}{\partial x} = 0. \qquad (12)$$

It will be shown later that this equation contains the jump relations derived by Oates and Cowley (32, 46).

Frictional Losses

A friction term is added to the momentum equation to account for viscous losses due to friction between the tube wall and the fluid. This added friction term is

$$F_{frict} = \frac{4\tau_w}{\rho De}, \qquad (13)$$

where

$$De = \begin{cases} \alpha Do, & \alpha < 1 \\ Do, & \alpha \geq 1 \end{cases}.$$

De is the hydraulic diameter used to account for the non-circular shape of the compressed tube for negative transmural pressures, and τ_w is the wall shear stress. τ_w is estimated by (47)

$$\tau_w = \frac{\rho f U^2}{8}, \qquad (14)$$

where f is a friction coefficient which can represent either laminar or turbulent friction losses. For laminar losses, f equals the following:

$$f_L = \frac{64}{Re_D} = \frac{64\mu}{\rho U De}, \qquad (15)$$

where Re_D is the Reynolds number and μ is the fluid viscosity. For stenotic arterial flow, the flow is expected to remain laminar throughout the region of concern except in the region of the elastic jump. The Re may approach and/or exceed the conventional value of transition Re for steady internal flows as the actual flow in a compliant stenosis reaches supercritical speeds. However, the flow should remain laminar since it is being accelerated by the converging tube area. Thus, the following friction term is added to the modified momentum equation, (eqn. 12):

$$F'_{frict} = \frac{32\mu f_L'}{\rho D e^2} UA \tag{16}$$

where f_L' will allow variations in the magnitude of laminar frictional losses. With this addition, the modified momentum equation becomes

$$\frac{\partial(AU)}{\partial t} + \frac{\partial(AU^2)}{\partial x} + \frac{A}{\rho}\frac{\partial(P - Pe)}{\partial x} + \frac{32\mu f_L'}{\rho D e^2} UA = 0. \tag{17}$$

Since a stenotic section has both converging and diverging area sections, separation losses may be important to consider. Separation losses will not occur until an adverse pressure gradient is created by the diverging section or by an elastic jump. For the latter case, the elastic jump relations incorporate separation losses. Thus, for critical flows, an additional separation loss term is not included in the baseline solutions. A separation term is added to the system of equations as an additional effect to account for possible separation due to the diverging section of the stenosis. In the comparison of the model with the experimental results of Powell (22), an additional empirical separation loss term is included. The experimental stenosis model was a rigid funnel with a sharp opening at the throat, which would form a separated jet. The separation term uses the following relationship to determine the pressure loss due to separation (47):

$$K_{Sep} = \frac{\Delta P_{Sep}}{\frac{1}{2}\rho U_1^2} \tag{18}$$

where ΔP_{Sep} represents the pressure loss resulting from separation. Thus, the separation pressure loss term reduces to

$$F'_{Sep} = \frac{\Delta P_{Sep}}{\rho} = \frac{1}{2} K_{Sep} U_1^2, \tag{19a}$$

which can be rewritten as the following by using continuity:

$$F'_{Sep} = \frac{1}{2} K_{Sep} \left(\frac{A_2}{A_1} U_2\right)^2 \tag{19b}$$

This separation term is incorporated in the modified momentum equation in the following manner:

$$\frac{\partial(AU)}{\partial t} + \frac{\partial(AU^2)}{\partial x} + \frac{A}{\rho}\frac{\partial(P-Pe)}{\partial x} + F'_{frict} + \frac{K_{sep}}{2}\left(\frac{A}{A_{th}}\right)^2\frac{AU^2}{L} = 0, \quad (20)$$

where F'_{frict} is the laminar losses defined in equation 16, L is the distance over which the separation term is applied, and A_{th} is defined as the area at the throat of the stenosis. For this model L is taken to be two tube nominal diameters, which was estimated from the experimental observations of Kececioglu et al. (34). This form of the modified momentum equation is applied at the onset of an adverse pressure gradient or on the subcritical side of the elastic jump up to the distance L.

Nondimensional Variables and Equations

Before the equations are input into a computational model, it is effective to non-dimensionalize the equations. The non-dimensional variables are defined in the following:

$$\tau = \frac{c_o}{D_o}t \qquad \xi = \frac{x}{D_o}$$

$$\lambda_A = \frac{A_o(x)}{A_{oo}} \qquad \lambda_K = \frac{Kp_o(x)}{Kp_{oo}} \quad (21)$$

$$u = \frac{U(x,t)}{c_o} \qquad \alpha = \frac{A(x,t)}{A_{oo}\lambda_A(x)}$$

$$\Pi = \frac{P(x,t)-P_e}{Kp_{oo}\lambda_K(x)} \qquad c_o = \sqrt{\frac{Kp_o(x)}{\rho}},$$

where D_o = nominal tube diameter

A_{oo} = nominal tube area

Kp_{oo} = nominal tube stiffnes

λ_A = stenosis shape function

λ_K = stiffness variation function.

with

$$\Pi = \alpha^{n1} - \alpha^{-n2}$$

Substituting these variables into equations 2i and 17 the following non-dimensional system of equations is established:

$$\frac{\partial}{\partial\tau}(\lambda_A\alpha) + \frac{\partial}{\partial\xi}(\lambda_A\alpha u) = 0 \qquad (22a)$$

$$\frac{\partial}{\partial\tau}(\lambda_A\alpha u) + \frac{\partial}{\partial\xi}(\lambda_A\alpha u^2) + \frac{Kp_o}{\rho c_o^2}\lambda_A\alpha\frac{\partial}{\partial\xi}(\lambda_K\Pi)$$

$$+ \frac{32\rho}{\mu c_o De}\frac{D_o}{De}f_L'\lambda_A\alpha u = 0. \qquad (22b)$$

In the third term of equation 22b, a non-dimensional parameter appears in the form

$$DS = \frac{Kp}{\rho V^2}, \qquad (23)$$

where DS refers to "dynamic stiffness" and V refers to a generic velocity term which can be the fluid velocity, the wave speed, or the nominal wave speed. If V is taken as the fluid velocity, U, DS can relate the tube stiffness, Kp, to the dynamic pressure of the flow, ρU^2. DS is directly relevant to collapsible tube flow since it represents the coupling of the flow with the structure of the tube, which is the driving mechanism of collapsible tube theory. The inverse of DS was used by Powell (22) to relate his experimental results to the inviscid solutions of Ziegler (42). This term should represent the tendency of a tube to collapse. Collapse should occur when DS, defined with respect to U, decreases within the stenosis to values below its nominal values outside of the stenosis. This decrease would represent a softening of the tube during dynamic flow conditions. The nominal value of DS is unity in the system of equation because of the definition of the nominal wave speed, c_o.

Other non-dimensional parameters, which appear in equation 22b, are a Re type term and a length term. Both of these terms appear in the frictional term of the equation. Thus, f_L' can also be used to modify the friction term for viscosity and length changes.

Equation 22b can be rewritten into the following:

$$\frac{\partial}{\partial\tau}(\lambda_A\alpha u) + \frac{\partial}{\partial\xi}\{\lambda_A[\alpha u^2 + \lambda_K(\alpha\Pi - \Gamma)]\}$$

$$+ \Gamma\lambda_A\frac{\partial\lambda_K}{\partial\xi} - \lambda_K(\alpha\Pi - \Gamma)\frac{\partial\lambda_A}{\partial\xi} + \frac{32\rho}{\mu c_o De}\frac{D_o}{De}f_L'\lambda_A\alpha u = 0, \qquad (24)$$

where

$$\Gamma = \int \Pi d\alpha.$$

This form of the equation isolates the forcing terms of area and stiffness variations and friction. The system of equations now becomes

$$\begin{Bmatrix} \lambda_A \alpha \\ \lambda_A \alpha u \end{Bmatrix}_\tau + \begin{Bmatrix} \lambda_A \alpha u \\ \lambda_A [\alpha u^2 + \lambda_K (\alpha \Pi - \Gamma)] \end{Bmatrix}_\xi$$

$$+ \begin{Bmatrix} 0 \\ \Gamma \lambda_A \dfrac{\partial \lambda_K}{\partial \xi} - \lambda_K (\alpha \Pi - \Gamma) \dfrac{\partial \lambda A}{\partial \xi} + \dfrac{32\rho}{\mu c_o De} \dfrac{D_o}{De} f_L' \lambda_A \alpha u \end{Bmatrix} = \begin{Bmatrix} 0 \\ 0 \end{Bmatrix}. \qquad (25)$$

with $$\Pi = \alpha^{n1} - \alpha^{-n2}$$

This complete system of equations has three equations with three unknowns. The unknowns are α, u, and Π. Only two boundary conditions and two initial conditions are required for a unique solution since the two partial differential equations are first order in both time and space.

Now, the elastic jump relations can be revisited to show that the modified system of equations contains these relationships. To show this equation 25 has to be integrated from a distance upstream of the jump, ξ_{up}, to a distance downstream of the jump, ξ_{down}, as in the following:

$$\int_{\xi_{up}}^{\xi_{down}} \{[\mathcal{A}]_\tau + [\mathcal{B}]_\xi + C\} d\xi = 0, \qquad (26)$$

where $\mathcal{A}$, $\mathcal{B}$, and C correspond to the terms in the brackets in equation 25. If the time derivative is carried through the integral, and if ξ_{up} and ξ_{down} approach the jump location, $\xi_J(\tau)$, then the following is obtained:

$$\frac{d\xi_J}{d\tau} [\mathcal{A}(\xi_{down}) - \mathcal{A}(\xi_{up})] - [\mathcal{B}(\xi_{down}) - \mathcal{B}(\xi_{up})] = 0, \qquad (27)$$

Note that the integral of C tends to zero as ξ_{up} and ξ_{down} both approach $\xi_J(\tau)$. If the jump is stationary or in a reference frame in which it appears stationary, the above equation reduces to the non-dimensional elastic jump relationships of Oates and Cowley (32, 46) as

$$(\lambda_A \alpha u)_{\xi_{up}} = (\lambda_A \alpha u)_{\xi_{down}} \qquad (28a)$$

$$(\lambda_A \alpha u^2 + \lambda_K (\alpha \Pi - \Gamma))_{\xi_{up}} = (\lambda_A \alpha u^2 + \lambda_K (\alpha \Pi - \Gamma))_{\xi_{down}}. \qquad (28b)$$

It should be noted that

$$\int \alpha \frac{d\lambda_K \Pi}{d\alpha} d\alpha = \alpha \lambda_K \Pi - \lambda_K \int \Pi d\alpha = \lambda_K (\alpha \Pi - \Gamma).$$

Experimental Evidence for Collapse Within a Stenosis

Binns and Ku (29) performed unsteady *in vitro* experiments on the possibility of stenosis induced collapse of a compliant tube model of the carotid artery. They used both snare stenoses of 50 and 68% (dia) and rigid stent stnoses of 69, 75, and 81% (dia) in the compliant tube which was placed in a Starling resistance chamber. The perfusion pressure was varied from 100 to 60 mmHg. The external pressure was increased to identified the collapsing pressures and flow rates. The nature of the unsteady flow was observed to have three regimes for different external pressure settings. In the first regime, the tube remained expanded during the entire cycle with increased expansion during systole. Thus, the flow remained subcritical throughout the cycle. In the second regime, distal collapse was observed only during systole with expansion occurring during diastole. The authors referred to this paradoxical motion as systolic wall collapse. In the third regime, distal collapse was established throughout the entire cycle. Thus, the flow remained supercritical throughout the cycle. Their findings showed that collapse occurred just distal to the stenosis at physiological flow rates and that the external pressure needed to cause collapse reduced with increasing degree of stenosis.

In another study, Powell (22) used a rigid funnel stenosis to better identify the conditions for distal collapse just past the stenosis. The rigid funnel shaped stenosis allowed the tube to be totally compliant just distal to the throat, but the tube was still restricted proximal to the throat. Steady flow measurements were obtained for variations in the distal and external pressure for stenoses of 70, 80, and 90% by diameter. Powell demonstrated that the flow became choked once collapse was initiated regardless of any further decrease in the distal pressure. As the distal pressure was decreased beyond the critical point, the degree of collapse was observed to increase. The limitation of these studies is that rigid stenoses were used in their models. However, they did show collapse just distal to the stenosis and the occurrence of choked flow at this point.

Two other experimental studies have considered the effects that an eccentric stenosis in a compliant tube has on the flow (48, 49). In their experiments, an eccentric shaped stenosis was created by the insertion of a plug into the tube that allowed a segment of the tube wall to remain free. Judd and Mates (48) observed steady state flow changes as the distal resistance was lowered for various perfusion pressures. For 61 and 78% (dia) stenoses, which were defined as the percentage of area reduction for a static perfusion pressure of 165 mmHg, the flow increased as the distal resistances was reduced. However, for a 86% (dia) stenosis, the flow initially increased then decreased slightly as the distal resistance was lowered. This observation of decreasing flow with an increasing pressure gradient across the stenosis has been referred to as *paradoxical* flow since this observation is contrary to our knowledge of flow through rigid pipes. At the point where the flow began to decrease, the tube collapsed at the distal end of the stenotic region. The effect of Reynolds number was also tested by reducing the fluid viscosity by a factor of 10. With the increased Reynolds number, paradoxical flow was again observed in the 86% (dia) stenosis.

The experiments by Young and Stergiopulos (49) involved pulsatile flow through eccentric stenoses. They noted two regions of stenoses, subcritical and critical. Under some of the flow conditions, small changes in the geometry of the stenotic region were observed during the cycle. For the critical stenoses, these changes affected the measured pressure gradient across the stenosis. In other tests, the vessel collapsed due

to the low pressures produced by the critical stenoses. Overall, these experimental observations provide good evidence that arterial collapse and flow choking can occur in a stenotic segment.

Physiological Evidence for Collapse and Choking of Arteries

Clinical studies by several authors have demonstrated that a stenosis affects the flow under moderate or high demand conditions, whereas no effect is seen under resting flow conditions (50-55). Several studies (52, 54-56) have also noted paradoxical flow through a stenotic artery. At low or resting flow rates, the stenosis has a small or no affect on the flow, but upon the initiation of high flow demands, i. e. lower distal resistance, the flow rate would actually decrease. Logan (1) stated experimental findings for flow through excised stenotic arteries in terms of stenotic resistance which increased with high flow. At low flow rates the stenotic resistance was constant with small changes in the flow rate. Under high flow conditions, the stenotic resistance increased by a factor of two to three. Logan reasoned that eccentric stenoses produced additional losses due to elastic effects of the stenosis which only appeared during high flow conditions.

Schwartz et al (54-56) and Higgins et al (57, 58) suggested that passive narrowing or collapse of the artery in the region of the stenosis might account for the paradoxical flow reduction. In experiments by Schwartz (54), a wire snare was utilized to create a stenosis in the coronary arteries of dogs. A wire snare encircles the exterior of the artery and is tightened to restrict the lumen. This type of device does not create a smooth, circular reduced lumen since the interior arterial wall will become crimped. This experiment demonstrated that the wire snare stenosis did not affect resting flow but caused a decrease in the flow when the distal resistance was lowered. Schwartz speculated that the stenotic lumen passively narrowed due to the reduction in the distal pressure. He discounted platelet thrombi by giving aspirin to some of the dogs to delay the development of any platelet thrombi and found that aspirin did not affect the results. This experiment provides a good demonstration of the paradoxical flow, yet the important parameter of the degree of stenosis was not measured or defined. In a follow-on experiment (55) to show exercise induced ischema in dogs, paradoxical flow was again demonstrated. A wire snare stenosis was used, and the degree of the stenosis was increased until decreased flow was observed under mild exercise conditions. The flow was observed to decrease with increasing degree of stenosis. Schwartz (56) suggested three possible mechanisms for the reduction in the flow upon lowered distal resistance. The first possibility was vasoconstriction of the artery which would reduce the lumen at the site of the stenosis. The second was passive narrowing due to lower pressures induced either by the stenosis or the distal resistance (52). The third was severe pressure loss due to turbulence past the stenosis (51, 59).

Passive narrowing has been put forth by Santamore et al (52) as the mechanism for the paradoxical flow. In their experiment, a balloon catheter was used to produce a stenosis with an annular lumen. This type of model stenosis allowed 100% of the arterial wall to remain active. Paradoxical flow was demonstrated in their experiments. Coronary angiograms showed stenotic area reductions, and reductions in both the distal intraluminal and aortic pressure were observed. These observations clearly showed that the artery is a compliant vessel and will react to changes in the intraluminal pressure. They also noted that distal coronary arteriolar vasodilation always increased the

hemodynamic severity of the stenosis. Vasoconstriction was induced in a few experimental trails to verify its affect on the flow. Their observation found no influence of vasoconstriction on their results.

Santamore and Bove (53) and Siebes et al (60, 61) developed simple models of flow through a stenotic artery. Their models incorporated basic friction loss terms to estimate the pressure drop across the stenosis for a given perfusion pressure and distal resistance. Dynamic pressure losses at the throat were also included at the throat of the stenosis, but they neglected any pressure recovery distal to the throat. A pressure/circumference relationship was used to model compliant effects of the artery. However, the relationships used in their models were restricted to positive pressures. The Santamore and Bove model separated the stenotic area into four sections with increasing steps in the plaque area. Siebes' model had a trapezoidal shaped stenosis with the minimum area extending for two nominal diameters. This trapezoidal stenosis was separated into 13 sections for the computation.

Santamore and Bove estimated with their model that paradoxical flow would start between low and high flow demands for a nominal area stenosis of 86%. Their model also predicted that the stenotic effect was enhanced (occurred at lesser degrees of stenosis) by vasoconstriction and lowered perfusion pressure. The model of Siebes et al simulated quasi-steady flow conditions with an inlet pressure waveform with a time varying distal resistance in order to mimic coronary flow conditions. Significant area reductions were shown to occur during the period of highest flow through the coronary arteries. From their model, Siebes and D'Argenio (60) speculated that as the degree of stenosis and the compliance increased, viscous losses would increase while separation losses would decrease. However, the results from the models of Santamore and Bove and Siebes et al are of limited value in estimating the effects of compliancy on flow through a stenotic artery since the pressure/area relationship was restricted to positive pressures.

In another experimental study which used excised human arteries (57), stenotic resistances were observed to increase dramatically in only a certain number of the arteries. The arteries which did not produce large resistance changes were referred as non-dynamic arteries. These non-dynamic arteries contained hard plaques, whereas the dynamic arteries, which produced large resistance changes, contained soft plaques. The degree of stenoses used in this study was not directly measured for each artery but was estimated to range from 80 to 94% by area. The experiment tested both vasodilated and vasoconstricted conditions at three perfusion pressures, 150, 100, and 75 mmHg, and with two distal resistance settings. The dynamic stenoses had larger stenotic resistances for all of the conditions when compared to normal arteries and non-dynamic stenotic arteries. Overall, the flow rate decreased with vasoconstriction versus vasodilation and with lower perfusion pressure. The stenotic resistance for the normal arteries and non-dynamic stenotic arteries remained constant with changes in the flow conditions, but for dynamic stenoses resistance increased significantly with decreases in the perfusion pressure. A combined effect was observed in the dynamic stenotic arteries when both the perfusion pressure and the distal resistance were lowered. In normal arteries and non-dynamic stenotic arteries, the flow increased by approximately 100% and the stenotic resistance remained fairly constant. Contrarily, in dynamic stenotic arteries, the flow rate decreased by approximately 40% and the stenotic resistance increased.

Another *in vitro* experiment by Higgins et al (58) declared that although passive narrowing was present in stenotic arteries, it was not related to a Starling resistor type phenomenon. In this experiment, silicon plugs were implanted in canine carotids to produce eccentric stenoses that were approximately 90% by area. The stenotic pressure was measured along with the distal pressure and the flow rate. The perfusion pressures were set at 149, 97, and 72 mmHg with either a high or low distal resistance. The results showed that flow rate and stenotic pressure decreased with decreasing perfusion pressure, while flow rate increased and stenotic pressure decreased with lower distal resistance. In this experiment the stenotic pressure was always greater than the distal pressure. This fact lead them to conclude that Starling resistor phenomenon did not occur in stenotic arterial flow since the stenotic pressure was always greater than the external pressure.

To add to the controversy of the mechanism which causes dynamic stenoses to affect the flow, Gould et al (51, 59) has suggested that geometric changes in the distal artery lead to greater separation losses and are the reason for the increased stenotic resistance under high flow conditions. In his experiments, a balloon constrictor was used to model the stenosis. This type of experimental stenosis restricts the movement of the artery wall. In the first experiment, high flow demand conditions were induced by the vasodilating drug, papaverine. The degree of stenosis ranged from 45 to 78% by diameter. The effect of vasodilation was observed to increase the flow rate and also increase the degree of the stenosis. This change in degree was caused by the dilation of the neighboring arterial segments. The segments next to the fixed stenosis increased in area while the stenotic area remained fixed. This geometric change increased the severity of the stenosis and lead to more separation of the flow. Gould noted that when matching the measured pressure loss across the stenosis, viscous and separation losses only accounted for one half of the losses. An additional loss term arising from the geometric changes was used to account for the additional measured loss. This additional term stated that changes in the area were directly equal to changes in the velocity. With this assumption, the additional loss term was proportional to the velocity raised to the third power. In the next study (59), better measurements of the artery dimensions were obtained during vasodilated flows. Their results again showed that geometric changes about the stenosis increased the hemodynamic severity of the stenosis while the stenosis itself remained unchanged. Upon the introduction of a vasodilating agent, the distal diameter was observed to narrow for a few seconds before dilating to a steady condition. Gould and Kelley discounted this narrowing as a transient artifact with no physical consequence. However, Schwartz (56) counters that the passive narrowing of the distal artery was prevented from establishing because of the drug induced vasodilation. The major problem of these experiments is the type of stenosis used. The balloon constrictor restricted artery movement within the stenotic region. Thus, the possibility of observing compliant affects within the stenotic region was greatly minimized.

In an *in vivo* experiment using dogs, Schwartz (56) demonstrated that distal vasodilation caused the distal diameter next to the stenosis to decrease. The model stenosis was created by a wire snare which allowed movement of the artery wall within the stenosis. The observations from this study showed that the distal diameter decreased even with flow increases in mild stenoses during distal dilation and for severe stenoses the flow decreased along with the distal diameter during vasodilation.

In another series of *in vitro* experiment with canine carotid and porcine coronary arteries, Tulenko et al (62) demonstrated altered responses to vasoconstricting agents due to the introduction of a stenosis. They utilized a silicone plug to produce eccentric stenoses. Without a stenosis, the vasoactive agents produced a 30 to 40% reduction in the lumen diameter without altering the flow rate or the distal pressure. However, in the presence of a stenosis, the introduction of vasoconstrictors resulted in decreased flow and distal pressure. This effect was amplified when the endothelial denudation was produced at the site of the stenosis. In a similar study, Li et al (63) demonstrated that a stenosis would accentuate the effects of vasoconstrictors by reducing the intraluminal pressure. This pressure reduction induced by the stenosis provided the potential for a positive feedback mechanism between the stenosis and the vasoconstricting agent. Their experiments used balloon stenoses which allowed 100% of the artery wall to remain active. Thus, the effects of the vasoconstriction were amplified (63). Their finding demonstrated that the stenotic diameter reduced significantly more than the proximal diameter. Thus, they concluded that the reduced stenotic diameters resulted from a combination of the vasoconstriction and the stenotic pressure reduction. These two studies show that the pressure reduction induced by the stenosis will amplify the effects of vasoconstriction to the point where flow will be decreased.

In summary, several researchers have attempted to identify the mechanisms behind increased stenotic resistance during high flow conditions and the reasons for the reduction of the flow. Their findings are contradictory to one another and still leave questions remaining. These questions include the following:

1. Can stenoses cause choked flow under physiological conditions?
2. If yes, What is the range of physiological conditions for choked flow?
3. What is the magnitude of the collapsed area from the nominal area of the throat?
4. What is the magnitude of the collapsing transmural pressure for physiological conditions?
5. How do variations within the physical parameters (i.e. compliance, frictional losses, mean pressure) affect physologic collapse?
6. What is the effect of pulsatile flow?
7. Can pulsatile flow create conditions for cyclic collapse of the stenosis?

Statement of Problem

Some previous computational models of compliant stenotic arteries have some shortcomings in properly modelling the physics of stenotic blood flow. The models of Santamore & Bove (53) and Gould (51) used overly simple empirical pressure loss equations to model the global flow through the stenotic segment without accounting for a choking phenomenon. Both of these models are simple in their description of the plaque characteristics and neglect any pressure recovery of the flow distal to the stenosis. The model developed by Ziegler (42) and modified by Ku et al (43) comes closer to modelling the system by solving the 1-D, steady, inviscid governing system of equations. This model highlighted the important choking characteristics of collapsible tube flow, but in simplifying the model frictional losses were neglected.

Thus, it is the goal of this investigation to study in more detail the coupling of hemodynamics with the structural characteristics of the arterial wall and plaque by considering a wide range of parametric effects which include frictional losses and unsteadiness. Moreover, this investigation aims to bracket the conditions leading to *physiological* collapse, which is a possible conducive mechanism for plaque fracture.

COMPUTATIONAL MODEL DESIGN

To improve upon the earlier models, this study's model uses 1-D unsteady equations to describe the flow, pressure, velocity, and tube area along a stenotic artery section. The basic assumptions of this model are that the flow can be model as basically one dimensional with the addition of empirical frictional loss terms to the system of equations, and the effects of longitudinal and bending tension, wall accelerations viscoelasticity properties, and tethering of the arterial wall can be neglected. The model includes smooth area and stiffness changes along with frictional losses at various driving pressure differences and perfusion pressures to the stenosis. Also, various tube and plaque characteristics are used to model the wide variations present in the physiological case of arterial plaques. The model also accommodates pulsatile flows. The results are verified by comparing them to the results obtained by the model of Ziegler (42) and the experimental results of Powell (22). This model also facilitates a thorough evaluation of the effects of physiological parameters have on the flow and the arterial shape. These attributes will provide a fuller understanding of the role hemodynamics has on a stenotic artery and specifically the role it has as a possible mechanism to the initiation of plaque instability.

The computational model solves one-dimensional unsteady flow through a compliant stenotic artery and is developed in the following discussion. The model consists of a compliant tube with a smooth, high-grade stenosis. The compliancy of the tube is defined by the tube law. The shape of the stenosis is a smooth area reduction which has a length of two nominal diameters and follows a $\sin^2\xi$ function. Figure 4 shows the basic shape of the model tube. The stenosis also includes smooth variation in the tube stiffness. The model accounts for frictional losses through an empirical friction term. Flow solutions are obtained for several conditions including changes in the degree of stenosis, in the driving pressures, in the stiffness, in the tube law, etc.

The advantages of a computer model in investigating collapse of an arterial stenosis includes time and control of the physical parameters. First, many conditions were needed to be modeled in order to bracket the conditions for physiologic collapse. This requirement can be fulfilled by a computer model in a relatively short time period since only values need to be changed instead of physical items. Second, a computer model also allows easy variations in single parameter so that trends can be estimated for the effect of the parameter. Moreover, the computational model optimizes experiments by allowing researchers to isolate the important parameters and to maintain the proper control over the other parameters during their studies.

Basic Model Characteristics

The basic area variation of the stenotic tube incorporated into this model is described by the following:

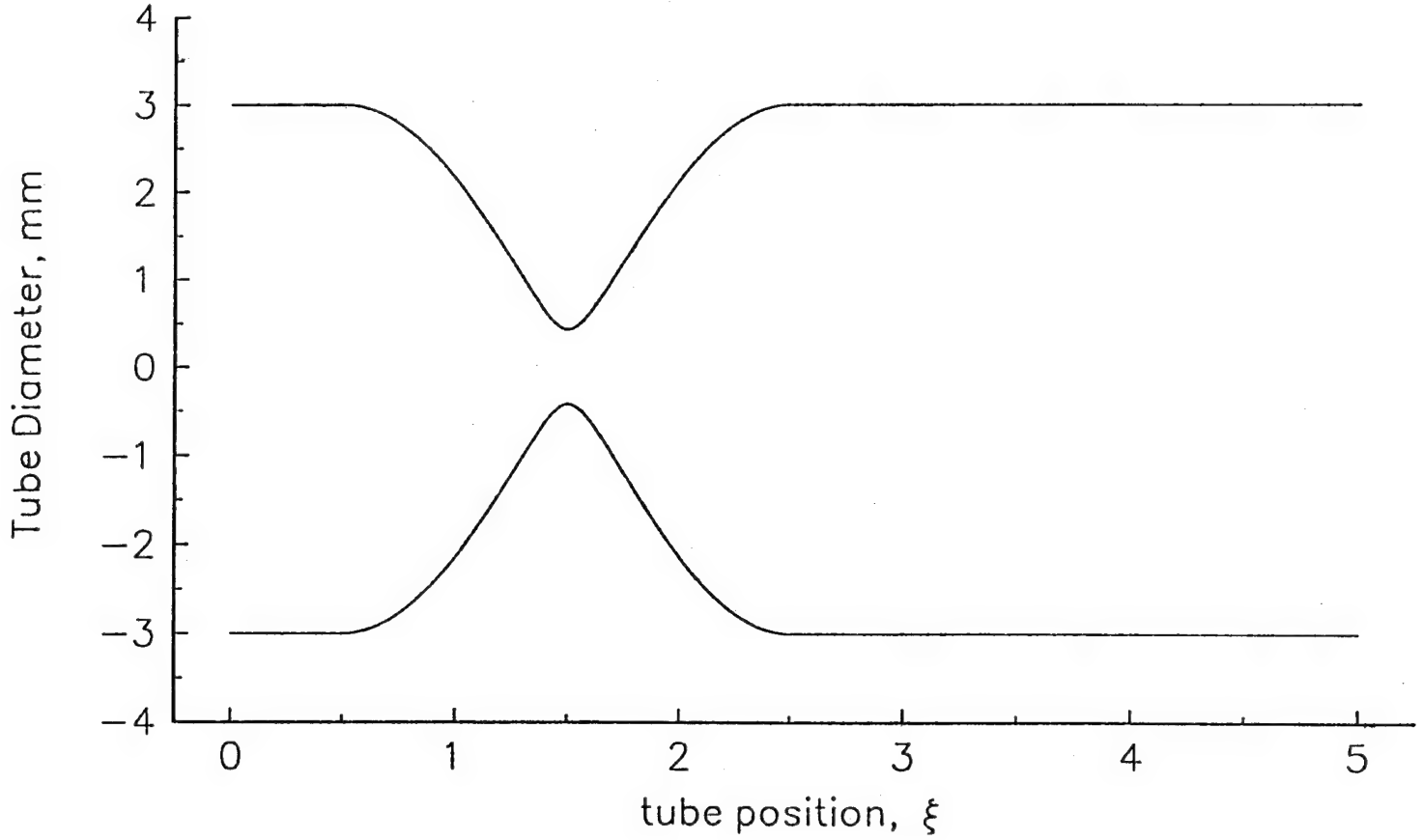

Figure 4 Shape of Computational Stenotic Tube

$$\lambda_A(\xi) = \begin{cases} 1.0 & \xi_i < \xi_{start} \\ 1 - \lambda_{A_o} \sin^2 \left[\pi \left(\frac{\xi_i - \xi_{start}}{\xi_{stop} - \xi_{start}} \right) \right] & \xi_{start} \le \xi_i \le \xi_{stop} \\ 1.0 & \xi_i > \xi_{stop} \end{cases} \quad (29)$$

where λ_{A_o} = area reduction amplitude

ξ_{start} = starting point of the stenosis

ξ_{stop} = stopping point of the stenosis.

This shape is a typical of stenotic arteries. λ_{A_o} is varied to change the degree of the stenosis for a set of conditions, and it is one of the basic input parameters. ξ_{start} and ξ_{stop} are set at 0.5 and 2.5, respectively.

The tube stiffness, Kp, is expected to vary along the stenosis because of geometric changes of the stenosis and possible variations in Young's modulus within the stenosis. Kp should increase as the wall thickens within the stenosis, since Kp depends on the ratio of wall thickness to tube radius, $\left(\frac{h_w}{R}\right)$. The relationship given by equation 4 was based on thin wall analysis (44) and for an 80% (dia) stenosis Kp would be increased by a factor of 250 at the throat. However, the thin wall assumption breaks down within the stenosis since the magnitude of the wall thickness becomes comparable to that of the radius. The actual Kp is much less within the stenotic section than the Kp evaluated by equation 4 (64). Therefore, the geometric variation should provide an increase in Kp along the stenosis which follows the stenotic shape and has an amplification factor of approximately an order of magnitude less that predicted by equation 4. Also, Young's modulus, E, may increase inside the stenosis because of the characteristics of the different materials within the plaque. No measurements of Young's modulus variations within a stenosis are available. It is likely that E will vary in a similar manner as the stenosis, itself. Therefore, the basic variation for the stiffness variation can also be approximated by a $\sin^2$ function, as described by the following:

$$\lambda_K(\xi) = \begin{cases} 1.0 & \xi_i < \xi_{start} \\ 1 + \lambda_{K_o} \sin^2 \left[\pi \left(\frac{\xi_i - \xi_{start}}{\xi_{stop} - \xi_{start}} \right) \right] & \xi_{start} \le \xi_i \le \xi_{stop} \\ 1.0 & \xi_i > \xi_{stop} \end{cases} \quad (30)$$

where λ_{K_o} = stiffness variation amplitude.

For the baseline solutions, the stiffness variation amplitude, λ_{K_o} is set at 10 with variations ranging from $\lambda_{K_o} = 0$ to 100. Although this range of λ_{K_o}'s is approximate, it should provide a representative range for the parametric evaluation of the effect of stiffness variations.

In comparison to the experimental results for the funnel shaped stenosis (22), this stiffness variation is modified to approximate the rigid funnel stenosis. This variation is defined by the following:

$$\lambda_K(\xi) = \begin{cases} \lambda_{Ko} & \xi_i < \xi_{throat} \\ (\lambda_{Ko} - 1)\cos^2\left[\frac{\pi}{2}\left(\frac{\xi_i - \xi_{throat}}{\xi_{stop} - \xi_{throat}}\right)\right] + 1.0 & \xi_{throat} \le \xi_i \le \xi_{stop} \\ 1.0 & \xi_i > \xi_{stop} \end{cases}, \quad (31)$$

The $\cos^2\xi$ part of the variation accounts for the stenting open of the tube at the throat of the rigid stenosis. For the comparison ξ_{throat} was set at 1.5, and ξ_{stop} was set at 2.5 resulting in a transition length of one nominal diameter. This variation is illustrated in figure 5. The proximal tube stiffness which is set at 20 times the nominal value of 125 Pa from the inlet to the throat of the stenosis approximates the rigid experimental stenosis. Also, since the rigid stenosis created an area discontinuity which would force flow separation, the additional separation loss term is included in this comparison. However, the area variation maintained a $\sin^2\xi$ shape since modeling the area discontinuity would make the computational method unstable when overlaid with the severe stiffness variation. Also, the nominal diameter for the prediction is set to equal the experimental value of 8.92 mm (22). Solutions are obtained for 70% and 80% stenoses (diameter).

Other input parameters include the inlet and outlet pressures, the friction coefficients, f_L' and K_{Sep}, if needed, and the nominal tube stiffness. The boundary pressures are input so that the proper α's can be determined for the boundary conditions.

Model Tube Laws

The parameters for the tube law are also input requirements for the model. This study considers three simplified tube laws and two physiologically based tube laws. The simplified tube laws consist of a highly, a moderately, and a lowly compliant tube. The parameters for the basic tube laws are given below

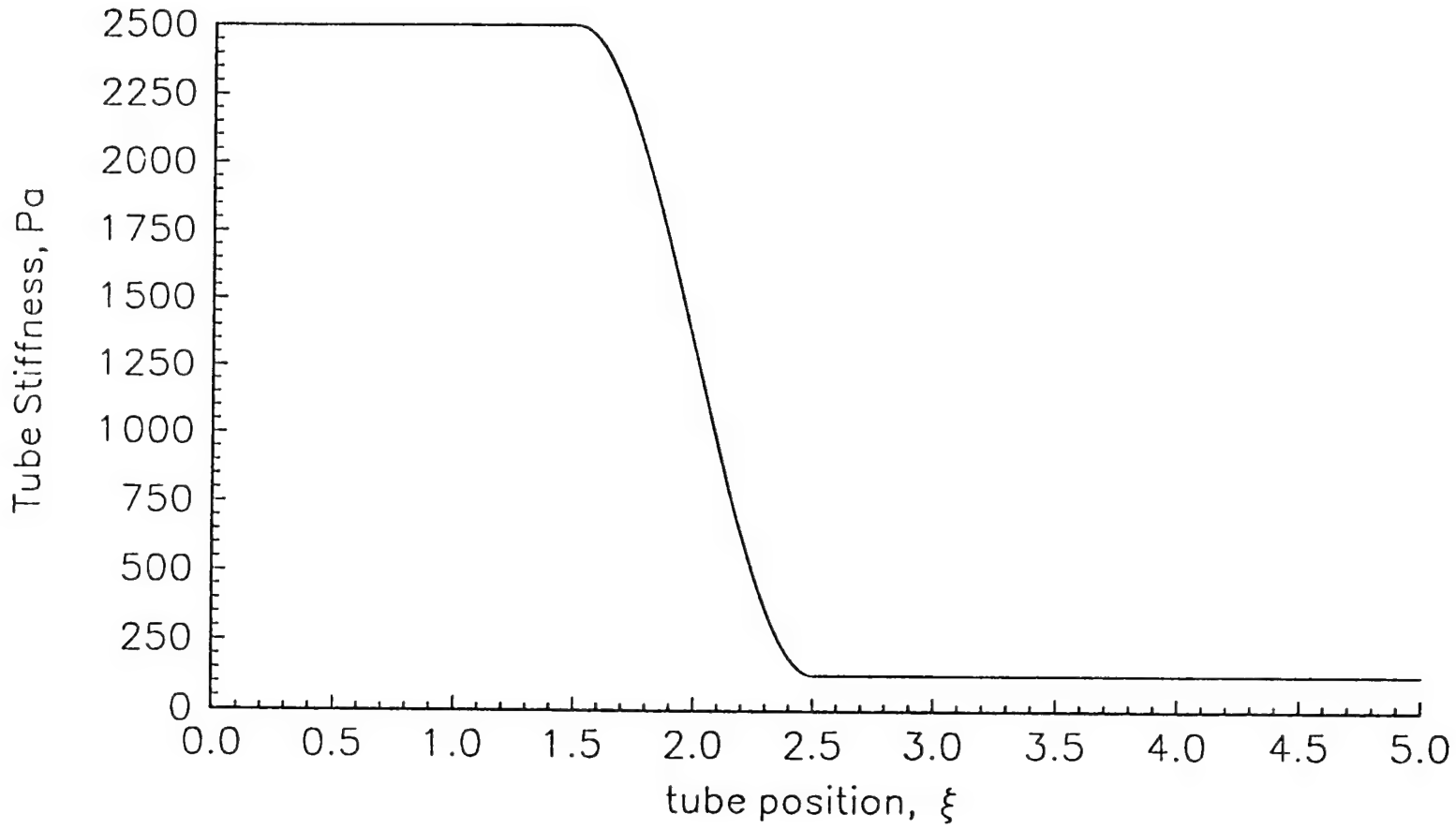

Figure 5 Stiffness Variation for Comparison to Powell's Experimental Observations

Table 1. Basic Tube Law: $\Pi = \alpha^{n1} - \alpha^{-n2}$			
Compliancy	Kp_o (Pa)	*n1*	*n2*
High	125	4	1.5
Moderate	125	7	2.5
Low	125	20	1.5

Arterial tube laws are harder to determine because of the wide variation in physical properties from one specimen to another. The arterial tubes used in this study were developed from experimental data on a bovine carotid artery and a canine carotid artery. The bovine tube law was determined by Powell (22) and is defined by the following:

$$\Pi = 0.13\alpha^{4.72} - 0.037\alpha^{-2.65}. \tag{32}$$

with $Kp_o = 3691.6$ Pa. The bovine tube law correlates to the moderately compliant basic tube law.

The canine tube law was determined from experimental pressure/area curves reported by Cox (65) and is defined by the following:

$$\Pi = 0.437\alpha^{3.77} - 0.63\alpha^{-1.5} \tag{33}$$

with $Kp_o = 463$ Pa. This tube law corresponds to the highly compliant basic tube law. Figure 6 plots all five of these tube laws to illustrate how they compare and the highlight how they effect the pressure/area curve. It should be noted that the response of human arteries should be between the response of the bovine and the canine arteries.

Definition of the Degree of Nominal and Dynamic Stenoses

The important descriptor of stenotic flow is the degree of area or diameter reduction produced by the stenosis. The degree of stenosis shows the relationship between the normal area and the minimum area of the stenosis. This study uses two definition for the degree of stenosis, nominal and dynamic. The nominal stenosis is defined by the degree of reduction in the nominal uninflated tube area. The value of the area reduction parameter, λ_{A_o}, is equal to the degree of nominal area stenosis,

$$\%\ \text{nominal stenosis (area)} = \lambda_{A_o} \times 100\% \tag{34}$$

The dynamic stenosis refers to the actual degree of stenosis produced in a perfused artery with flow and is defined by

$$\%\ dyn\ stn_{Area} = \left(1 - \frac{A_{\min}}{A_{in}}\right) \cdot 100\%, \tag{35}$$

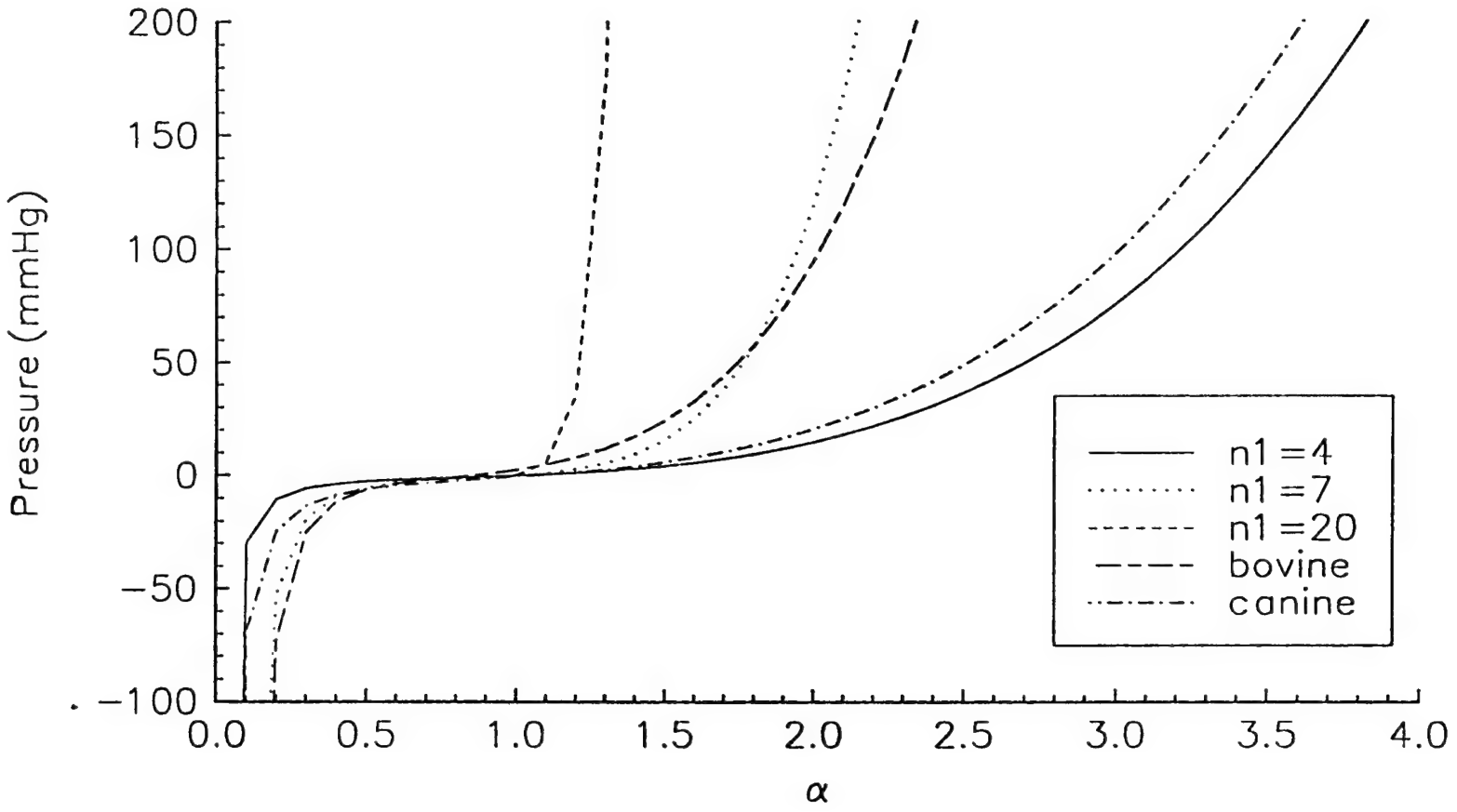

Figure 6 **Tube Laws: Simplified and Arterial**

where A_{min} is the minimum cross-sectional area and A_{in} is the perfused area at the inlet. This definition of dynamic stenosis is also the degree of stenosis determined from clinical measurements. The difference between nominal and dynamic stenoses is highlighted in figure 7.

This definition differs from the ones used by Gould and Kelley (59) who related the minimum pressure to the normal area distal to the stenosis. Also, the use of the term dynamic stenosis in this study differs from how Higgins et al (57) used it to define a class of stenotic arteries.

For the computational results, the nominal stenosis was an input into the solution, and the dynamic stenosis was a variable determined from the solution. Thus, the area reduction parameter was varied until the desired dynamic stenosis was obtained.

Numerical Approach: MacCormack Method

With the system of non-dimensionalized equations, the computational solution approach can now be summarized for the model description given in the above section. The system of equations is hyperbolic so that discontinuous solutions, such as to shock waves in gas dynamics, are admitted. This similarity has led others (37, 38, 66) to use a modified form of the explicit MacCormack predictor/corrector scheme (67). This method is advantageous since it requires only two first order finite difference steps, yet it is accurate to second order in both space and time. This method is simple and straight forward in its application to non-linear hyperbolic equations. Moreover, it does not involve the Jacobian as with the Lax-Wendroff method, and it evaluates the equations only at the grid points without the need of intermediate grid values. MacCormack's method is a robust tool and is well established in the field of CFD for solving hyperbolic problems which contain discontinuities. The MacCormack difference steps for equations in the form of equation 25 are given as

$$\text{Predictor:} \quad \overline{\mathcal{A}_i^{n+1}} = \mathcal{A}_i^n - \frac{\Delta\tau}{\Delta\xi}[\mathcal{B}_i^n - \mathcal{B}_{i-1}^n] + \Delta\tau C_i^n \tag{36a}$$

$$\text{Corrector:} \quad \mathcal{A}_i^{n+1} = \frac{1}{2}\left\{\mathcal{A}_i^n + \overline{\mathcal{A}_i^{n+1}} - \frac{\Delta\tau}{\Delta\xi}\left[\overline{\mathcal{B}_{i+1}^{n+1}} - \overline{\mathcal{B}_i^{n+1}}\right] - \Delta\tau\overline{C_i^{n+1}}\right\}, \tag{36b}$$

where $\overline{n+1}$ indicates the intermediate values after the predictor step.

To apply this algorithm to equation 25, the space domain must be divided into an evenly spaced grid which is fixed along the axial direction of the tube. Once the space step, $\Delta\xi$, is defined, the time step, $\Delta\tau$, is calculated by the following equations as the solution marches forward in time:

$$\Delta\tau = \frac{\eta\Delta\xi}{(u+c)_{max}}, \tag{37}$$

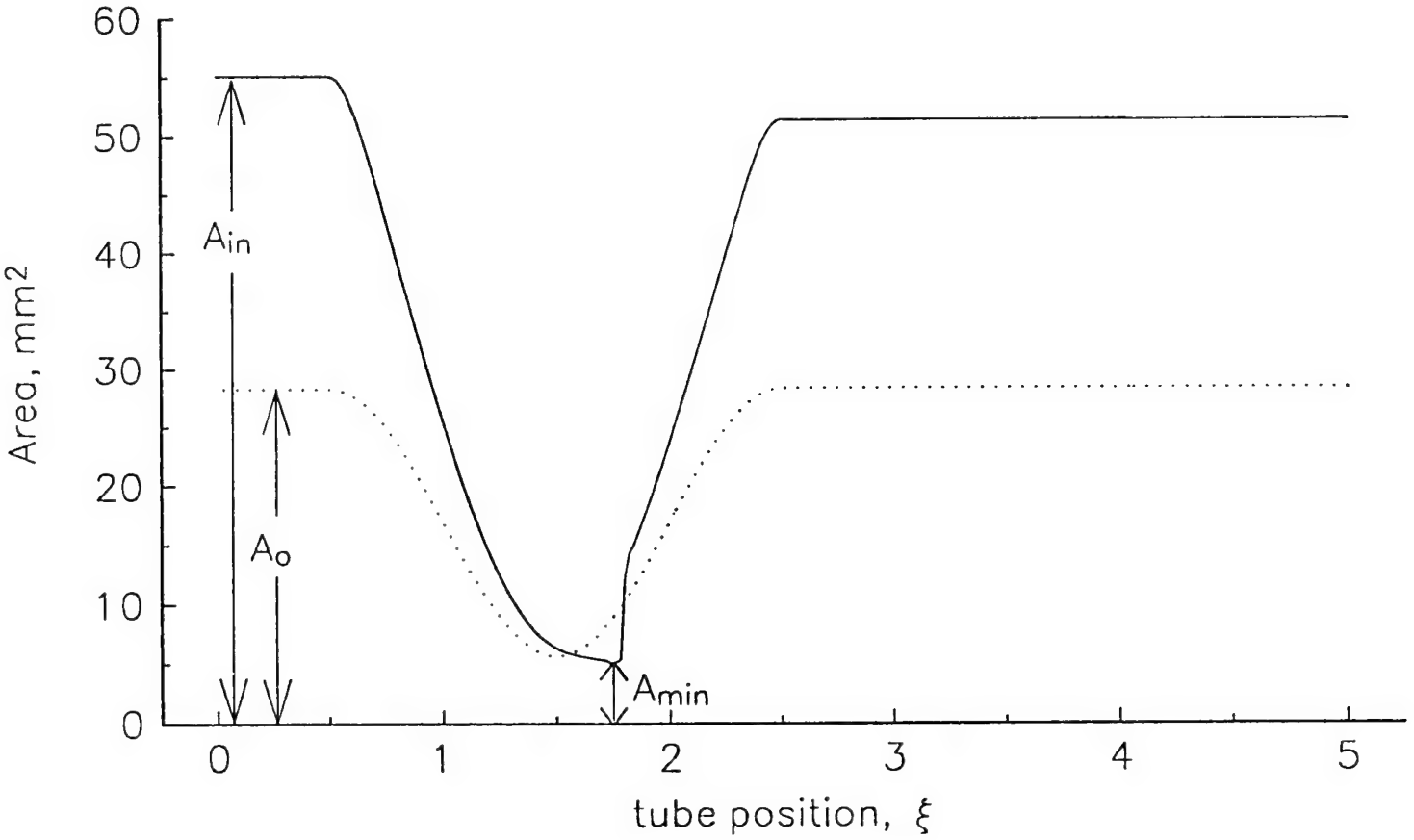

Figure 7 Nominal vs. Dynamic Stenosis

where η is a safety factor and is less than 1.0 (67). Equation 37 has been determined empirically and allows the solution to remain stable. This relationship ensures that the speed of computational information, $\frac{\Delta\xi}{\Delta\tau}$, exceeds the physical speed at which disturbances travel in the system, u+c. Thus, one of the computational stability requirements for this scheme is that $\eta < 1.0$. In this study most of the solutions used $\eta = 0.7$ to 0.9.

Program Outline: Steady

The implementation of MacCormack's method is simple and proceeds in the following manner. First, the initial conditions for α and u are set. These conditions are very basic, such as letting $\alpha = 1$ with a set flow rate throughout the domain to define the initial velocity array, u_i^0. Second, the computation starts by applying the inlet boundary condition followed by the predictor step, which marches forward to the outlet. Next, the outlet boundary condition is applied, and it is followed by the corrector step, which also marches forward. In the third step of the scheme, the dependent variables are checked for convergence and the time step is determined. The convergence check inspects the field variables to see if they are stable and have remained unchanged within a set tolerance from the last time step. Once the dependent variables are stable and steady, the computation is stop and the solution is saved. This check does not occur until a set time has elapsed. The computational flow for a steady state solution is shown in figure 8.

Steady solutions are obtained by maintaining steady boundary conditions and allowing the solution to reach steady state. The computational time required to reach steady state is at least $\tau = 3\frac{L}{Do}$, where L is the tube length. This time period is needed to ensure that transient disturbances have propagated out of the domain and that the boundary characteristics are established throughout the solution.

The two boundary conditions are applied at the inlet and the outlet for either the area or the velocity. When transients are present at the start of the solution, it is necessary to slowly vary the boundary conditions in time. This slow variation is usually small in amplitude and short in duration. This approach allows the transients to propagate out of the solution without piling up at the boundaries. On the boundaries, the other dependent variable must be determined by a compatibility condition. A compatibility condition must not specify the variable, but evaluate it so that it is compatible with the governing equations and its corresponding boundary condition. For this model the modified momentum equation is used to generate the compatability condition for evaluating u on the boundaries. The application of the compatability condition is shown in Appendix B

The actual boundary conditions used for the steady state solutions in this study were applied on α at the inlet and the outlet and corresponded with the prescribed inlet and outlet pressures. α was set at a desired value and the boundary velocities were determined by compatibility conditions which involved the modified momentum equation. This compatibility condition used a second order difference scheme to determine the velocity by using the updated boundary value for α.

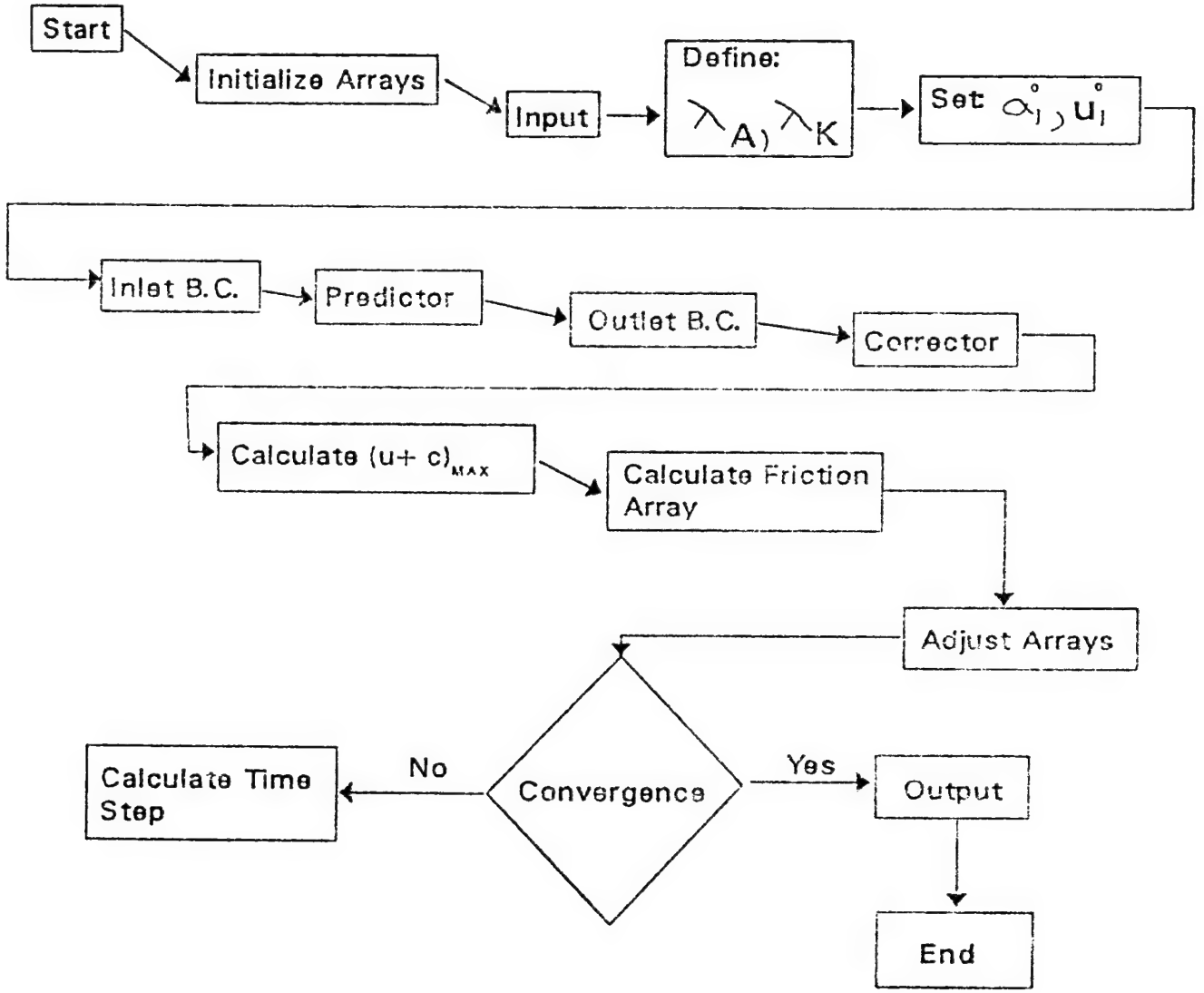

Figure 8 Computation Code Organization

Unsteady Solution Outline

For unsteady solutions, the process is similar except for the application of the unsteady boundary conditions. The unsteady boundary conditions must be applied only after a stable solution has been established with all the numerical transients out of the solution domain. With the application of unsteady boundary conditions, the time evolution of the solution can be observed. For this study, the inlet boundary condition has a prescribed sinusoidal time variation in pressure. The outlet boundary condition imposes a constant downstream resistance. The boundary velocities are determined by the same compatibility condition as in the steady case.

Several unsteady solutions were obtained to illustrate the effects of pulsatile flow condition. These solutions demonstrate conditions which would induce cyclic collapse of the stenosis. For this series of solutions, a deterministic variation was applied to the inlet pressure in the following manner:

$$P_1(t) = 100 + 20\sin(2\pi f t) \tag{38}$$

where f is the frequency of the cycle. This variation mimics an arterial pressure pulse of 120/80 mmHg. A constant distal resistance is used as the downstream boundary condition. Solutions were calculated for f=1, 5, and 10 Hz with low, moderate, and high distal resistance settings. Thus, this series includes pulsatile variations in the perfusion pressure for a range of frequencies and distal resistance settings.

For collapsible tube, unsteady solutions in the form of oscillations may also occur with steady boundary conditions. Modelling of this type of unstable solution does not relate to the physical situation of flow through a compliant stenotic artery, and, thus, it is not within the scope of this study.

Artificial Viscosity

In the region of the elastic jump, there is a discontinuity in the dependent variables. In this region, the space grid does not have the proper length scale to model the actual physics of the jump. Thus, numerical oscillations will appear in this region due to the inaccurate grid spacing. These oscillations are similar to Gibb's phenomenon and can make the solution unstable. Therefore, it is necessary to smooth out these oscillations to maintain a stable solution. This smoothing process is referred to as artificial viscosity in computational fluid dynamics since it involves adding additional dissipation to the solution in this region.

The approach used in this study is normal stress dampening (67). This approach uses the normal stress term to dampen out the oscillations in the region of the elastic jump. This term comes from the following definition of normal stress:

$$\sigma_{11} = -P + 3\lambda\frac{\partial u_1}{\partial x_1} + 2\mu\frac{\partial u_1}{\partial x_1}, \tag{39}$$

where λ is usually taken to equal $-\frac{2}{3}\mu$. The second term in equation 39 becomes important only in the region of the discontinuity. Since the physics is not properly modelled in this region, λ can be modified to add dissipation to the system without affecting the solution elsewhere in the domain. First, the sign of λ is changed such that $\lambda = +\frac{2}{3}\mu$. Second, an additional coefficient is added to increase λ

$$\lambda = +\beta\frac{2}{3}\mu, \tag{40}$$

where β can range from 1 to 1000. The actual effect of this term is to smooth the solution only in the region of the discontinuity. The term artificial viscosity can be misleading since it connotes the application of a physically artificial term to the physical solution. The real function of this term is to modify the second coefficient of viscosity in the discontinuous region where the computational grid does not properly model the physics. Thus, artificial viscosity modifies the solution only in the region where the solution is improperly modelled. Therefore, artificial viscosity only affects the solution in a region where the solution is known to be invalid. Figure 9 shows the effect β has on the solution of α in the region of a elastic jump. This figure demonstrates that increasing β smooths out the oscillations without affecting the solution outside of the jump region. It should also be noted that no stable solution was obtained with $\beta = 0$. While this smoothing technique stabilizes the solution about the elastic jump, it does not completely smooth the field variables in the jump region for all of the solutions. Thus, some values of the solution, such as the minimum pressure and area, are estimated when numerical oscillations are present in the solution. The oscillations resulted in an error in the degree of dynamic stenosis of $\pm 0.3\%$.

Other smoothing approaches tried with this model during this study include simple dissipation term, flux correction, upwind differencing, and higher order differencing. However, these techniques were not as successful in dampening the numerical oscillations.

Computer Implementation

The computer model is written in FORTRAN and compiled on a 33MHz 486 based personal computer. The program code is contained in Appendix C along with a detailed flow chart of the program. The code is fairly small because of the efficiency of the MacCormack method, yet the run time required to obtain a solution varies from 10 minutes to two hours. The solution time depends mostly on the domain size of the tube length and the grid spacing. The code was compiled with the Lahey FORTRAN Compiler version 5.0, which takes advantage of the 486 based personal computer and the Weitek coprocessor. The code was also compiled on a MircoVax 3300 computer, which had run times that were three to five times longer.

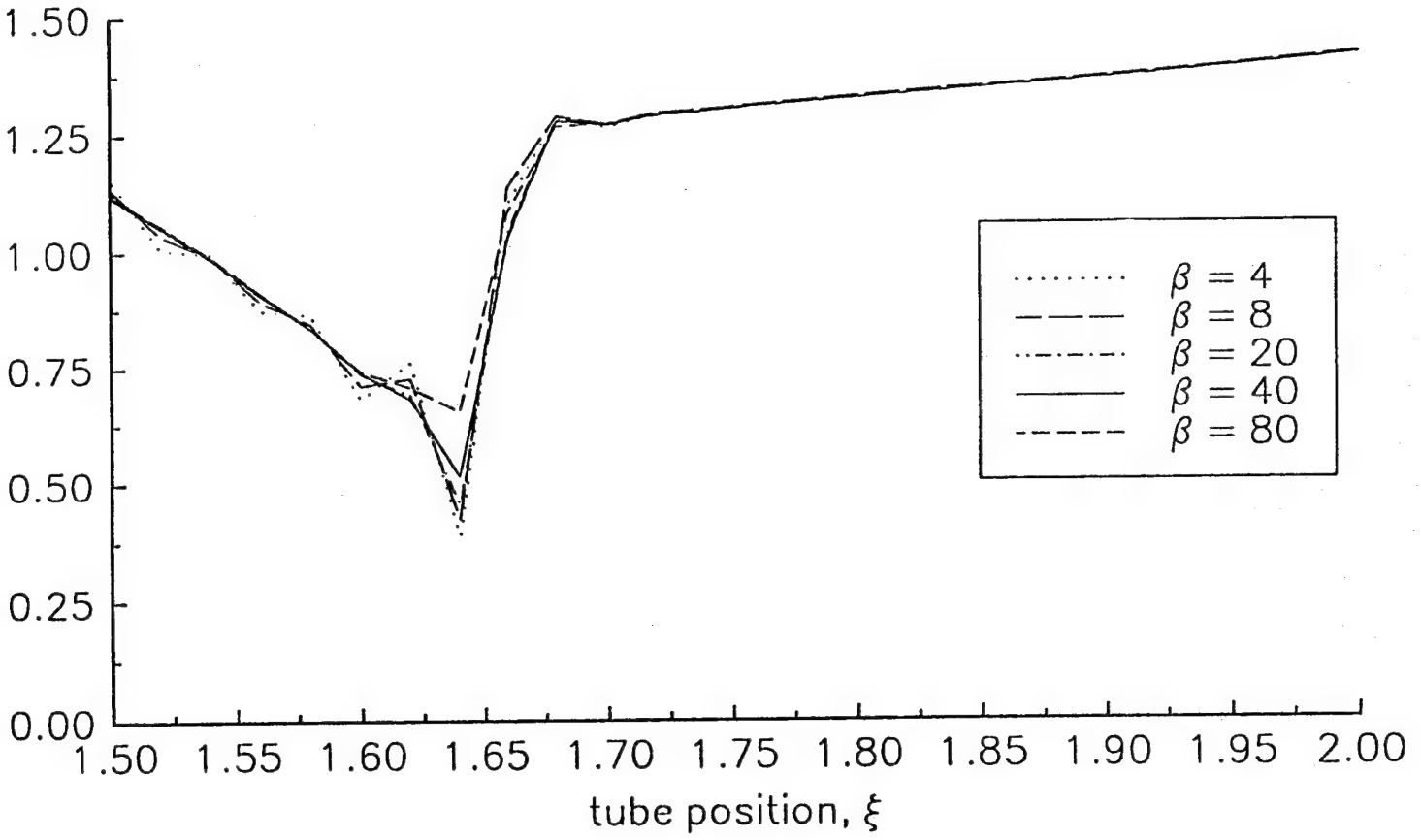

Figure 9 Effect of Normal Stress Dampening Coefficient,β

Expectations

This computer model is developed to predict the flow through a compliant stenotic artery. The model estimates the flow rates and the pressure conditions required to obtain critical flows through a stenotic artery. These estimates are used to relate the critical flow rates with the degree of dynamic stenosis for various parametric conditions. The minimum pressures are also obtained to estimate the hemodynamically induced stresses on the plaque caused by stenotic blood flow.

The physical parameters are varied to investigate their influence on the flow. These parameters include the tube compliancy, frictional losses, mean pressure, stiffness variations, changes in nominal stiffness, and unsteadiness. These parametric effects are further examined to clarify when critical flow rates overlap with physiological conditions. Such an overlap suggests that vessel collapse may occur in a stenotic artery. Moreover, the collapse of the artery at the site of a plaque may be the mechanism which generates sufficient stresses to cause plaque disruption.

The model is first compared to the experimental results of Powell (22) to demonstrate that the model provides good estimates of observed data. Second, steady state solutions are obtained for wide variations of the parameters to highlight their individual affect on the flow, the minimum pressure, and other flow characteristics. Finally, unsteady solutions are obtained to demonstrate that cyclic collapse may indeed be produced under physiological conditions.

RESULTS

First, baseline solutions are furnished to describe some of important characteristics of collapsible tube flow. Second, an evaluation of the computational results is provided. This evaluation includes variations in the nominal dimensions of the tube, comparison with the experimental results of Powell (22), and determination of the effect between the utilization of physiological and basic tube laws. Third, results highlighting the effects of individual parametric variations are provided. These variations involve changes in the tube compliance, frictional losses, and mean pressure. Finally, the effect of unsteady deterministic boundary conditions is presented in a series of computational solutions. This full range of results provides the background for discussing collapsible flow through a compliant stenotic artery. These results demonstrate where the phenomena of collapsible tube flow can occur under physiological conditions and how variations in the physical system influence physiologic collapse.

Baseline Observations

Variation in Degree of Stenosis

A baseline series of solutions were grouped so that the only variable to change was the degree of dynamic stenosis. In this solution series the following parameters were held constant:

Tube Law: $n1$=7, $n2$=2.5
P_1= 100 mmHg
P_2= 60 mmHg
Kp_o=125 Pa
$\lambda_{K_o} = 10$
D_o = 6.0 mm
Length = $5D_o$
f_L = 5
K_{Sep} = 0 (no additional separation).

These conditions are referred to as the baseline parameter settings, and they were used throughout these results except where noted. The critical flow rates decreased as the degree of dynamic stenosis increased, as shown in figure 10a which plots critical flow rate, Q_c, versus the degree of dynamic stenosis. This figure displays the inverse relationship between Q_c and the degree of stenosis. This relationship arose from the increased fluid acceleration that resulted from an increase in the stenosis. Thus, as the degree of stenosis increased, less flow was needed to reach the critical point, which is the choked flow condition when S=1 within the stenosis. For this series Q_c was reduced by 90% when the dynamic stenosis was increased from 70 to 90% by diameter.

Also, the degree of stenosis affected P_{min} and S_{max}. These effects are provided in figure 10b and c, respectively. P_{min} remained fairly constant until the stenosis reached 89% where P_{min} increased dramatically with further increases in the stenosis. Likewise, S_{max} remained constant up to the 89% stenosis point where it started to decrease. At a 95% stenosis, S_{max} was decreased to subcritical levels, and P_{min} was increased to positive, uncollapsed values. This increase in P_{min} and decrease in S_{max} resulted from

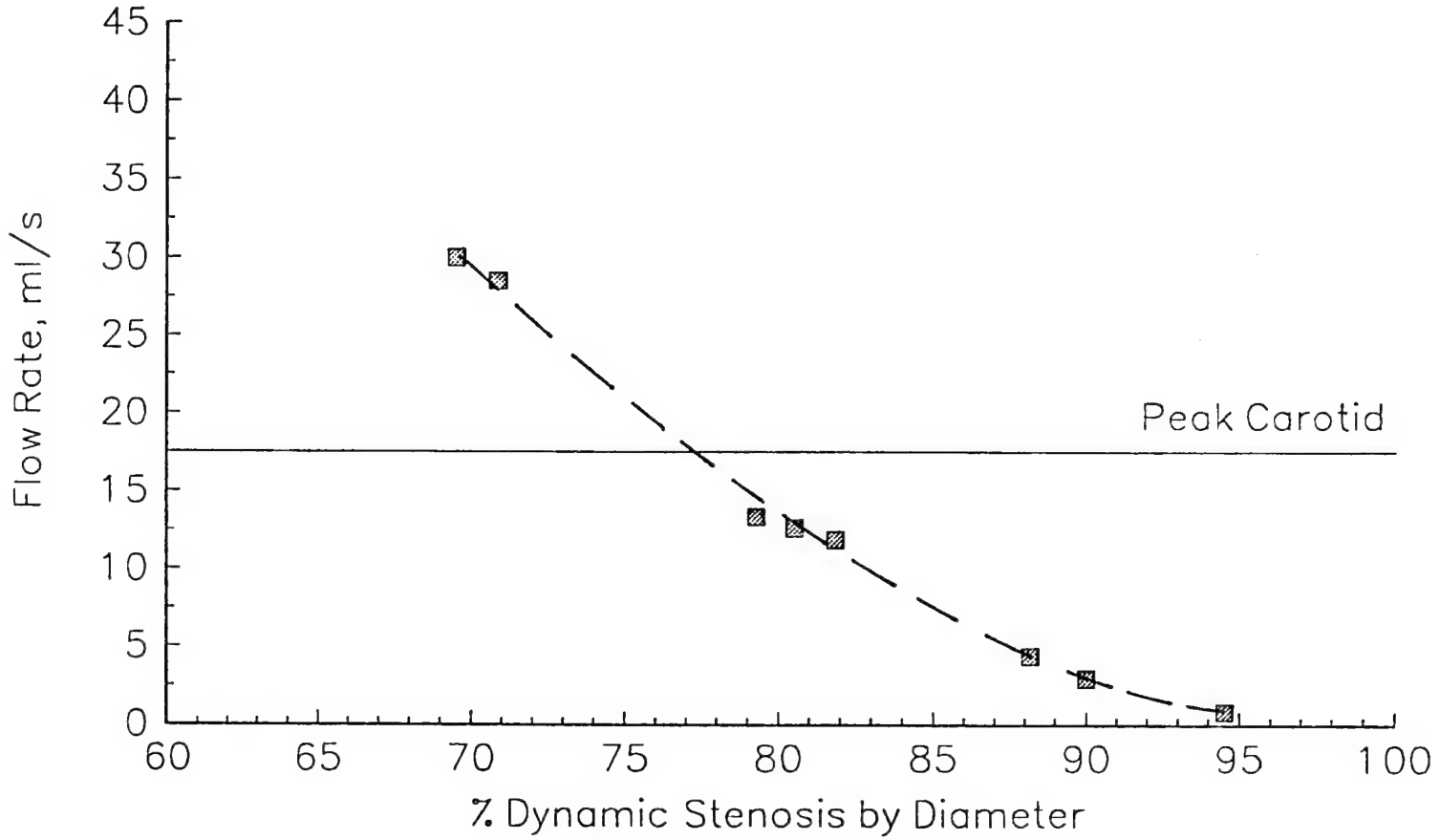

Figure 10a Critical Flow Rate vs Dynamic Stenosis. Solutions calculated with the following constant values: Tube Law $n1$=7, $n2$=2.5; Kp_o=125 , λ_{K_o}=10, D_o=6.0mm, f_L=5 and K_{Sep}=0.0

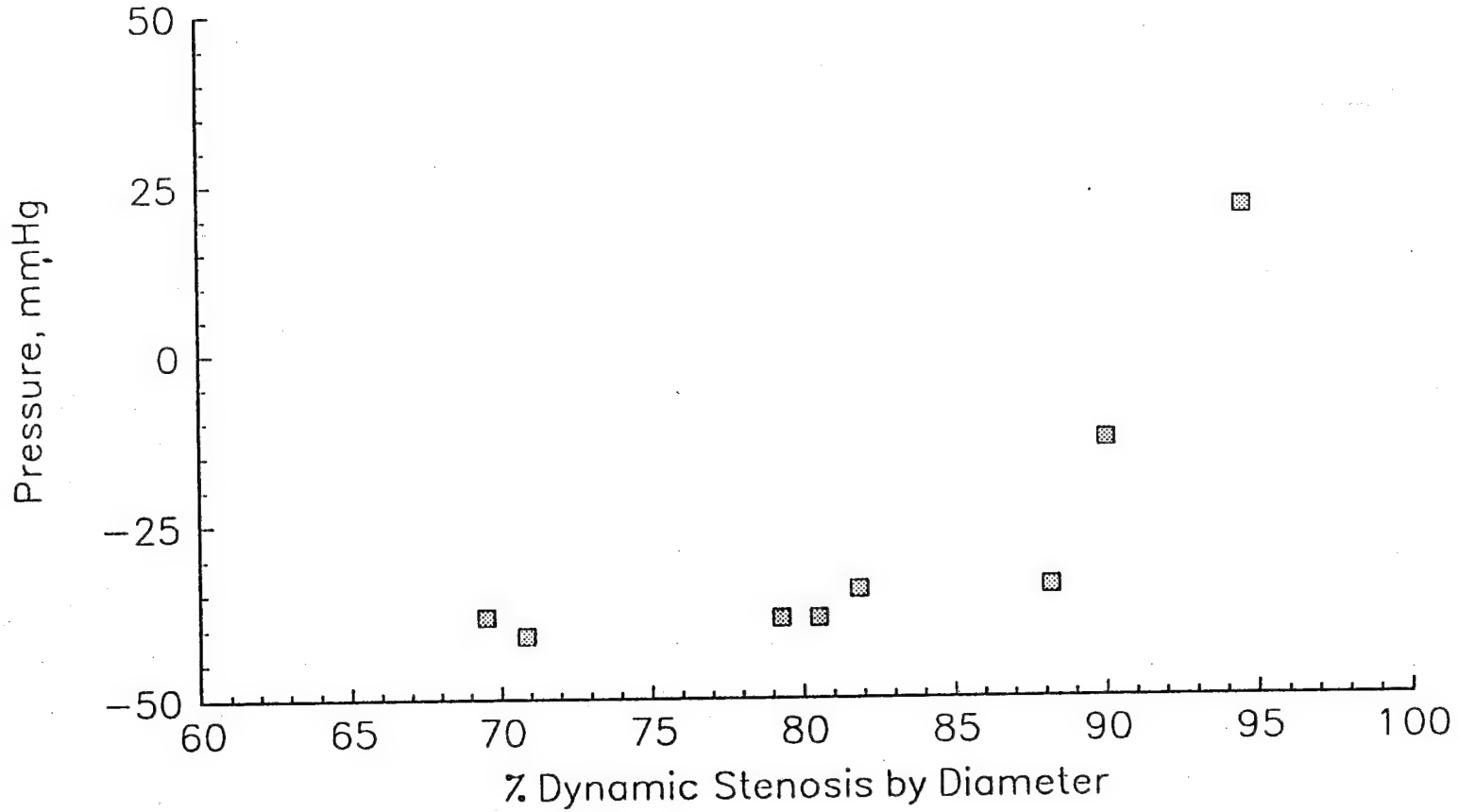

Figure 10 b Minimum Pressure vs Dynamic Stenosis. Solutions calculated with the following constant values: Tube Law *n1*=7, *n2*=2.5; Kp_o=125 , λ_{K_o}=10, D_o=6.0mm, f_L=5 and K_{Sep}=0.0

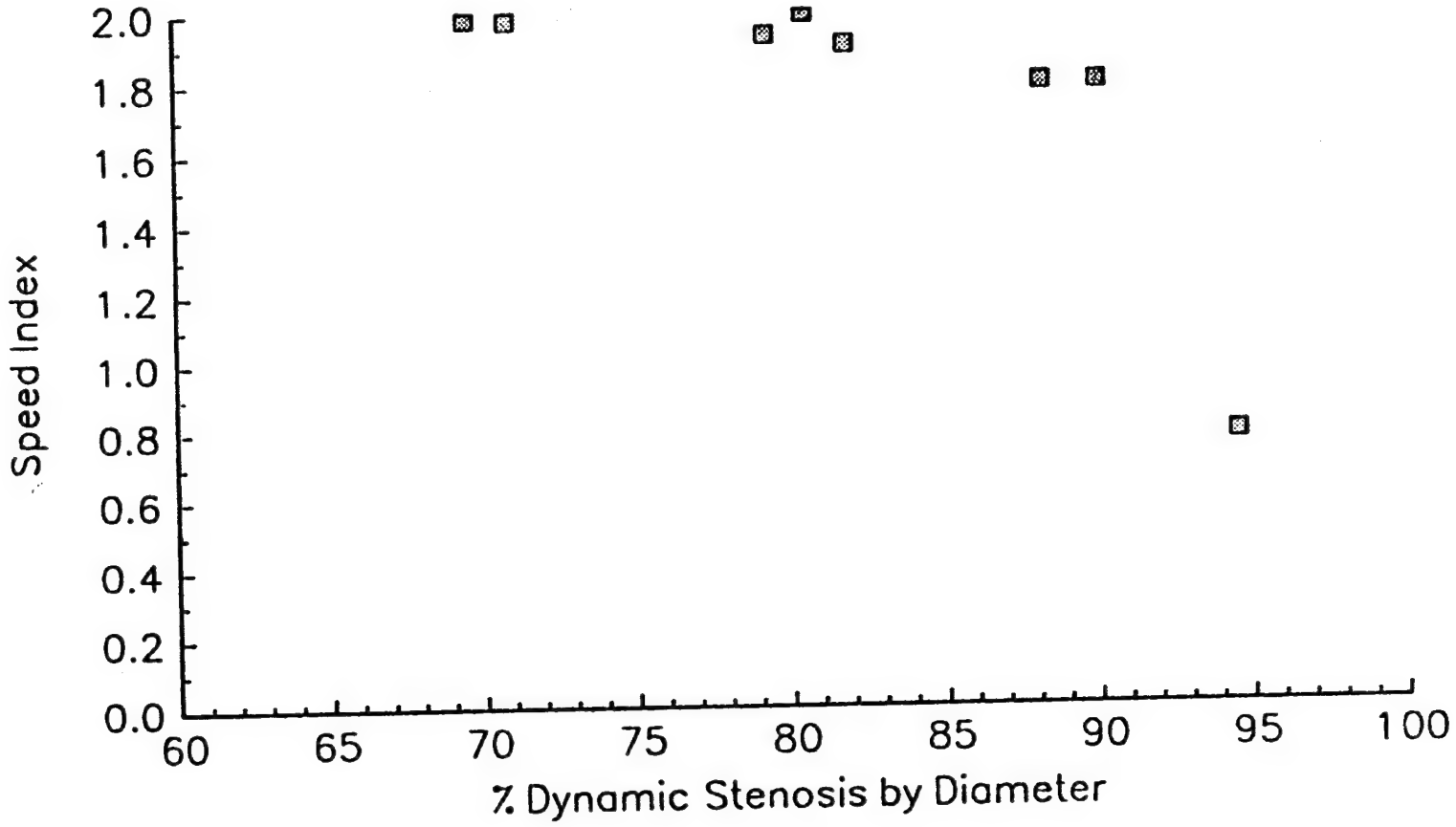

Figure 10 c Maximum Speed Index vs Dynamic Stenosis. Solutions calculated with the following constant values: Tube Law $n1$=7, $n2$=2.5; Kp_o=125 , λ_{x_o}=10, D_o=6.0mm, f_L=5 and K_{Sep}=0.0

increasing frictional losses which impeded the flow as the restricted luminal area became smaller. Since these losses are inversely proportional to the luminal area, the 95% (dia) dynamic stenosis produced sufficient losses so that the 40 mmHg pressure drop was not able to establish critical flow through the stenosis. Thus, as the stenosis increases, frictional losses grow in magnitude and can impede the flow from becoming critical. These observations agree with the analogy to compressible flow.

This series of solutions can also be used to demonstrate the variations in DS, (dynamic stiffness number). The DS curves for dynamic stenoses of 70 and 80% (dia) are provided in figure 10d. These plots show that the minimums in DS coincided with collapse of the stenotic segments. These curves illustrate that at first DS increased as the stenosis stiffens, but it decreased below its nominal values in the region of the throat. Thus, in the throat region, the velocity was sufficiently accelerated to overcome the tube stiffness and to generate collapse. Although DS clearly represents the relation of the tube stiffness versus the dynamic pressure, it does not appear to have any straight forward clinical value since arterial stiffness measurements could not be realistically obtained.

This series demonstrates that the critical flow rate is highly dependent on the degree of dynamic stenosis and greatly influences the possibility of collapsed flow with physiological conditions. A possible peak carotid artery flow is 17.5 ml/s, as noted in figure 10a. For this case, physiologic collapse occurs at a dynamic stenosis of 83% (dia). If the flow rates are scaled for high demand coronary flow of 5 ml/s, which corresponds to a plotted flow rate of 20 ml/s in figure 10a, collapse starts at a dynamic stenosis of 76% (dia). These points agree very well with clinical findings which observed symptomatic plaques ranging from 75% to 90% of the lumen diameter (3). Also, in this collapsed region, the artery was compressed by a negative transmural pressure down to -40 mmHg as shown in figure 10b. Thus, the baseline computational results demonstrate that the overlap of the collapse regime with physiological flows starts in arteries which have dynamic stenoses greater than 75% (dia), and the collapse induces bending and compressive stresses on the plaque.

The baseline solutions for the critical flow rate versus the degree of stenosis can be compared to estimated flow rates through a rigid tube. For this comparison the rigid tube area variation was the same as the dynamic area variation of the compliant tube. The estimated flow rates for the rigid tube include viscous and separation losses were estimated by

$$\Delta P = \frac{128\mu}{\pi D^4} Q \Delta x + \frac{k\rho}{2}\left\{\frac{1}{A_{th}} - \frac{1}{A_{out}}\right\}^2 Q^2 \frac{\Delta x}{2D_o} \qquad (41)$$

where k is the separation coefficient and A_{th} and A_{out} are the throat and outlet area, respectively. The flow rates for the compliant tube were evaluated at the baseline conditions, and the flow rates for the rigid tube were estimated with P1 = 100 mmHg, P2 = 20 mmHg, and k=0.5. A compliant tube produces lower flow rates than flows through a rigid tube as shown in figure 10e. This reduction in the flow occurs because a compliant stenosis can produce choking conditions. The choking reduces the flow rate by approximately 45% compared to flow for an 80% stenosis. Flows through the rigid and compliant stenosis are highly dependent on the degree of constriction, and the actual difference in the flow rates diminishes with increasing degree of stenosis.

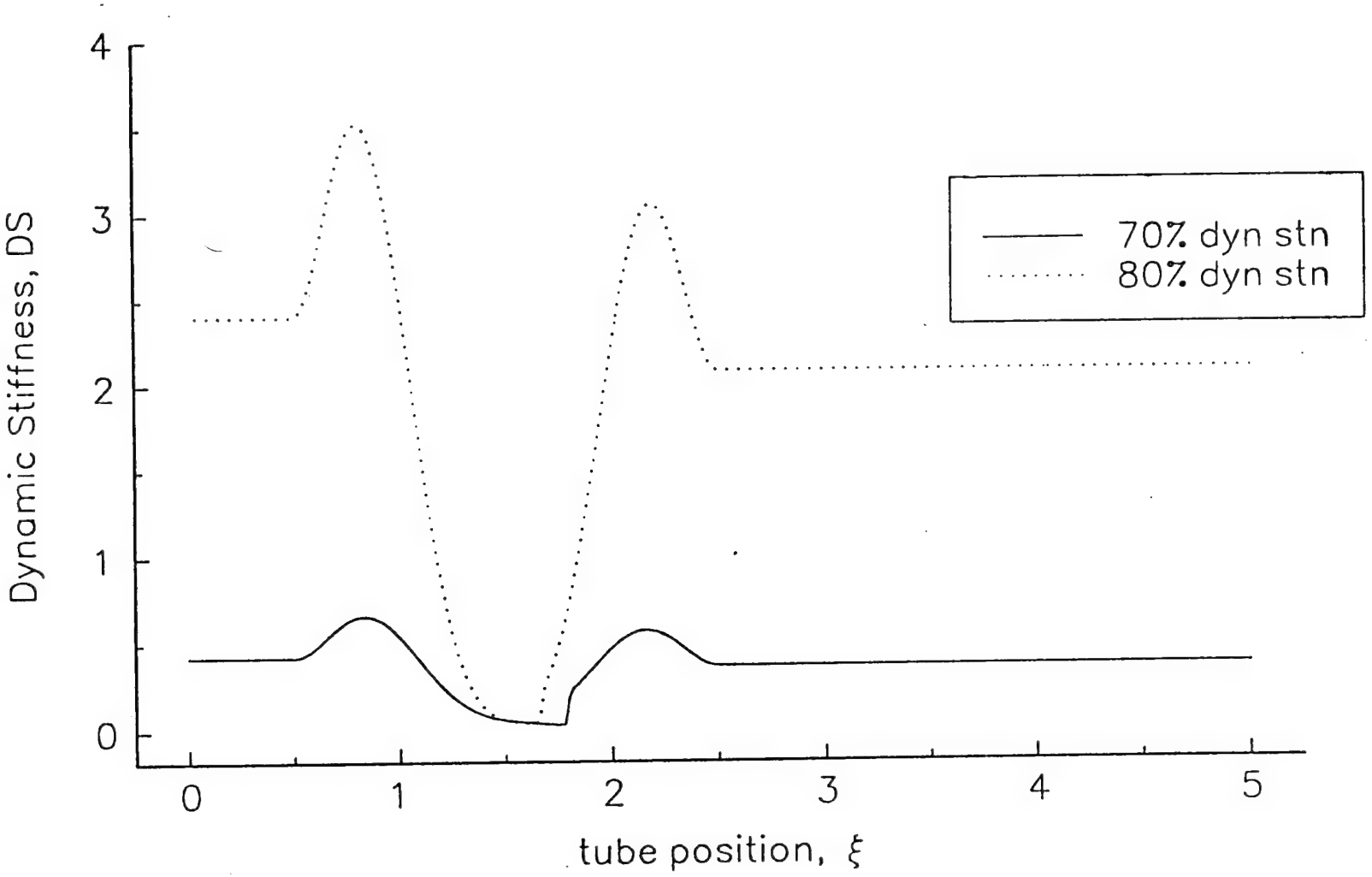

Figure 10d Dynamic Stiffness for 70% and 80% (dia) Dynamic Stenoses for the Baseline Conditions

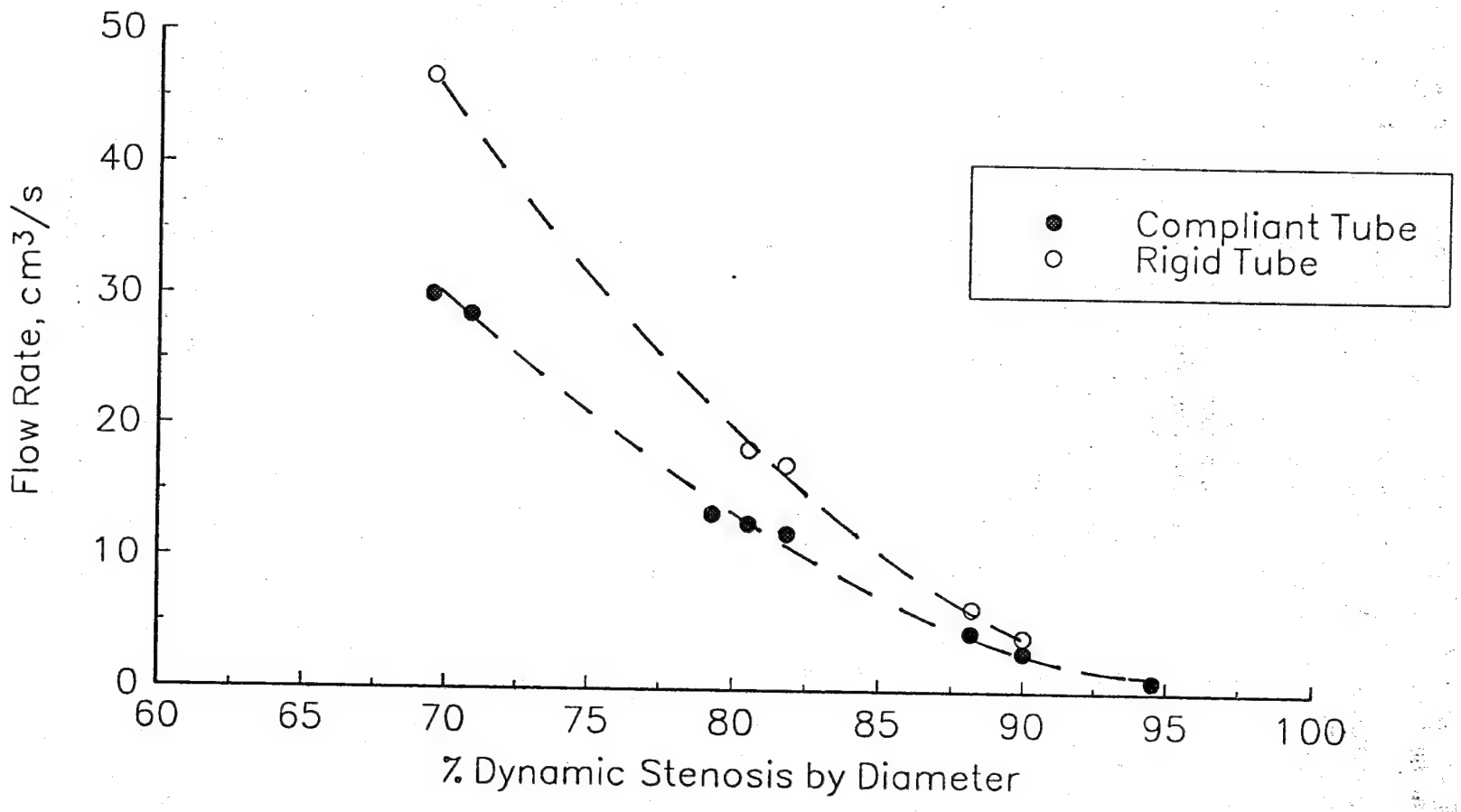

Figure 10 e Comparison of Flow Rates between Rigid and Compliant Tubes with a Stenosis

Variations in Distal Pressure, P_2

The next series of baseline solutions are provided to demonstrate the effect of variations in the distal pressure. Also, in this series, the basic characteristics of collapsible tube flow through a stenotic artery is highlighted (figures 11a-e). For this series, the distal pressure, P_2, was varied from 100 mmHg to 20 mmHg in 20 mmHg steps, and the nominal area reduction was set at 91.5%. The solution with $P_2 = 100$ mmHg resulted in a static no flow condition since no driving pressure was applied across the stenosis. For all of the dynamic solutions, the flow was critical, (choked), with a value of 12.6 ml/s and a nominal Re_D of 725. For the decrease in P_2 from 80 to 20 mmHg, the dynamic stenosis was increased from 95.9% to 96.8% by area or 79.8% to 82.1% by diameter. The increase in the dynamic stenosis resulted from a reduction in the minimum area of 0.5 mm^2 (from 2.24 mm^2 to 1.76 mm^2) or the minimum diameter of 0.2 mm (from 1.69 mm to 1.50 mm). The minimum pressure just downstream of the throat, P_{min}, varied from -25.0 mmHg to -120.5 mmHg, and the maximum speed index, S_{max}, was constant at 1.92. Critical flow is demonstrated by the fact that all of the curves for each of the variables are equal upstream of the throat and are not affected by changes in the distal boundary condition (figures 11a-e). Changes in P_2 did affect the location of the elastic jump. As P_2 decreased, the elastic jump moved downstream which is directly analogous to the shock wave in a supersonic diverging nozzle.

The area variation as a function of tube position, (figure 11a), includes four dynamic solutions along with two static curves for P=100 and 0 mmHg. The P=0 mmHg curve corresponds to the nominal area curve. The dynamic area curves did not deviate from the 100 mmHg static curve until a tube position of about 1.3. The deviation corresponded directly with the start of the sharp decrease in the pressure, which is given in figure 11b. This point also corresponded to the decrease in the wave speed, c, and the increase in the speed index, S, (figures 11 c & d), respectively. In both of these plots, the critical point, U=c or S=1, was shifted just distal to the throat (less than 0.12 mm) because of the presence of viscous losses. If viscosity was not included, the critical point would have to coincide exactly with the throat since the local maximum in the stiffness and the local minimum of the nominal area coincide at the throat. At this point the stenosis had greatly accelerated the fluid velocity by reducing the cross-sectional area of the artery. The acceleration, in turn, reduced the pressure, which decreased the area. This cycle continued until the elastic jump was encountered. In this supercritical region where $U > c$, the pressure became negative, and compressive and bending stresses were applied to the artery. The induced negative pressure reduced the luminal area to values less than the nominal static area corresponding to P=0 mmHg. Hence, the artery is said to be collapsed. The collapsed state for this solution started at a tube position of 1.54 and extended up to the elastic jump. For the variations in P_2 shown, the range of collapse varied from 0.5 to 1.2 mm in length.

Downstream of the elastic jump, the pressure recovered to positive values, and the tube area was expanded above its nominal value. The elastic jump decelerated the fluid velocity, and the flow returned to subcritical values, $U < c$. Just distal to the elastic jump, the pressure had a small recovery as the velocity was further decelerated by the diverging section of the stenosis. Pressure, area, and velocity varied only marginally as they propagated further downstream of the stenosis.

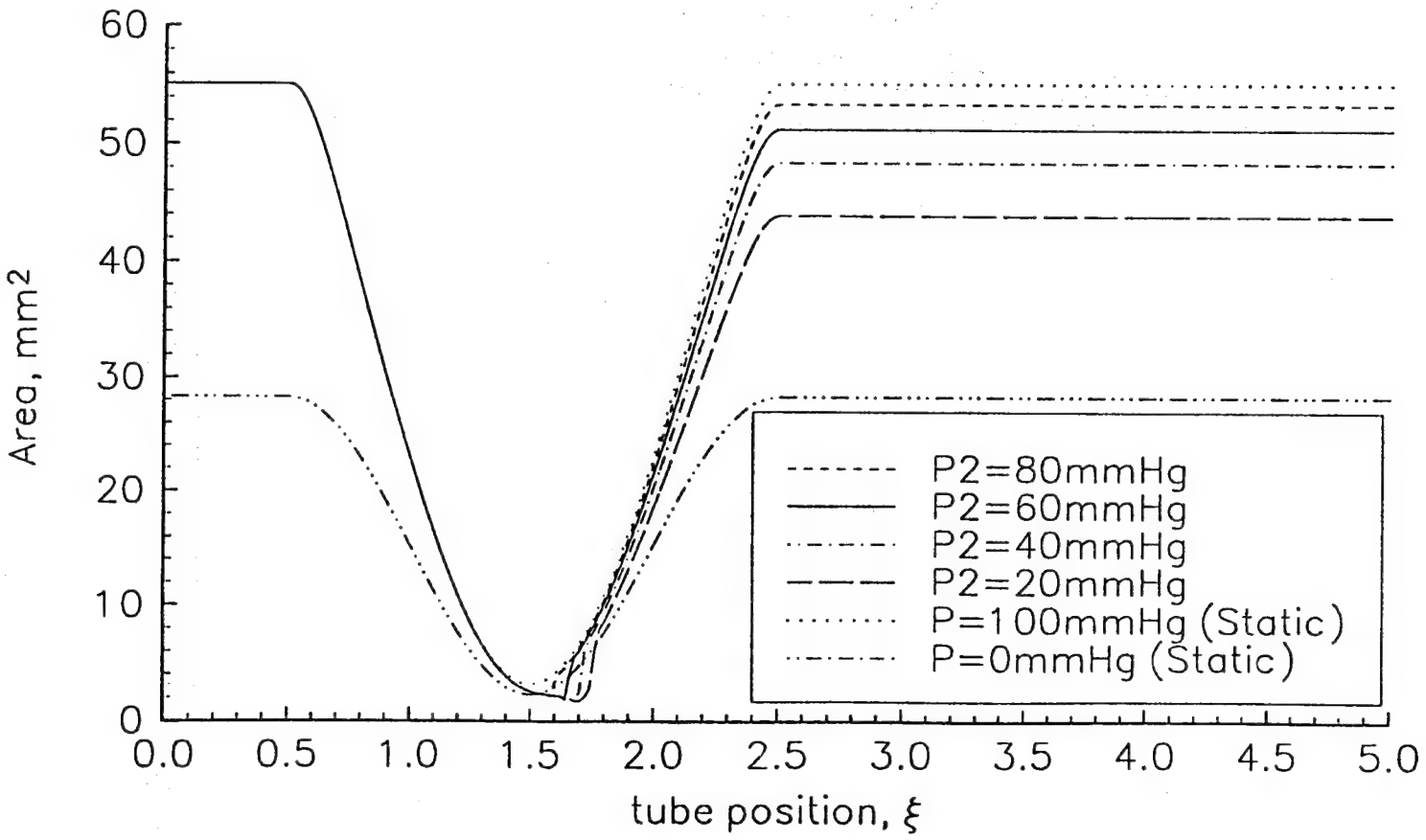

Figure 11 a Area Curves from a Representative Solution of Collapsible Tube Flow Through a Stenotic Artery with the following parameters: Tube Law: $n1$=7, $n2$=2.5; Kp_o=125 , λ_{k_o}=10, λ_{A_o}=0.915, D_o=6.0mm, f_L=5, and K_{Sep}=0.0

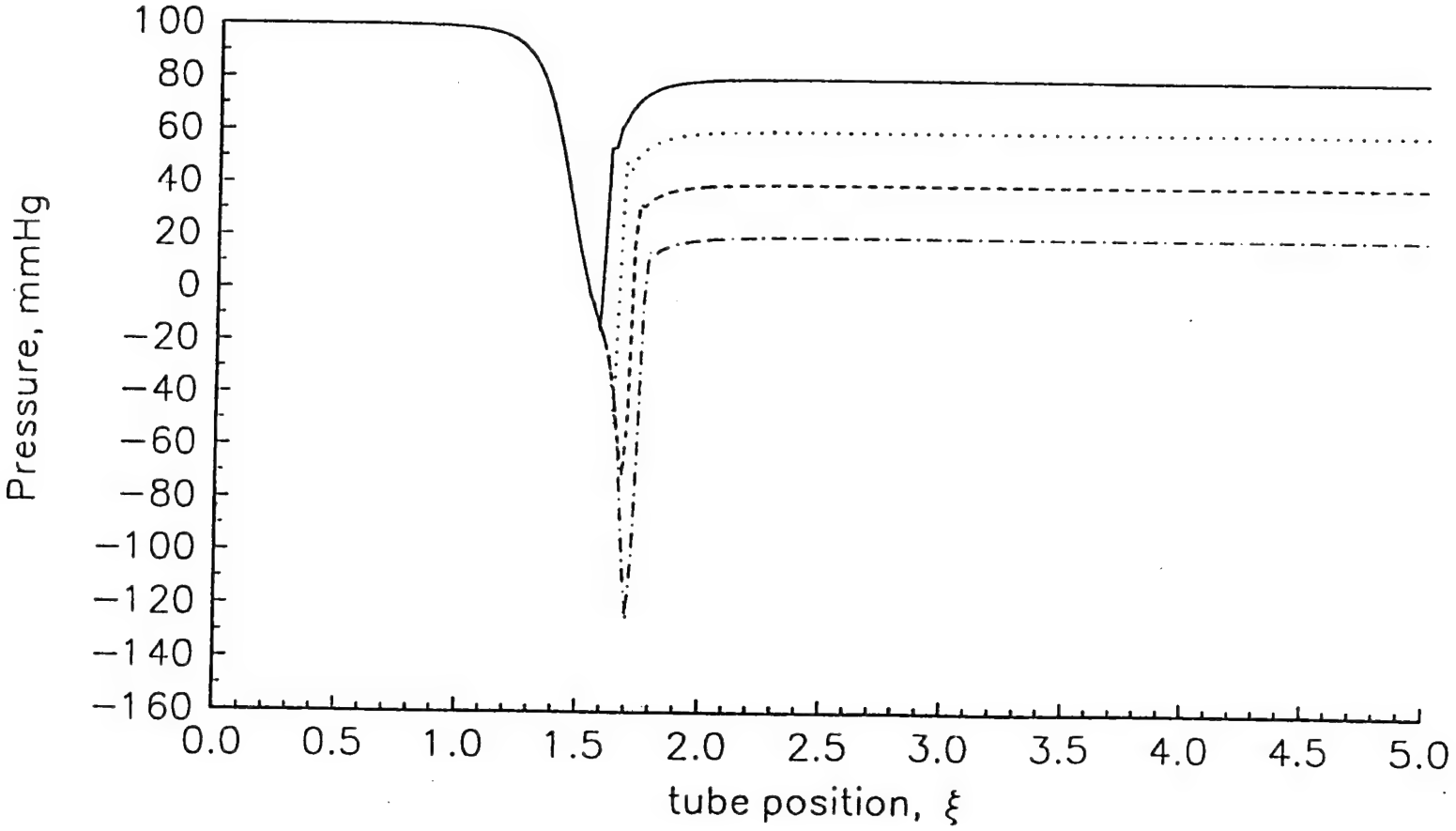

Figure 11b Pressure Curves from a Representative Solution of Collapsible Tube Flow Through a Stenotic Artery with the following parameters: Tube Law: $n1$=7, $n2$=2.5; Kp_o=125 , λ_{k_e}=10, λ_{λ_e}=0.915, D_o=6.0mm, f_L=5, and K_{Sep}=0.0

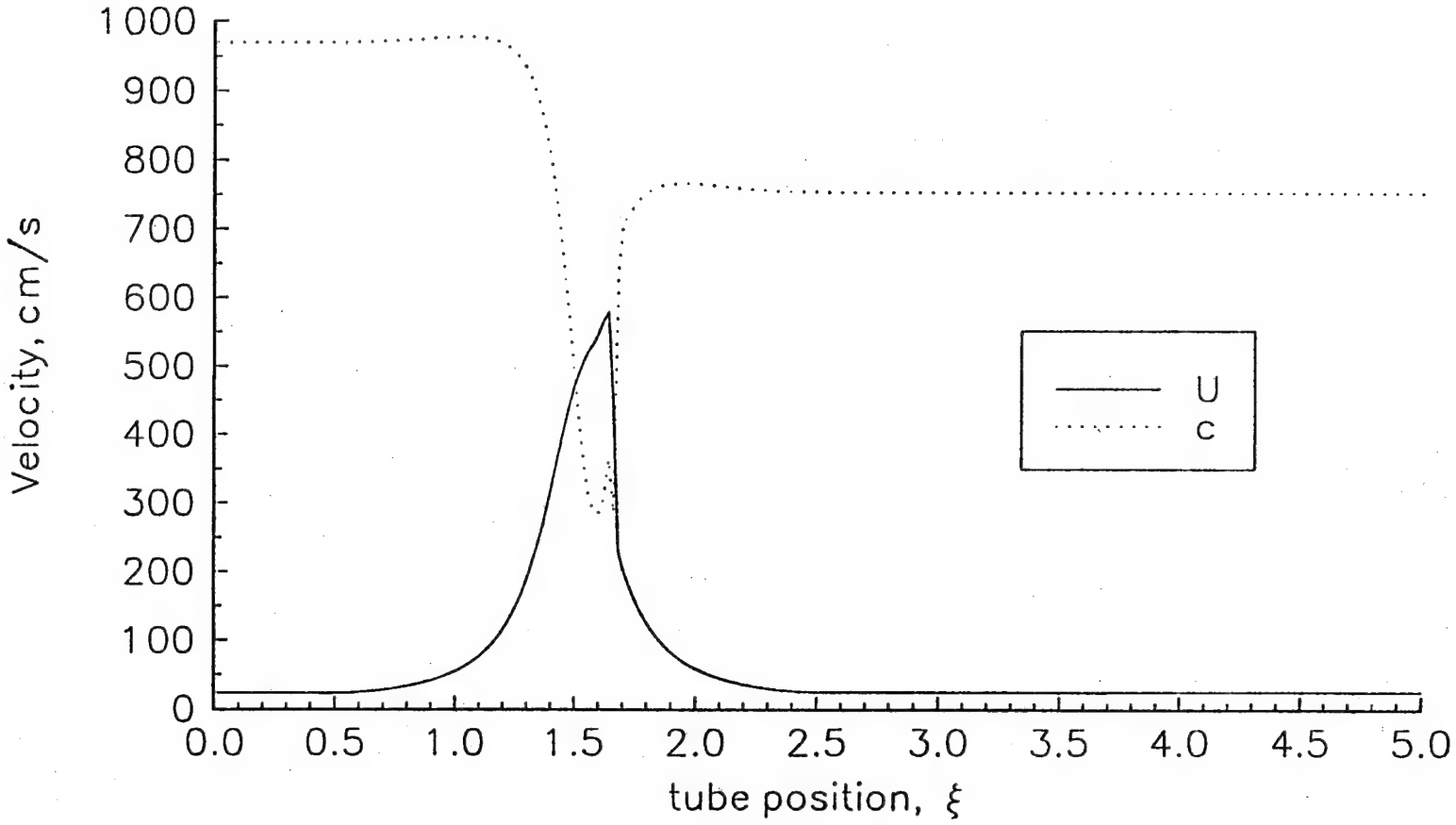

Figure 11c Velocity Curves from a Representative Solution of Collapsible Tube Flow Through a Stenotic Artery with the following parameters: Tube Law: $n1$=7, $n2$=2.5; Kp_o=125 , λ_{k_o}=10, λ_{A_o}=0.915, D_o=6.0mm, f_L=5, and K_{Sep}=0.0

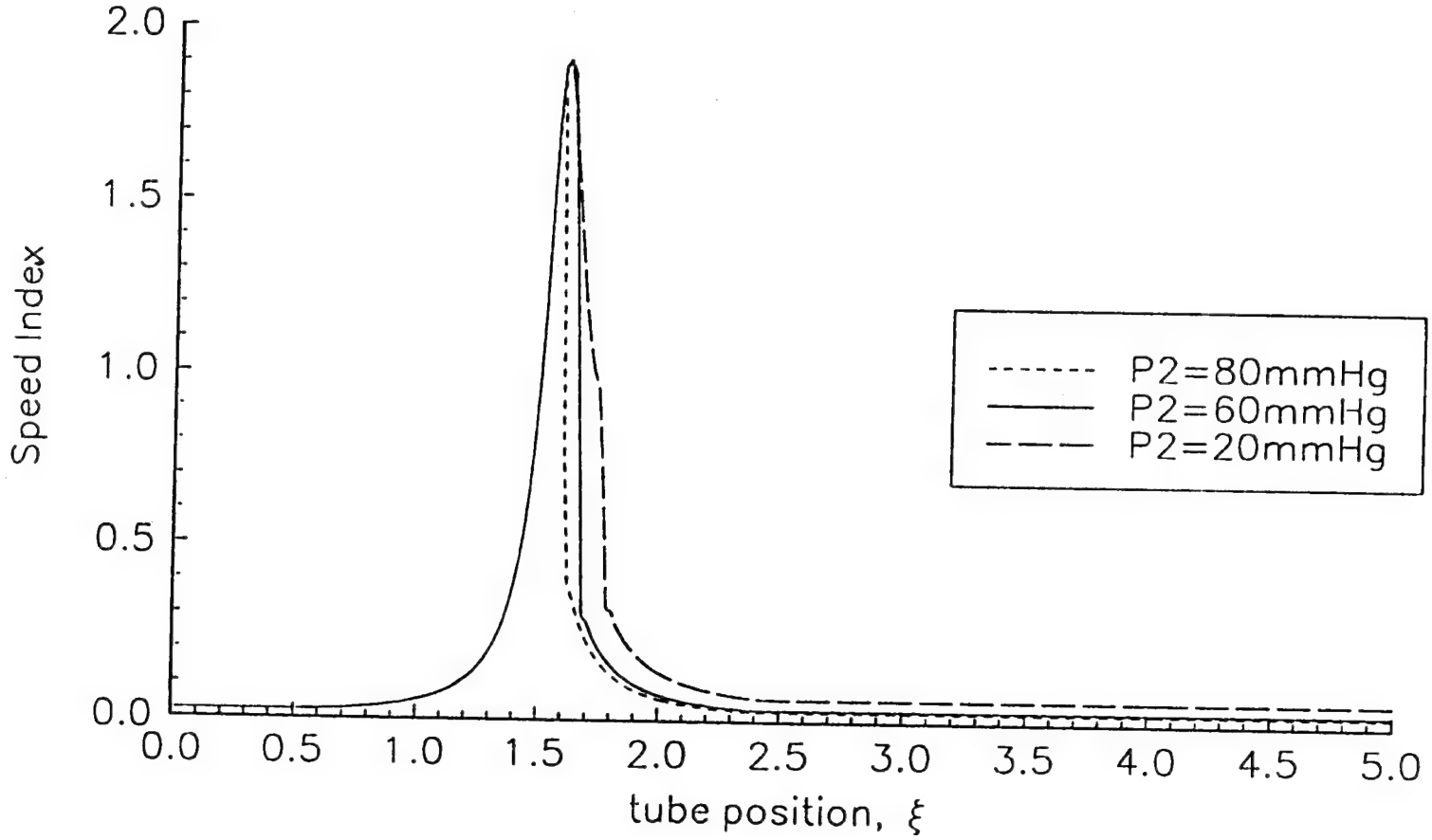

Figure 11d Speed Index Curves from a Representative Solution of Collapsible Tube Flow Through a Stenotic Artery with the following parameters: Tube Law: $n1$=7, $n2$=2.5; Kp_o=125, λ_{k_o}=10, λ_{A_o}=0.915, D_o=6.0mm, f_L=5, and K_{Sep}=0.0

A stiffness variation was also included in this solution. This variation is illustrated in the α curves, (figure 11e). For the no flow case with P=100 mmHg, α varied from 1.95 to a minimum of 1.40. This variation was caused by a increase in the stiffness about the throat. As the tube became more stiff, the amount of expansion of the tube area under a constant pressure was reduced. Sharp bends in the curves for α, figure 11e, are noted at the start and end points of the stenosis and within the stenotic region. These bends resulted from the two forcing terms which exist in the alternate momentum equation, as expressed in equation 24. These terms involve the effects of the prescribed variations in the tube area and stiffness. Outside of the stenosis both terms were 0 and have no effect on the flow, as shown in figure 11f. However, at the ends of the stenosis both terms had large gradients. As seen in figure 11f, the stiffness variation term dominated the area variation term. In the subcritical sections, the two terms opposed each other, but in the supercritical region, they were both negative.

In summing, the distal pressure was shown to be the next important parameter in influencing physiologic collapse. The baseline steady solutions which were provided in figure 11a-e demonstrated the influence of the distal pressure. These solutions showed that lowering the distal pressure or resistance would enhance the likelihood that collapsed flow could become established. Once collapsed flow was presence, further decreases in the distal pressure would increase the collapsed pressure and extent by allowing supercritical flow further downstream of the stenotic throat. Also, since the flow is limited by collapse, further decreases in the distal pressure would increase the stenotic resistance. Clinically, if collateral flow was present, it would impede collapse since a reduced flow would be going through the stenosis with a smaller pressure gradient.

Quasisteady Approximation

To assess the validity of applying steady flow solutions to model physiological flows through a high grade stenosis, a simple order of magnitude analysis was calculated from this solution to evaluate the relative magnitude of the unsteady term compared with the other terms in the linear momentum equation. First, the following values were needed to perform this calculation:

$A_{in} = 55.1 \text{ mm}^2 = 55.1 \text{ X } 10^{-6} \text{ m}^2$
$A_{th} = 2.53 \text{ mm}^2 = 2.53 \text{ X } 10^{-6} \text{ m}^2$

$P_{in} = 100. \text{ mmHg} = 13300.0 \text{ Pa}$
$P_{th} = 14.9 \text{ mmHg} = 1990 \text{ Pa}$

$U_{in} = 0.215 \text{ m/s}$
$U_{th} = 4.68 \text{ m/s}$

$De_{,in} = 8.38 \text{ mm} = 8.38 \text{ X } 10^{-3} \text{ m}$
$De_{,th} = 1.80 \text{ mm} = 1.80 \text{ X } 10^{-3} \text{ m}$

$\mu = 2.63 \text{ X } 10^{-3} \text{ kg/(ms)}$
$\rho = 995 \text{ kg/m}^3$

$\Delta x = 0.009 \text{ m}$

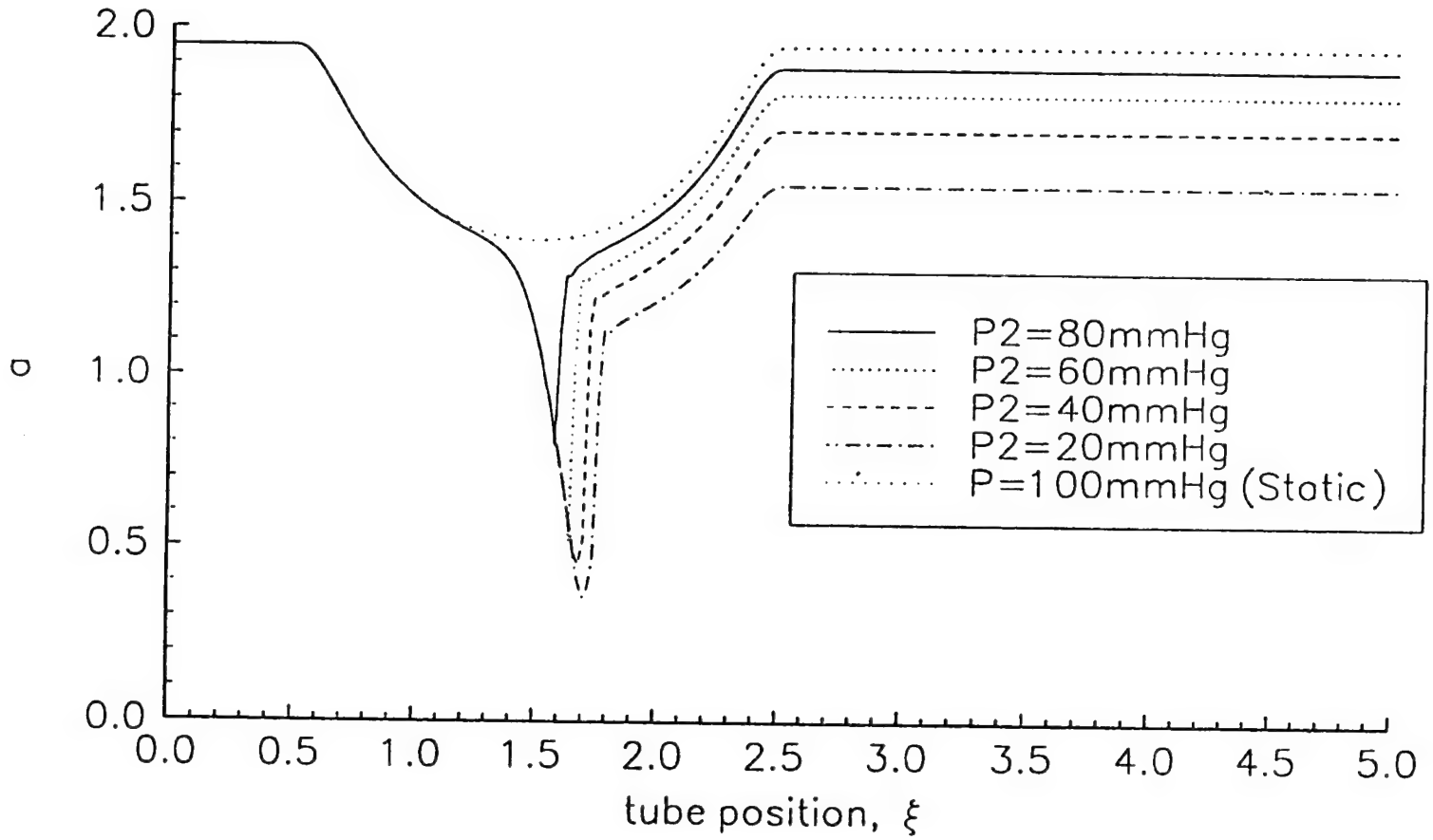

Figure 11e Nondimensional Area, α, Curves from a Representative Solution of Collapsible Tube Flow Through a Stenotic Artery with the following parameters: Tube Law: *n1*=7, *n2*=2.5; Kp_o=125, λ_{k_o}=10, λ_{A_o}=0.915, D_o=6.0mm, f_L=5, and K_{Sep}=0.0

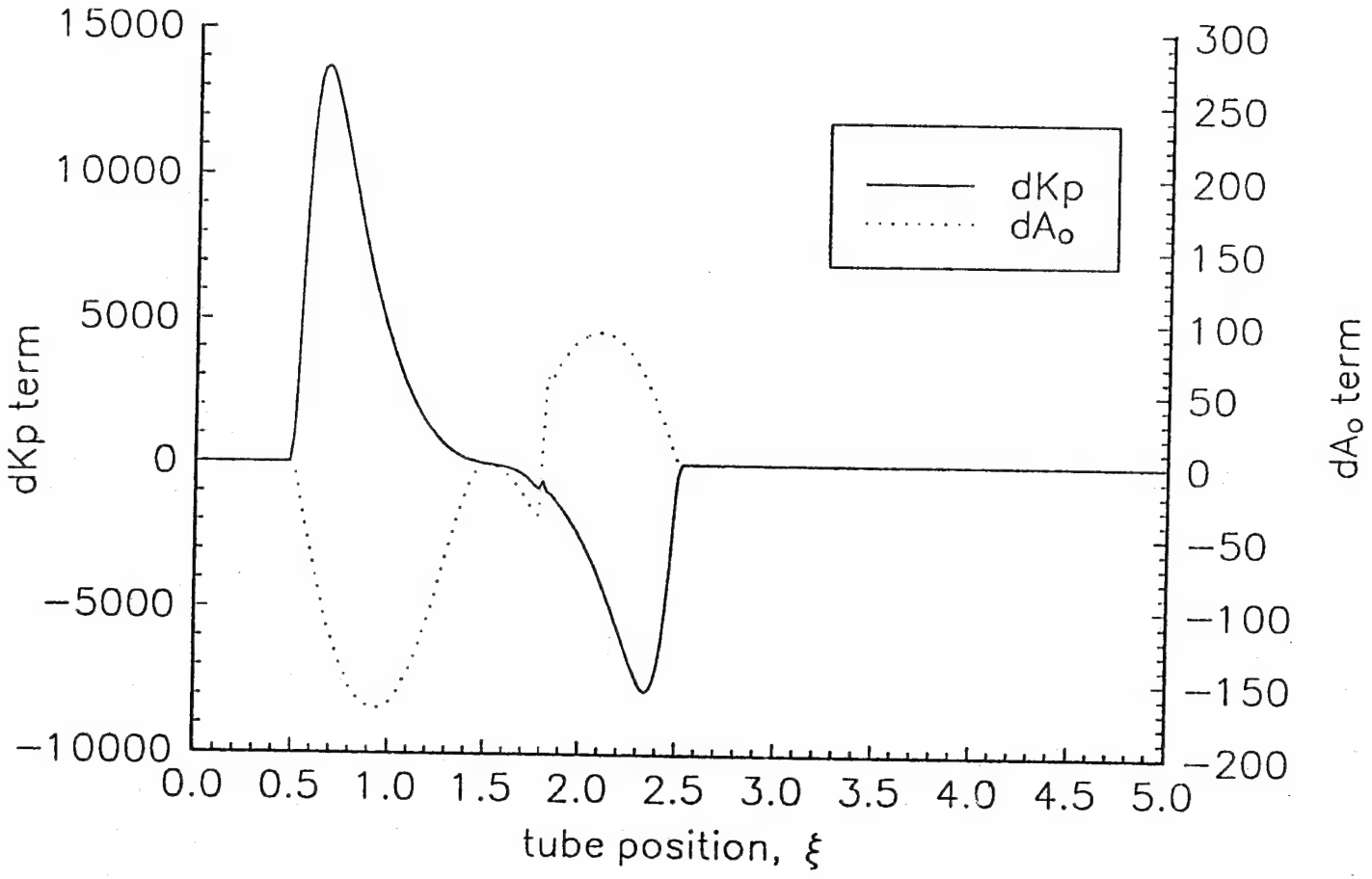

Figure 11f Nominal Area and Stiffness Forcing Function Curves from a Representative Solution of Collapsible Tube Flow Through a Stenotic Artery with the following parameters: Tube Law: $n1$=7, $n2$=2.5; Kp_o=125, λ_{k_o}=10, λ_{A_o}=0.915, D_o=6.0mm, f_L=5, and K_{Sep}=0.0

where the subscripts in and th refer to the inlet and throat values, respectively. The spatial gradient was taken as the difference between the conditions at inlet and at the throat of the nominal stenosis. Thus, the magnitude of the convection term was approximated as

$$\frac{\partial}{\partial x}\frac{1}{2}U^2 \;:\; \frac{1}{2}\frac{\Delta U^2}{\Delta x} = \frac{1}{2}\left(\frac{4.68^2 - 0.215^2}{0.009}\right) = 1200\frac{m}{s^2}.$$

The pressure gradient term was

$$\frac{1}{\rho}\frac{\partial(P - P_e)}{\partial x} \;:\; \frac{1}{\rho}\frac{\Delta(P - P_e)}{\Delta x} = \frac{1}{995}\left(\frac{1990 - 13300}{0.009}\right) = 1300\frac{m}{s^2}.$$

The magnitude of the basic friction term at the inlet was

$$\mathit{Frict.} \quad \frac{32\mu f_L}{\rho D_e^2}U_e = \frac{32 \cdot 2.63 \cdot 10^{-3} \cdot 5}{995 \cdot 8.38 \cdot 10^{-3}}0.215 = 1.3\frac{m}{s^2},$$

and at the throat it is

$$\mathit{Frict.} \quad \frac{32\mu f_L}{\rho D_e^2}U_{th} = \frac{32 \cdot 2.63 \cdot 10^{-3} \cdot 5}{995 \cdot 1.80 \cdot 10^{-3}}4.68 = 600\frac{m}{s^2}.$$

For the unsteady term, the unsteady velocity was estimated from the expected time variation in the flow rate during the cardiac cycle and was taken to be

$$\frac{\partial U}{\partial t} \approx \frac{1}{A}\frac{\partial Q}{\partial t},$$

which neglects area changes with respect to time. This assumption increased the magnitude of the acceleration term since the area also varies with time. The magnitude of the acceleration term was

$$\left|\frac{\partial U}{\partial t}:\right|: \quad \left|\frac{\Delta U}{\Delta t}\right| \approx \frac{1}{A}\left|\frac{\Delta Q}{\Delta t}\right| = \frac{1}{55.1 \cdot 10^{-6} mm^2}\left(100 \cdot 10^{-6}\frac{mm^3}{s^2}\right) = 1.8\frac{m}{s^2},$$

at the inlet, and it was

$$\left|\frac{\Delta U}{\Delta t}\right| \approx \frac{1}{2.54 \cdot 10^{-6}}(100 \cdot 10^{-6}) = 39.5\frac{m}{s^2}$$

at the throat. Thus, even with large time variations in the flow rate, the magnitude of the unsteady term was much smaller compared to the other terms. Therefore, steady state solutions should provide good illustrations on the individual effects of various parameters since the flow system can be approximated as quasisteady. Later, the unsteady term will be used to demonstrate the conditions under which flows may oscillate between critical and subcritical flows.

Verification of Compuational Solutions

Diameter Changes: Simple Scale Factor

Changes in the nominal diameter should result in a simple scaling of the results since the nominal diameter was one of the normalizing constants. Solutions using tube diameters of 6.0 mm and 9.5 mm and two different tube laws were obtained to test the affect of changes in the nominal diameter. The results for the flow rates are provided in Table 2a and show that the ratio of the flow rates was equal to the square of the ratio between the nominal diameters of 0.399. This scaling factor was independent of the tube law. Also, the results for the minimum areas are provided in Table 2b. This table shows that the minimum areas can be scaled to within 1% by the square of the nominal diameter ratio. Since the area ration accounted for the entire flow rate changes due to changes in the nominal diameter, the velocity curves remained unaffected by these changes, as demonstrated in figure 12 Constant velocity curves were expected since the solution is independent of the nominal area. Changes in the tube law displayed a marginal effect in A_{min} of about 0.5%. This marginal effect can be explained by the numerical error introduced by the oscillations about the jump, which lessened the accuracy of the variable predictions about the elastic jump region.

Table 2a. Flow Rates from Model Solutions with 6 mm and 9.5 mm Nominal Diameters.

Tube Law *n1*	% Stenosis (dia)	Q_6 (ml/s)	$Q_{9.5}$ (ml/s)	$Q_6/Q_{9.5}$
4	70.0	44.4	112.	.397
7	69.5	30.0	75.6	.397
4	80.0	19.9	50.2	.397
7	81.8	11.9	29.9	.397

Table 2b. Minimum Area from Model Solutions with 6 mm and 9.5 mm Nominal Diameters.

Tube Law *n1*	% Stenosis (dia)	A_{min6} (mm^2)	$A_{min9.5}$ (mm^2)	$A_6/A_{9.5}$
4	70.0	8.20	20.4	.402
7	69.5	5.10	12.8	.397
4	80.0	3.66	9.11	.402
7	81.8	2.05	5.18	.397

Thus, the predicted solution can be scaled directly for the tube diameter of interest by multiplying the solution flow rate and area with the square of the ratio of the desired diameter to the solution diameter. The minimum pressure, P_{min}, and the maximum speed index, S_{max}, were also only marginally affected (less than 2%) by nominal

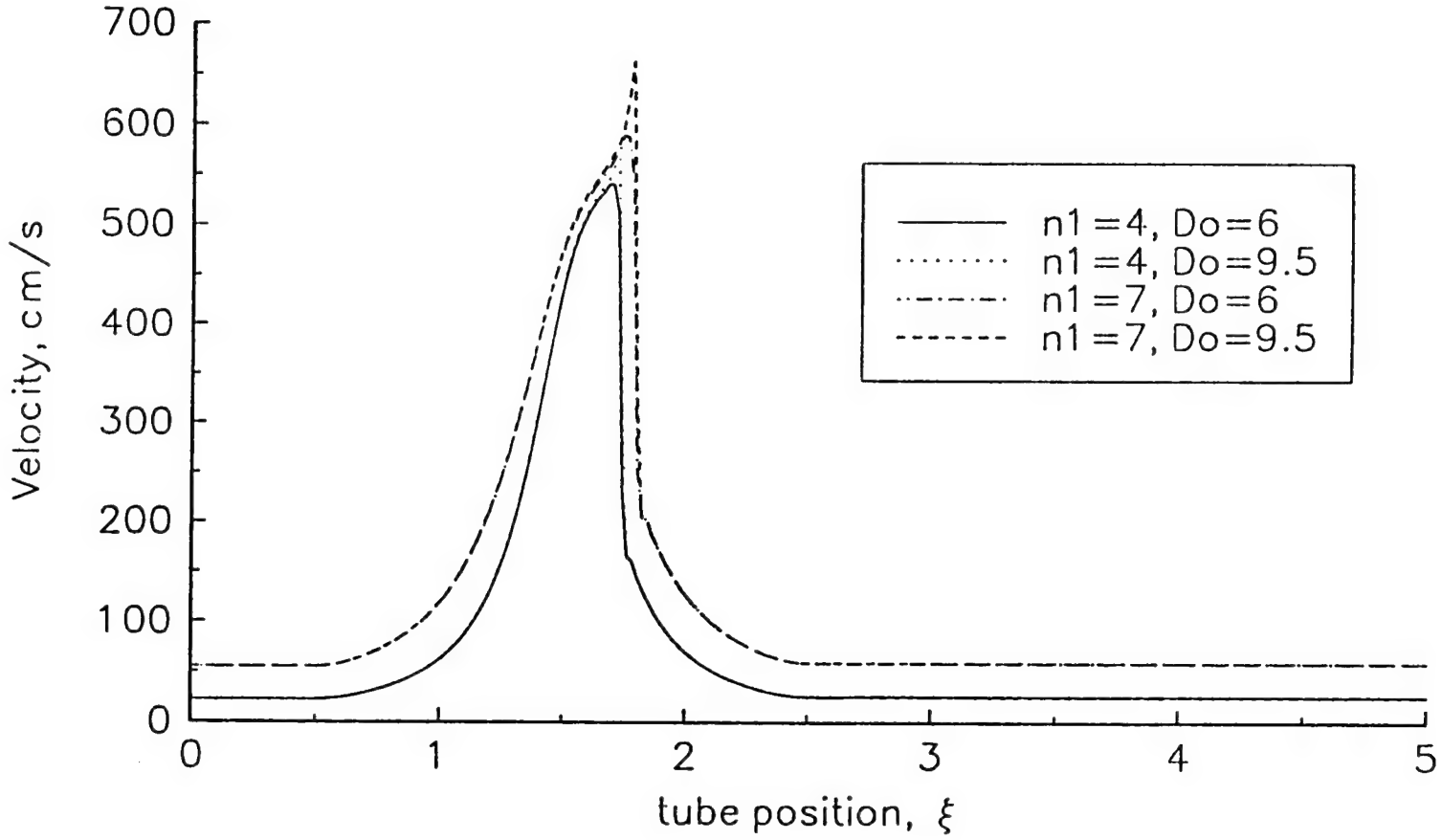

Figure 12 Changes in Nominal Diameter: No Effect on Velocity Curves

diameter changes. This marginal effect resulted from the numerical oscillations which persist in some of the solutions. The degree of dynamic stenosis remained unchanged with changes in diameter.

Length Changes: No Effect

Another modeling factor to consider is the exit length of the tube. Two solutions were obtained for tube lengths of $10D_o$ and $5D_o$ with the same boundary conditions. These solutions were identical in the stenotic region as shown in figure 13 which displays the pressure variation along the tube. In this figure, it can be seen that the elastic jump location and the minimum pressure were not affected by extending the exit length of the tube. Also, the critical flow of 44.4 ml/s remains unchanged along with A_{min} and S_{max}. This comparison demonstrates that tube exit length has little affect on the flow through the stenosis when only small viscous losses are modelled outside of the stenotic region.

Comparison with the Experimental Observation of Powell

Next, the computational results are compared to experimental results of Powell (22). This comparison provides an estimate of the accuracy of the model results in matching actual physical observations. The prescribed stiffness variation employed by the model was modified to approximate the rigid funnel stenoses used in the experimental study. The modification was shown in figure 5 and was defined by equation 31. Solutions were obtained for 70% and 80% stenoses (diameter). The model predictions used an f_L=20 and K_{sep}=0.5 for the 70% stenosis case and an f_L=20 and K_{sep}=0.2 for the 80% stenosis. The predicted flow rates were within 15% of the measured values, and the predicted distal pressure, P_2, required for the onset of critical flow was within 5 mmHg, as shown in figure 14a. The degree of dynamic stenosis varied by about 2%, as shown in figure 14b which plots the flow rate as a function of the degree of stenosis. For the computational model the degree of stenosis was defined as the percentage of area reduction at the initiation of critical flow. Thus, the degree of stenosis in the computational model varied over the range of P_2 settings, whereas the degree of experimental stenoses remained constant. Overall, this comparison demonstrates that the model estimates the flow rates reasonably well given the approximate nature of modeling the rigid funnel stenosis used in the experimental approach.

Arterial Tube Laws

Another important consideration is the type of tube law employed in the computational model. Two different types of tube laws, simplified and arterial, were considered. The simplified tube laws were defined in Table 1, and the arterial tube laws were defined by equation 31 and 32. The arterial tube laws considered were a bovine carotid artery and a canine carotid artery. The bovine artery tube law was derived from actual measurements (22) and was compared to the moderately compliant tube law ($n1$=7). The canine tube law was roughly derived from pressure/circumference data reported by Cox (65) and was compared to the highly compliant tube law ($n1$=4). Comparison values between the solutions using the

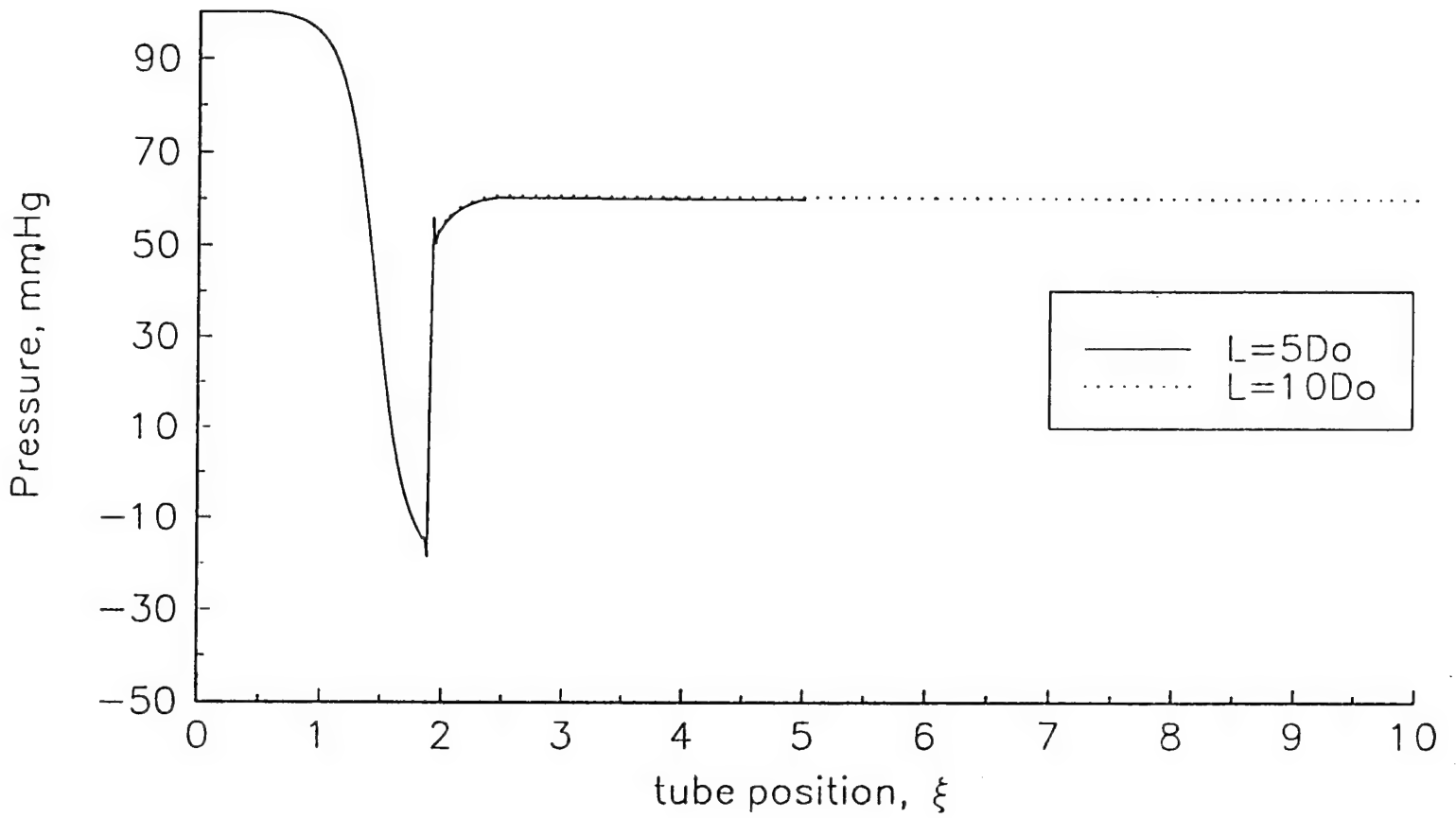

Figure 13 Tube Exit Length: Effect on Solution

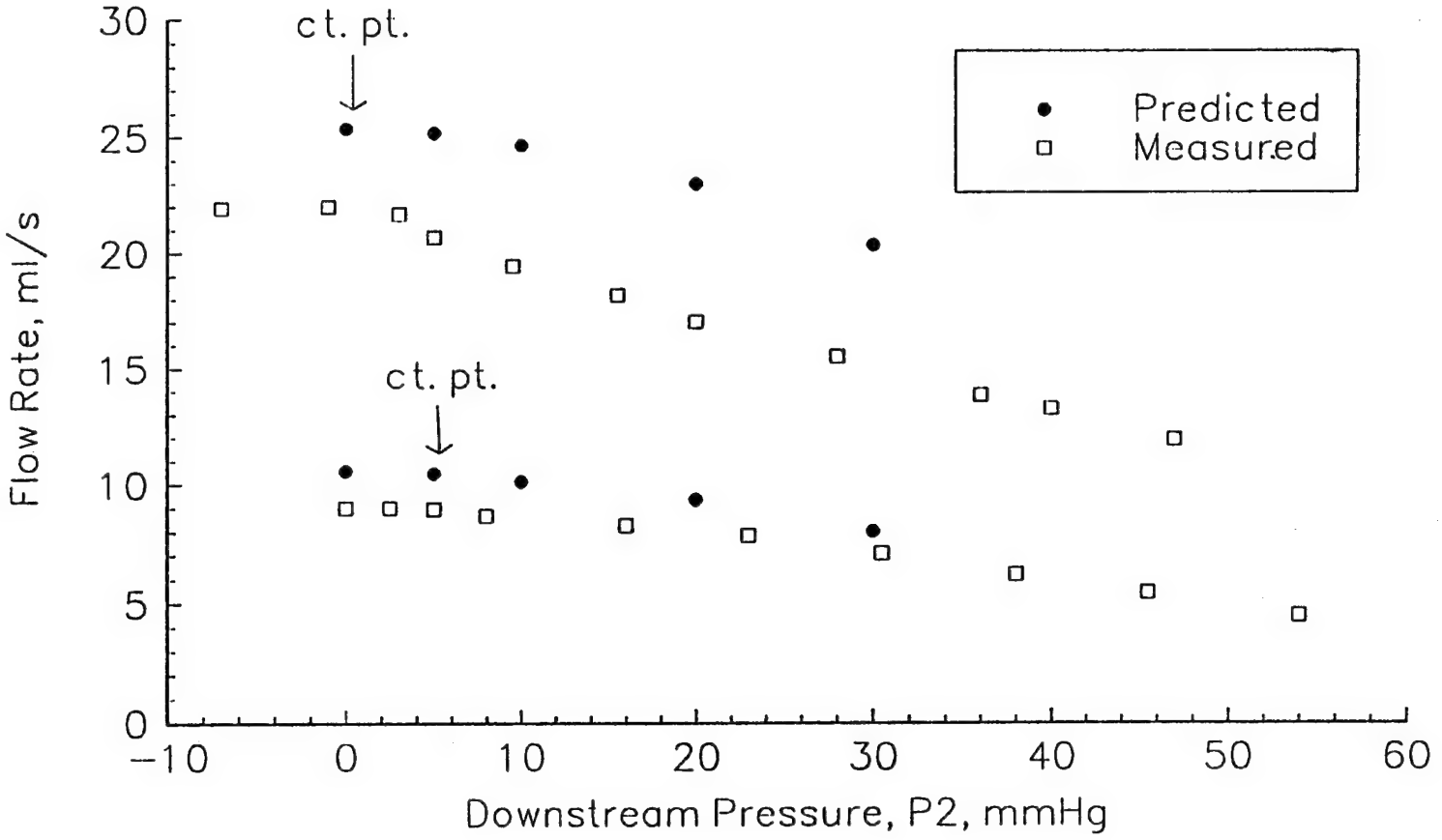

Figure 14 a Comparison of Model Predictions to Powell's Experimental Results: Flow Rate vs P_2 with P1=70mmHg

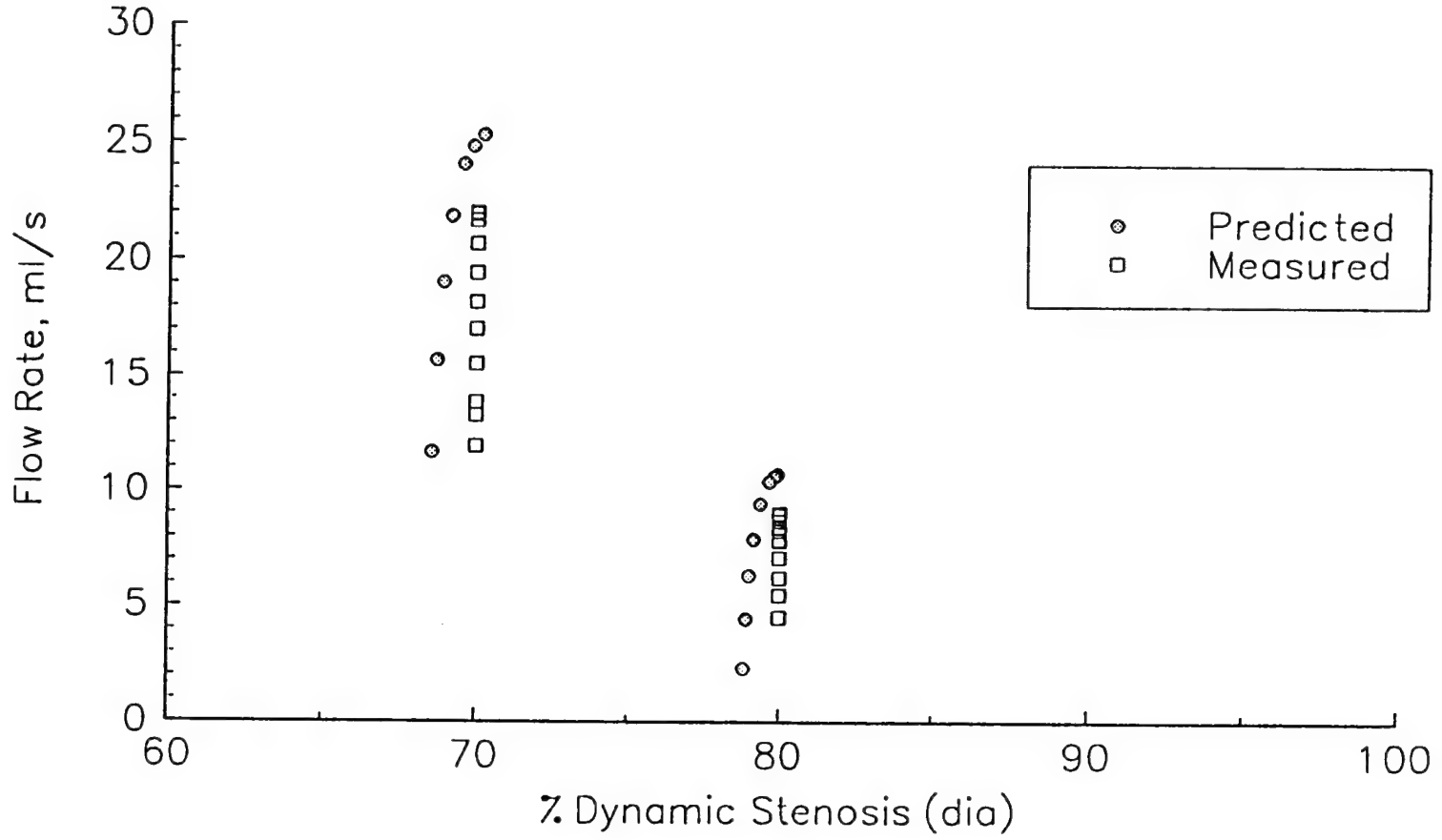

Figure 14b Comparison of Model Predictions to Powell's Experimental Results: Flow Rate vs Dynamic Stenosis

simplified and arterial tube laws are listed in Tables 3a and b. The critical flow rates obtained with the moderately compliant tube law ($n1$=7) were within 10% of the bovine critical flow rates, and the critical flow rates for the highly compliant tube law ($n1$=4) were within 9% of the canine results. Although the values for P_{min} did not agree as well, the pressure curves for both the bovine and the moderately compliant tube law solution for an 80% stenosis, as shown in figure 15a, had the same general trends within the stenotic region. P_{min} for the bovine case was 9 to 38 mmHg higher than the P_{min} for the $n1$=7 tube law. Also, S_{max} was lower in the bovine solutions than in the $n1$=7 solutions. The pressure curves comparing the canine and the highly compliant tube law solutions for a 80% stenosis, figure 15b, again demonstrated that although they do not match exactly they did show the same general trends. In this figure, P_{min} for the canine solution was 23 mmHg lower than the $n1$=4 solution, and S_{max} for the canine solution was lower than the $n1$=4 solution as noted in Table 3. These difference existed because of the approximation of the negative portion of the arterial tube laws and not the positive response defined by n1. The negative pressure region of the tube law is difficult to measure accurately because of the complex dumbbell shape of a collapsed tube. However, all of the solutions demonstrate the same trends in the data within the stenotic region. Thus, the simplified tube laws can be used with good confidence to estimate the characteristics of flow through a stenotic artery.

Table 3a. Comparison between Simplified and Bovine Arterial Tube Law

% Stenosis (dia)	Q_c (ml/s)	P_{min} (mmHg)	S_{max}	Tube Law
70.5	28.6	-29.3	1.46	bovine
69.5	30.0	-38.3	1.98	$n1$=7
79.8	11.3	-0.5	1.09	bovine
81.8	12.6	-38.3	1.92	$n1$=7

Table 3b. Comparison between Simplified and Canine Arterial Tube Law

% Stenosis (dia)	Q_c (ml/s)	P_{min} (mmHg)	S_{max}	Tube Law
70.2	42.8	-37.6	1.97	canine
70.0	44.4	-15.6	2.79	$n1$=4
80.3	18.2	-42.2	1.85	canine
80.0	19.9	-19.5	2.54	$n1$=4

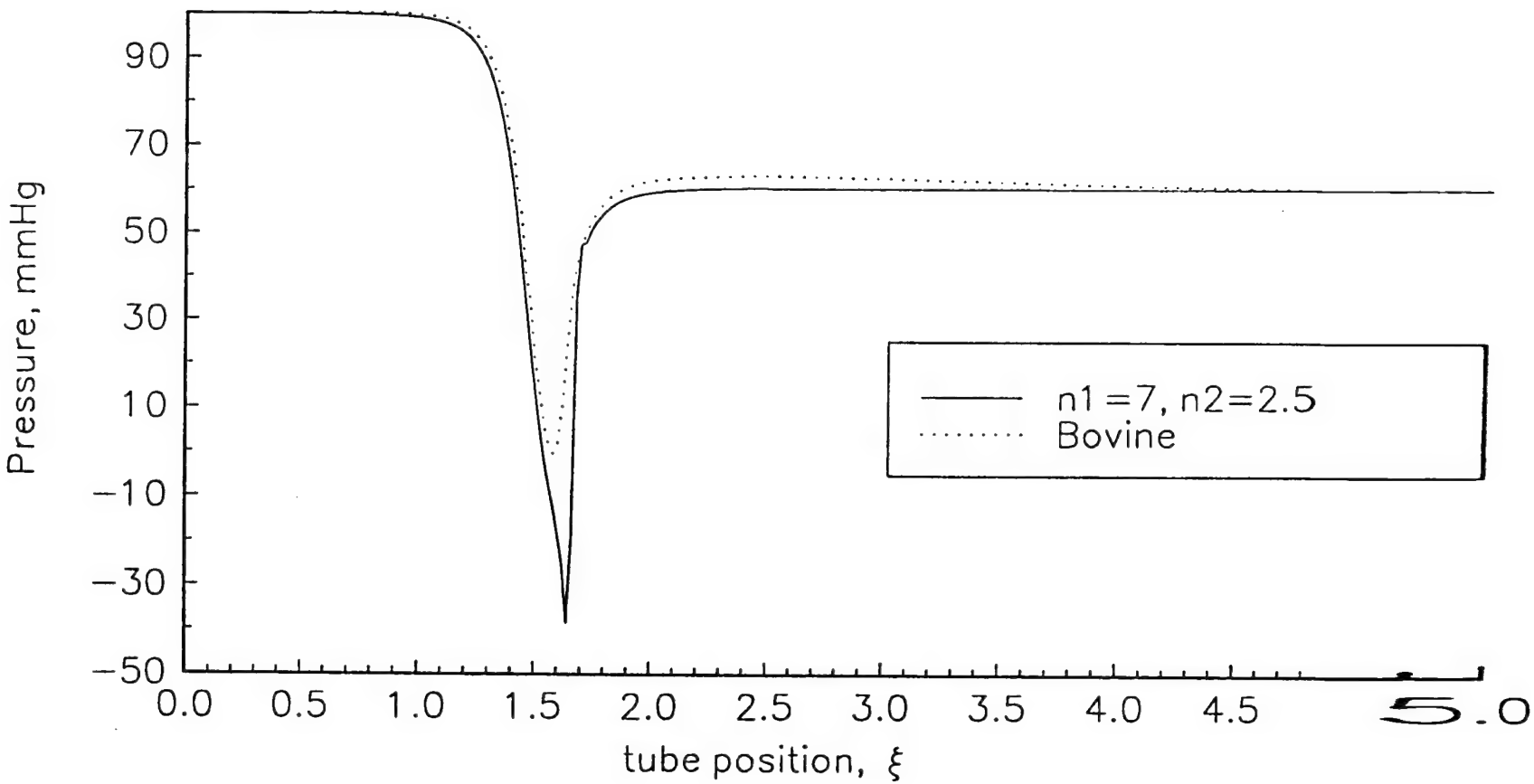

Figure 15a Pressure Curves Comparing Simplified (*n1*=7, *n2*=2.5) and Bovine Tube Laws for an 80%(dia) Dynamic Stenosis.

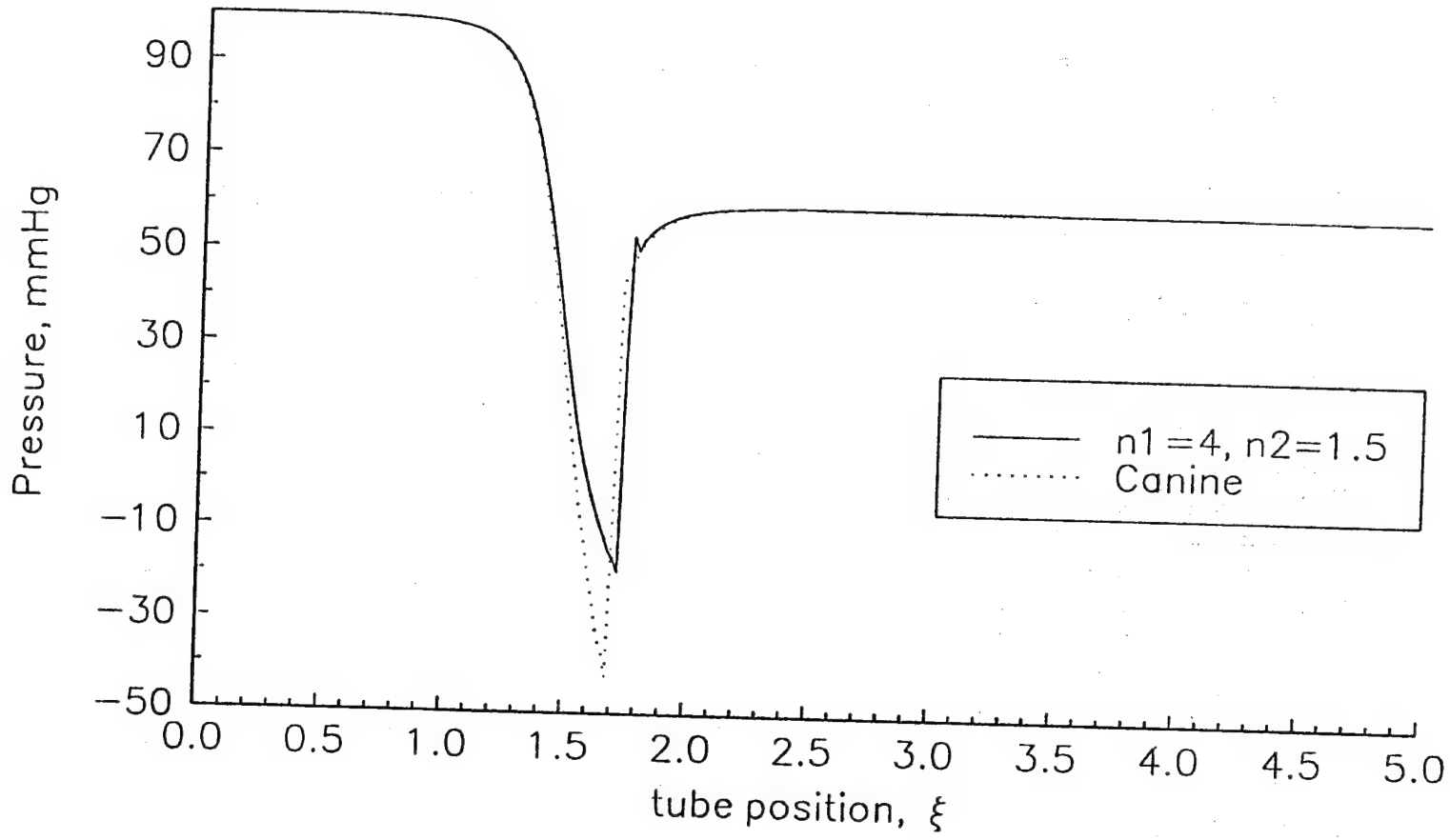

Figure 15b Pressure Curves Comparing Simplified (*n1*=4, *n2*=1.5) and Canine Tube Laws for an 80%(dia) Dynamic Stenosis

Parameter Variations Steady

Next, solutions which include variations in the tube compliance, frictional losses, and mean pressure are used to describe the various effects of the different parameters.

Tube Compliance

The tube compliance can vary widely for physiological vessels. Thus, this study considered several parameters which affected the relationship between the transmural pressure and the cross-sectional area of the tube. These parameters included variations in *n1* and *n2* in the basic tube law relationship, in the amplitude of the stiffness variations along the stenosis, and in the nominal tube stiffness. The *n1* variations affected the positive pressure region of the flow for a given nominal diameter, and the values chosen were *n1*=4, 7 and 20. The *n1*=4 tube modeled a highly compliant tube; *n1*=7 tube modeled a moderately compliant tube, and the *n1*=20 tube represented a stiff, lowly compliant tube. Variations in *n2* affected the negative pressure region of the flow and, thus, mainly influenced the super-critical region of the flow. Variations in stiffness influenced the flow rate and the magnitude of the pressure since the stiffness was used to normalize the pressure in the tube law relation.

Variations in *n1*. The *n1* parameter defines how the tube area expands with respect to positive pressure, as shown in figure 2.3. Therefore, variations in *n1* affected the amount of tube expansion in the positive pressure regions of the flow. As *n1* increased, the lumen expanded less. Thus, for a given nominal diameter, the lumen was smaller for a tube defined by a larger *n1*. With this influence of the *n1* parameter, solutions are discussed for the following conditions: 1) nominal diameter was held constant and 2) dynamic inlet area was held constant.

For the first case with the nominal diameter set at 6 mm, the resulting inlet areas, A_{in}, for the three *n1* values of 4, 7, and 20 were 91 mm^2, 55 mm^2, and 36 mm^2, respectively. This reduction in A_{in} with increasing *n1* resulted in decreasing Q_c. Figure 16a, which plots Q_c versus the degree of dynamic stenosis for the three *n1* values, shows this decrease in Q_c with increases in *n1*. Tables 4a-c provide a summary of the results for these solutions. The summaries include Q_c, P_{min}, S_{max}, A_{in}, A_{min}, jump location, and the degree of stenosis. From these tables, it can be seen that for a 70% dynamic stenosis, Q_c increased by 160% between *n1*=20 and *n1*=4 tube laws and increased by 74% between *n1*=20 and *n1*=7 tube laws. For a 80% dynamic stenosis, the resulting increased are 170% and 70%, respectively, and were 140% and 60% for a 90% stenosis. As can be seen in figure 16a, the difference between Q_c for the three different *n1* solutions decreased with increasing degree of stenosis.

However, if the critical flow rates for the three *n1* values were scaled for a constant dynamic inlet area (A_{in}), then the dependence of Q_c on *n1* disappeared, as demonstrated in figure 16b. It should be noted that the only variables affected by the scaling were D_o, Q_c, and the area. P_{min}, S_{max}, the degree of dynamic stenosis, and the velocity remain unchanged by the scaling.

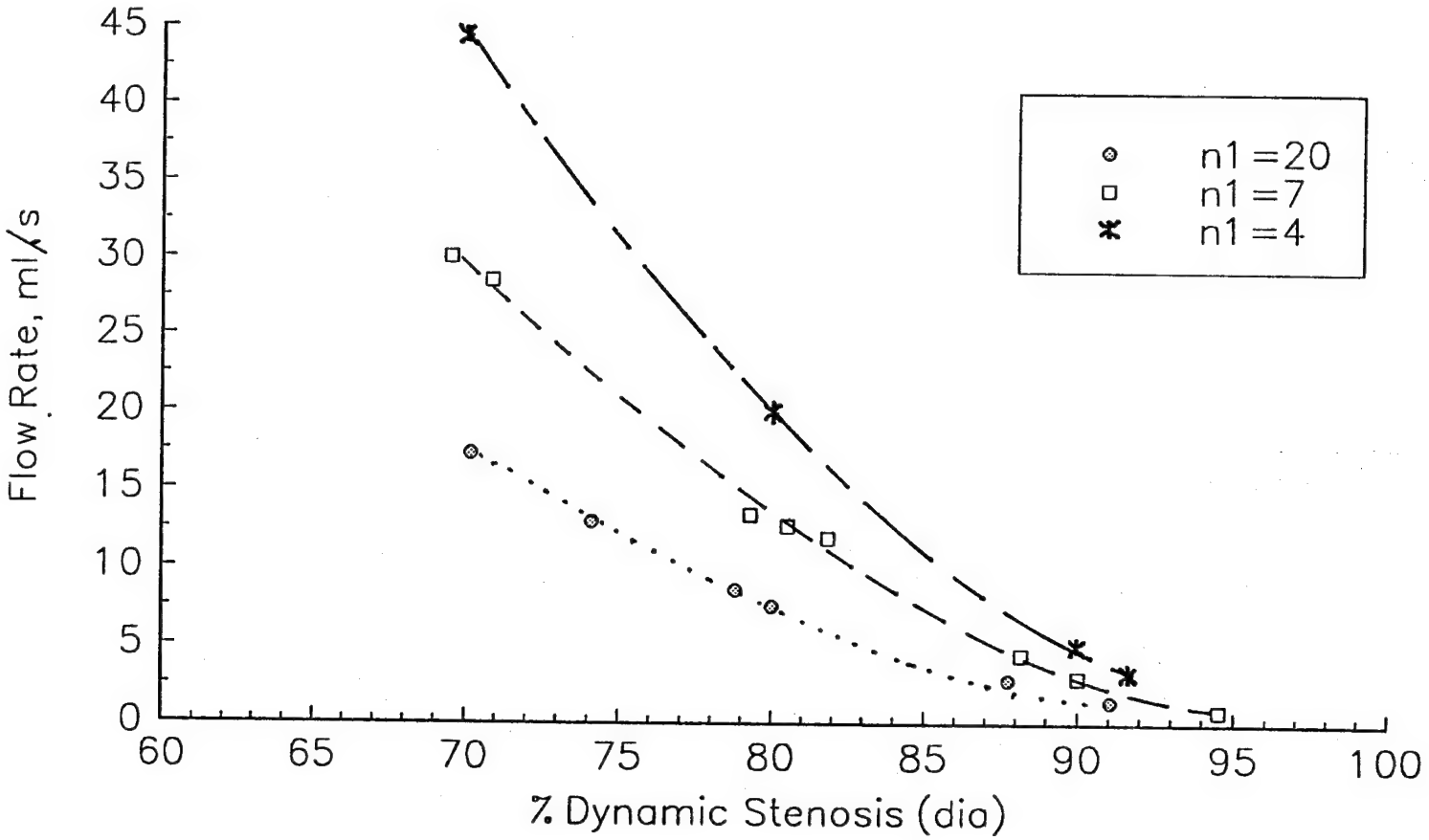

Figure 16a Critical Flow Rate vs Dynamic Stenosis for the Simplified Tube Laws ($n1$=4, 7 & 20) with a Constant Nominal Diameter of 6mm

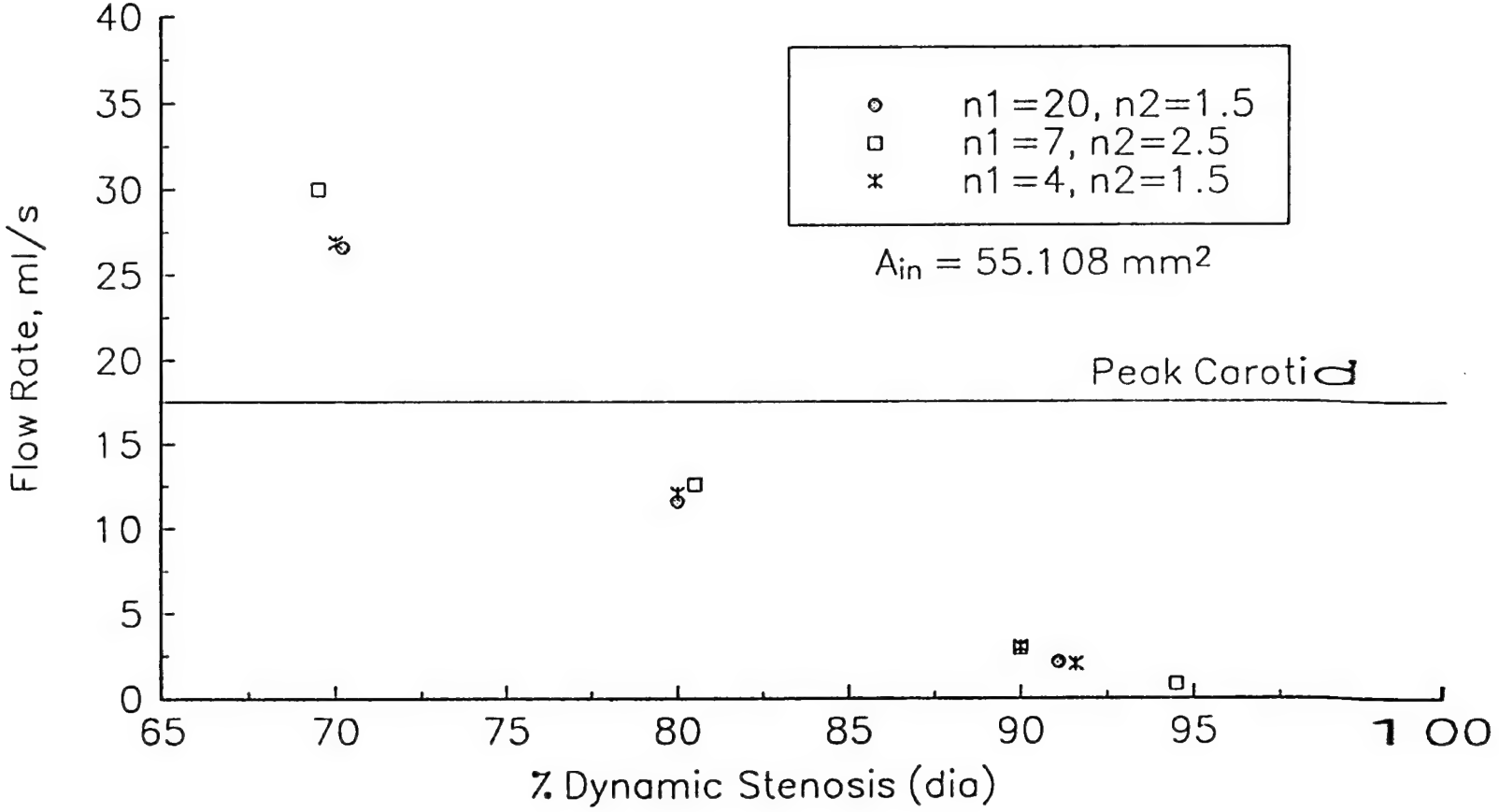

Figure 16 b Scaled Critical Flow Rates vs Dynamic Stenosis for Simplified Tube Laws (*n1*=4, 7 & 20) with a Constant Dynamic Inlet Area of 55.1 mm^2

Figure 16c plots P_{min} versus the degree of stenosis for the baseline solutions. P_{min} remained fairly stable until about 90% stenosis was reached. About this point, P_{min} began to increase with further increases in the degree of stenosis. P_{min} was lower for the *n1*=7 solutions since these solutions utilized an *n2*=2.5, while the other two solutions had an *n2*=1.5. More detailed effects of *n2* variation will be shown in the next section.

n1 influenced the size of the underlying stenosis needed to produce the same degree of dynamic stenosis. As *n1* increased, the nominal stenosis would also have to increase to maintain a constant dynamic stenosis. This relationship between the nominal area reduction, λ_{A_o}, and the degree of stenosis (by area) is displayed in figure 16d. The degree of the dynamic stenosis was increased from the nominal stenosis by flow through the stenosis. This increase was greatest for the highly compliant tube, but it diminished as the degree of stenosis approached 90% by diameter. Therefore, this comparison has illustrated the marginal effect of *n1* on the critical flow rate. For a given nominal diameter, *n1* affected the critical flow only by restricting the amount of expansion of the proximal area. However, for a constant dynamic inlet area, the dependence of Q_c on *n1* disappeared. The important effect of *n1* was on the degree of nominal stenosis require to achieve a given degree of dynamic stenosis. Thus, the less compliant that an stenotic artery is, more underlying plaque build up is required to create a critical stenosis. Also, *n1* was shown to have little effect on P_{min}, S_{max}, and the velocity.

Table 4a Summary of Results for *n1* Variations: *n1*=4

λ_{A_o} (area)	P_2 (mmHg)	% dyn stn (dia)	Q (ml/s)	P_{min} (mmHg)	S_{max}	A_{min} (mm^2)	Jump Location (ξ)
.735	80	69.7	44.4	-8.5	2.3	8.35	1.76
	60	70.0	44.4	-15.6	2.79	8.20	1.90
	40	70.0	44.4	-17.5	2.82	8.20	2.10
	20	70.0	44.4	-17.5	4.6	8.20	2.74
.88	80	79.5	19.9	-8.5	2.33	3.78	1.66
	60	80.0	19.9	-19.5	2.54	3.66	1.74
	40	80.0	19.9	-32.5	2.54	3.62	1.84
	20	80.0	19.9	-39.6	2.54	3.62	1.98
.97	80	89.5	4.94	3.3	1.62	1.01	1.56
	60	90.0	4.98	-19.6	2.38	.93	1.62
	40	90.0	5.00	-33.7	2.38	.923	1.66
	20	90.0	5.02	-38.6	2.38	.923	1.70
.98	60	91.6	3.28	-12.1	2.3	.615	1.60

Table 4b Summary of Results for *n1* Variations: *n1*=7.

λ_{A_o} (area)	P_2 (mmHg)	% dyn stn (dia)	Q (ml/s)	P_{min} (mmHg)	S_{max}	A_{min} (mm^2)	Jump Location (ξ)
.80	80	68.7	30.0	-15.0	1.96	5.39	1.70
	60	69.5	30.0	-38.3	1.98	5.10	1.80
	40	71.4	30.0	-82.1	1.98	4.51	1.90
	20	73.2	30.0	-148.4	1.98	3.99	2.00
.915	80	79.8	12.6	-25.0	1.92	2.24	1.62
	60	80.5	12.6	-38.6	1.92	2.1	1.68
	40	81.3	12.6	-100.0	1.92	1.95	1.72
	20	82.1	12.6	-120.5	1.92	1.76	1.74
.98	80	89.0	2.89*	22.3	.779	.659	--
	60	90.0	2.91	-12.8	1.79	.567	1.58
	40	90.0	2.91	-42.4	1.86	.533	1.60
	20	90.5	2.91	-65.8	1.85	.502	1.62
.99	60	94.5	0.80*	21.4	.782	.164	--

Table 4c Summary of Results for Baseline solutions with *n1*=20

λ_{A_o} (area)	P_2 (mmHg)	% dyn stn (dia)	Q (ml/s)	P_{min} (mmHg)	S_{max}	A_{min} (mm^2)	Jump Location (ξ)
.88	80	70.0	17.2	-15.2	3.02	3.22	1.64
	60	70.2	17.2	-23.1	3.02	3.17	1.72
	40	70.3	17.2	-34.0	3.02	3.15	1.80
	20	70.3	17.2	-42.1	3.02	3.15	1.92
.947	80	80.0	7.51	-8.3	1.62	1.435	1.54
	60	80.0	7.51	-22.5	2.98	1.419	1.64
	40	80.3	7.51	-32.3	2.90	1.41	1.68
	20	80.3	7.51	-39.0	2.91	1.41	1.74
.99	80	90.3	0.70*	68.8	.148	.611	--
	60	91.1	1.36	-4.3	1.06	.524	1.54
	40	91.1	1.36	-16.9	2.6	.523	1.58
	20	91.1	1.36	-24.1	2.6	.540	1.60

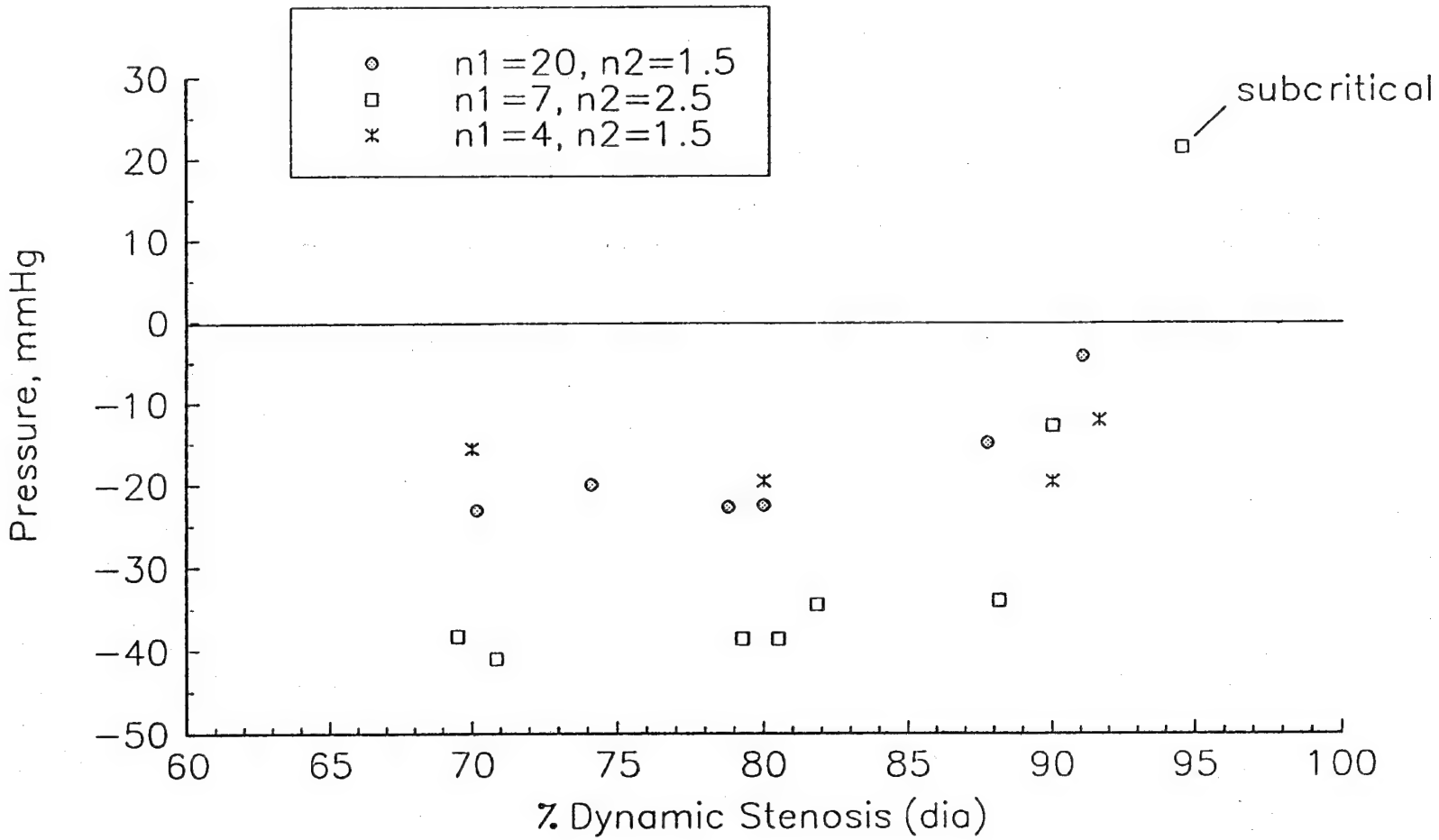

Figure 16c Minimum Pressure vs Dynamic Stenosis for the Simplified Tube Laws (*n1*=4, 7 & 20).

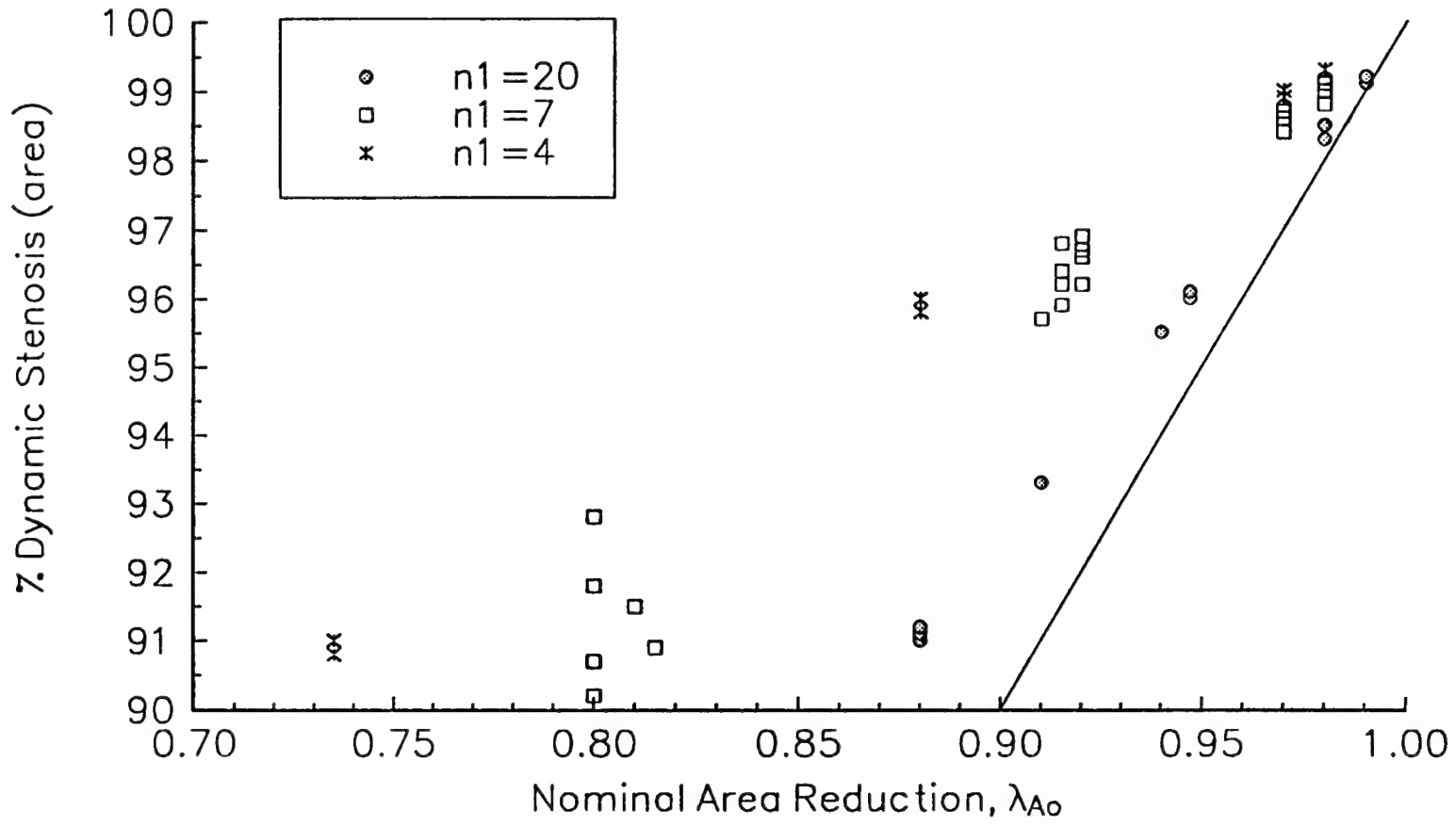

Figure 16d Nominal Area Reduction, λ_{A_o}, vs Dynamic Stenosis for Simplified Tube Laws ($n1$=4, 7 & 20)

Variations in *n2*. Since the negative portion of the tube law is difficult to measure, variations in *n2* were considered to estimate the impact of variations in this parameter. Solutions were calculated for *n2* values of 1.5, 2.5 (baseline), 3, and 4 with *n1*=7. The other parameters were set at the baseline conditions. The values of Q_c obtained for the four values of *n2* showed no effect from variations in *n2*. This negligible effect on Q_c is clearly seen in Figure 17a. However, the *n2* variation caused large changes in the values of P_{min}. These changes were from -20 mmHg for *n2*=1.5 to -100 for *n2*=4, as shown in figure 17b. Figure 17c plots S_{max} versus *n2*. S_{max} remained supercritical for these variations, but it was reduced with increasing magnitude of *n2*. Also, changes in the dynamic stenosis are noted in these figures. Increases in *n2* from 1.5 to 4 tended to increase the dynamic stenosis from 96.2% to 96.9% by area or 80.5 to 82.4 by diameter. These results were as expected since *n2* influences the flow mainly in the negative pressure, or collapsed, region of the flow where the flow was supercritical.

Plaque Stiffness Variation: λ_K. In a stenotic artery, the arterial wall thickens with the enlargement of plaque. Thus, the arterial stiffness is expected to vary along the stenosis. Moreover, because of the wide variation in plaque structural qualities, a wide range of stiffness variations may exist in a stenotic artery. This increased stiffness should not reach the maximum stiffness, that would be calculated by equation 4, since the thin wall assumption breaks down as the arterial wall thickness becomes comparable to the arterial radius. A series of solutions were calculated with a wide range of amplitudes for the stiffness variations as defined in chapter 2. The previous solutions included a stiffness variation amplitude, λ_{K_o}, equal to 10 to model a plaque which added some structural support to the wall. The other solutions for this comparison have λ_{K_o}'s ranging from 0 to 100 with the other parameter held at baseline values. The range of solutions included dynamic stenoses varying from 62% to 91% by diameter. Table 5 lists the values obtained for Q, P_{min}, and S_{max} for this series.

From these solutions, Q_c increased with λ_{K_o} which agrees with the analysis of Shapiro (33). Shapiro stated that an decreasing stiffness gradient moved the flow toward the critical point. Thus, an increasing gradient retarded the propagation toward the critical point, and a higher initial flow rate was needed to reach the critical point. Also, the degree of dynamic stenosis increased with λ_{K_o} for the same underlying nominal area reduction. Figure 18a shows Q versus the degree of dynamic stenosis for the range of λ_{K_o}'s. This figure illustrates the effect of λ_{K_o} which tended to increase the critical flow rate and the degree of the stenosis. This trend is seen in the data points shifting upward and to the left. However, the magnitude of the increases in the flow and the degree of stenosis diminished as the underlying nominal stenosis becomes more severe. With a constant area reduction of 0.80, the flow rate increased by 6.96 ml/s (23%) with a tenfold increase in λ_{K_o} (from λ_{K_o}=10 to 100) and the dynamic stenosis increased from 69.5% to 75.5 % (dia). However, with a nominal area reduction of 97%, the flow rate increased by only 0.91 ml/s (21%), and the

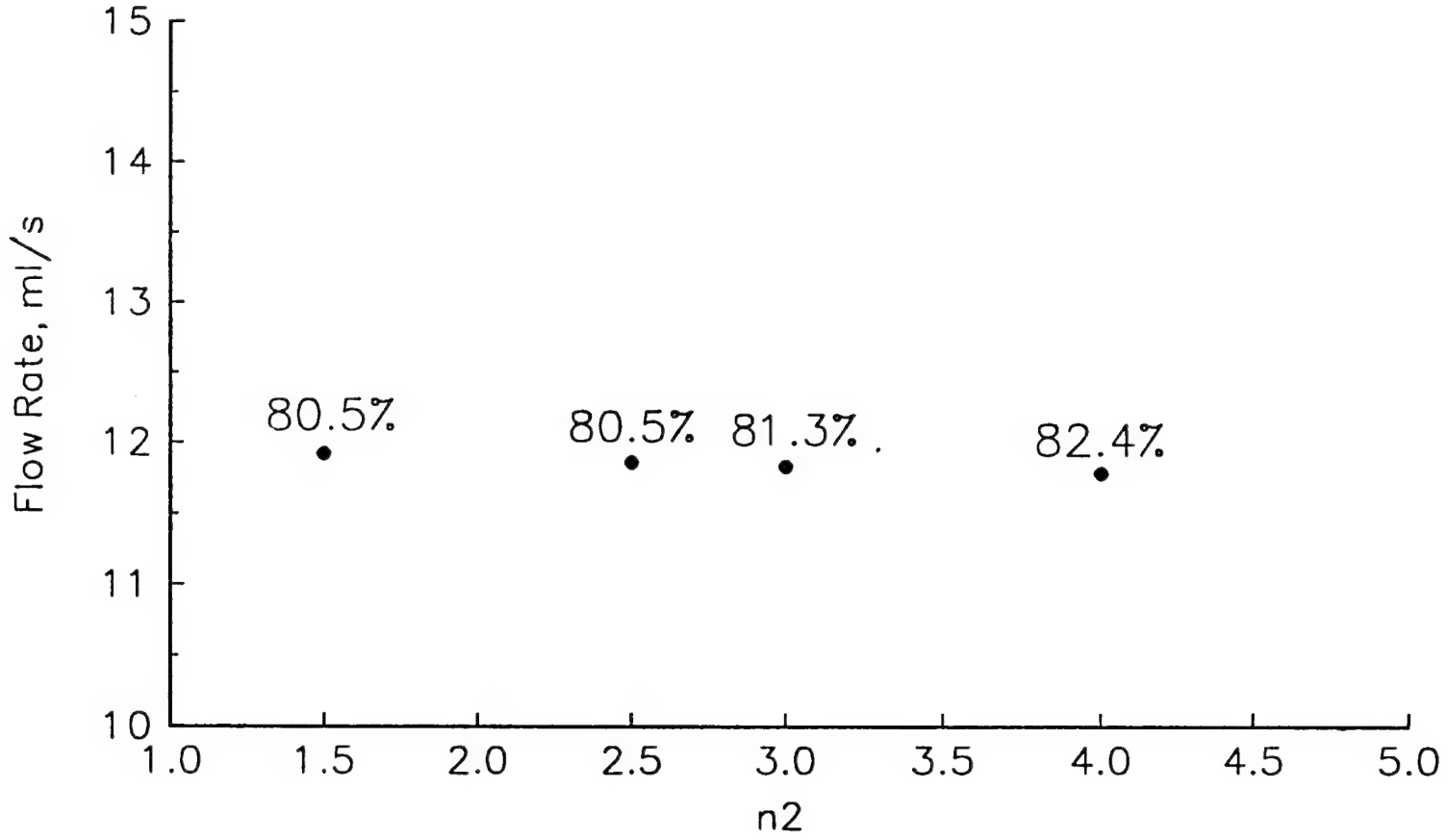

Figure 17 a Effect of *n2* on the Critical Flow Rate with the following constant values: λ_{A_o}=.92, *n1*=7, Kp_o=125 Pa, λ_{K_o}=10, P_1=100 mmHg, P_2=60 mmHg, f_L=5, K_{Sep}=0
(Note: % stenosis has an error of ±.3%)

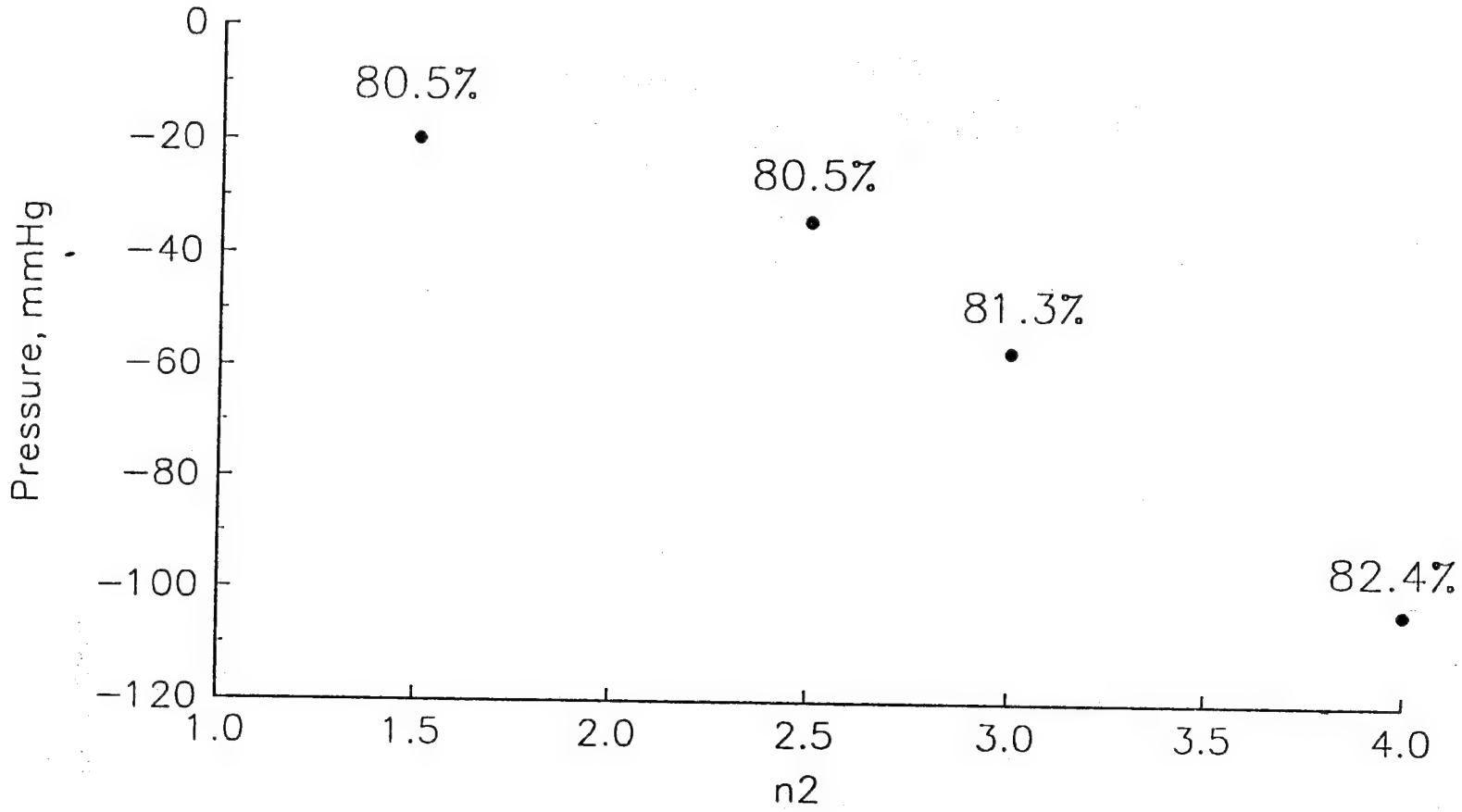

Figure 17b Effect of *n2* on the Minimum Pressure with the following constant values: λ_{A_o}=.92, *n1*=7, Kp_o=125 Pa, λ_{K_o}=10, P_1=100 mmHg, P_2=60 mmHg, f_L=5, K_{Sep}=0

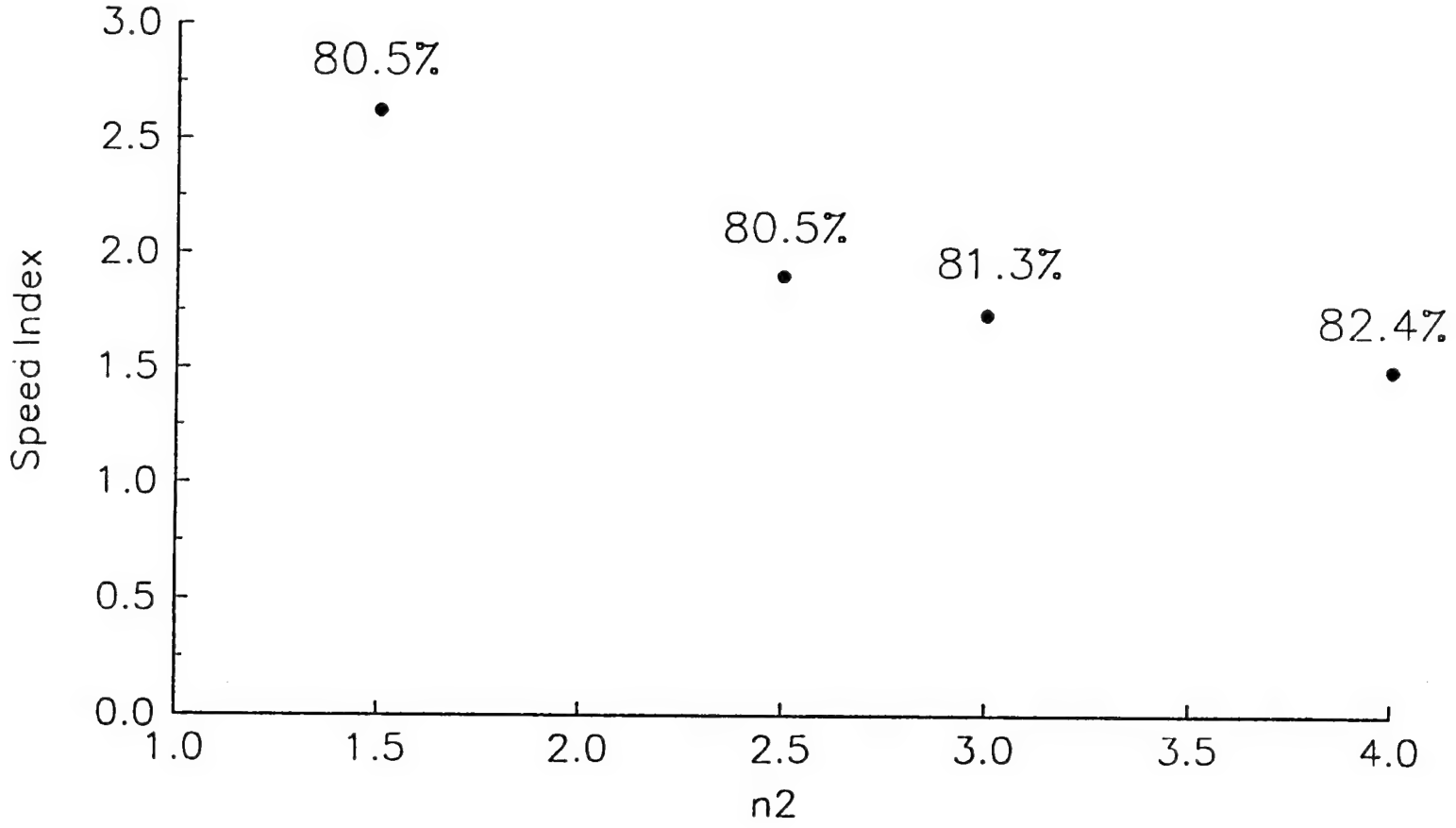

Figure 17c Effect of *n2* on the Maximum Speed Index with the following constant values: λ_{A_e}=.92, *n1*=7, Kp_o=125 Pa, λ_{K_e}=10, P_1=100 mmHg, P_2=60 mmHg, f_L=5, K_{sep}=0

Table 5 Summary of Results for Variations in the Tube Stiffness

Stiffness Var. λ_{K_o}	Area Red. λ_{A_o}	% Stenosis (dia)	Q (ml/s)	P_{min} (mmHg)	S_{max}
0	.800	62.3	25.2	-2.0	1.88
	.870	69.8	26.2	-1.6	1.78
	.945	80.5	11.0	-0.5	1.68
	.975	87.8	4.96	-2.0	1.60
10	.800	69.5	30.0	-38.3	1.98
	.915	80.5	12.6	-38.6	1.92
	.920	81.2	11.9	-34.0	1.90
	.970	88.2	4.39	-34.0	1.79
	.980	90.0	2.91	-12.8	1.79
	.995	94.5	0.80	21.4	.78
15	.785	70.3	31.5	-55	1.69
	.800	71.4	29.4	-67.7	1.69
	.902	80.5	14.1	-68.8	1.64
	.920	81.8	11.6	-58.6	1.65
	.980	90.0	2.85	-22.9	1.51
20	.770	70.3	33.5	-86.6	1.52
	.800	73.4	29.0	-111.	1.52
	.900	80.0	14.4	-73.0	1.50
	.920	81.8	11.5	-70.8	1.48
	.970	88.6	4.3	-44.1	1.47
	.980	90.5	2.9	-34.6	1.38
30	.720	69.3	41.3	-145.	1.34
	.738	70.3	38.6	-148.	1.33
	.800	73.9	29.3	-146.	1.32
	.890	80.3	16.0	-134.	1.31
	.920	82.7	11.6	-95.7	1.31
	.965	88.2	5.04	-64.5	1.27
	.980	90.5	2.88	-43.2	1.24
40	.800	74.7	30.0	-187.	1.22
	.875	79.5	18.7	-161.	1.22
60	.800	75.5	32.1	-275.	1.11
	.870	79.5	20.8	-231.	1.11
100	.800	75.5	37.0	-396.	1.01
	.920	83.3	14.7*	-241.	.996
	.970	88.6	5.3*	-116.	.831

dynamic stenosis increased from 87.4% to 88.6% (dia). λ_{K_o} also greatly decreased P_{min}. This relationship is provided in figure 18b which displays P_{min} versus the degree of dynamic stenosis over a range of λ_{K_o} values. The case with λ_{K_o}=100 and λ_{A_o}=.80 resulted in a dynamic stenosis of 76% by diameter with a P_{min} of -396 mmHg, whereas with λ_{K_o}=10 and λ_{A_o}=.80, the solution resulted in a dynamic stenosis of 69.5% with a P_{min} of 38.6 mmHg. Thus, a tenfold increase in λ_{K_o} resulted in a tenfold decrease in P_{min}. The above figure also reveals that with no stiffness variation, λ_{K_o}=0, negative pressures were barely obtained and were very small in magnitude. This relationship between P_{min} and λ_{K_o} can be explained through the tube law. Since the tube law relates the normalized pressure to the area ratio, for a given area ratio, the magnitude of the dimensional pressure increased with increases in the local stiffness. Another trend illustrated in this figure is that the bend in P_{min} curve occurs at a lower dynamic stenosis with increasing λ_{K_o}. This shift was produced by the increased frictional losses arising from the increases critical flow rates and the degree of stenosis.

It is also interesting to note that with λ_{K_o}=100 and λ_{A_o}=.97 the flow rate was increased from the λ_{K_o}=10 case, yet critical flow was not established. Thus, increasing λ_{K_o} also affected S_{max} as shown in figure 18c. From this figure it was observed that any increased stiffness variation decreases S_{max}. For the λ_{K_o}=0 case, S_{max} reached a value of 6.0, while with λ_{K_o} ranging from 10 to 100 S_{max} reached values of 2.0 to 1.1.

Overall, the amplitude changes in the stiffness variation enhanced both the flow rate and the degree of dynamic stenosis. Increasing λ_{K_o} also generated much larger negative pressures while decreasing S_{max}. An interesting occurrence arises with λ_{K_o}=100 and λ_{A_o}=.97 in that critical flow was not established, yet the flow rate was increased by 20% from the λ_{K_o}=10 solution for the same boundary conditions.

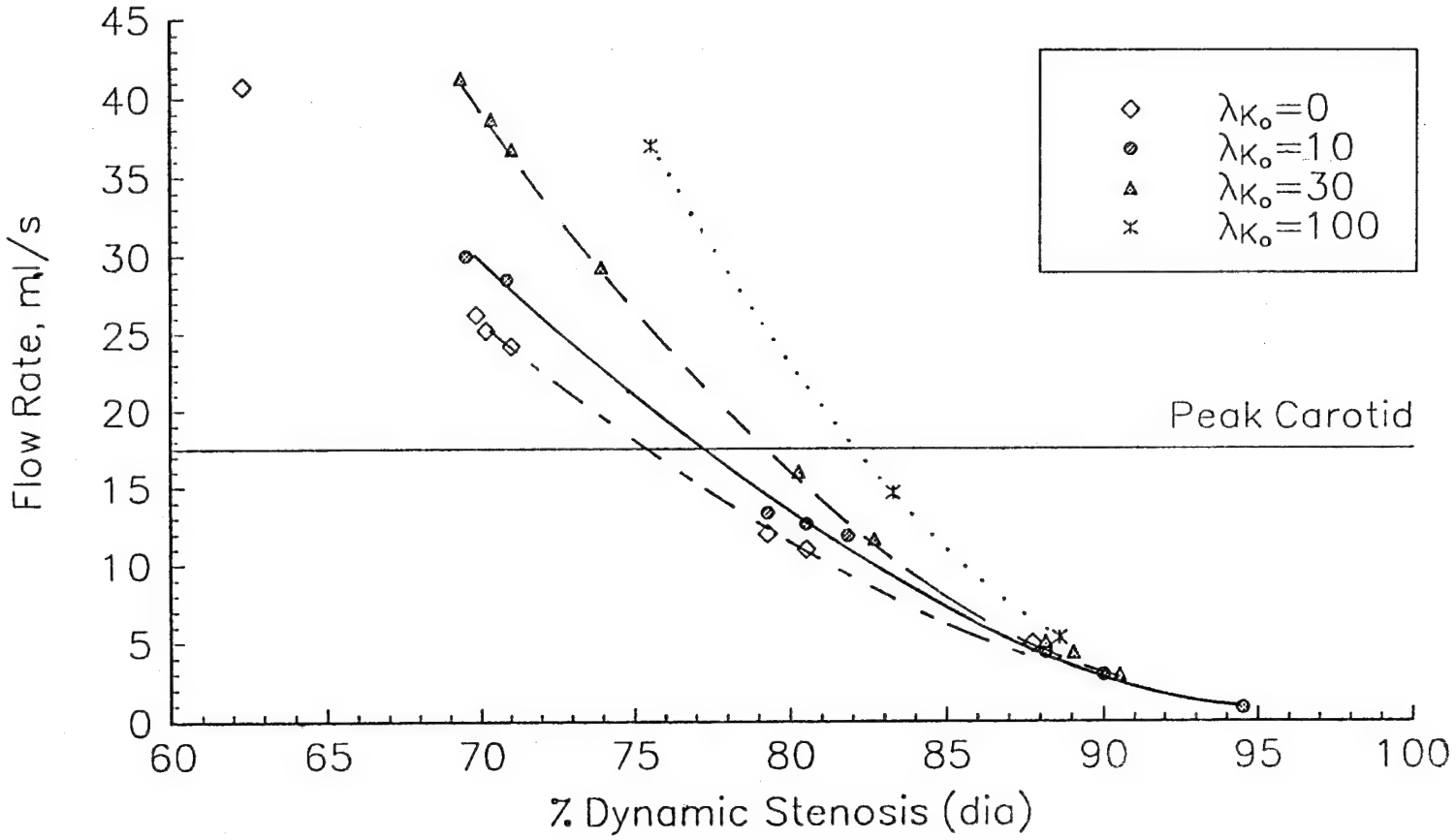

Figure 18a Effect of Stiffness Variations on the Critical Flow Rate versus Dynamic Stenosis Relationship.

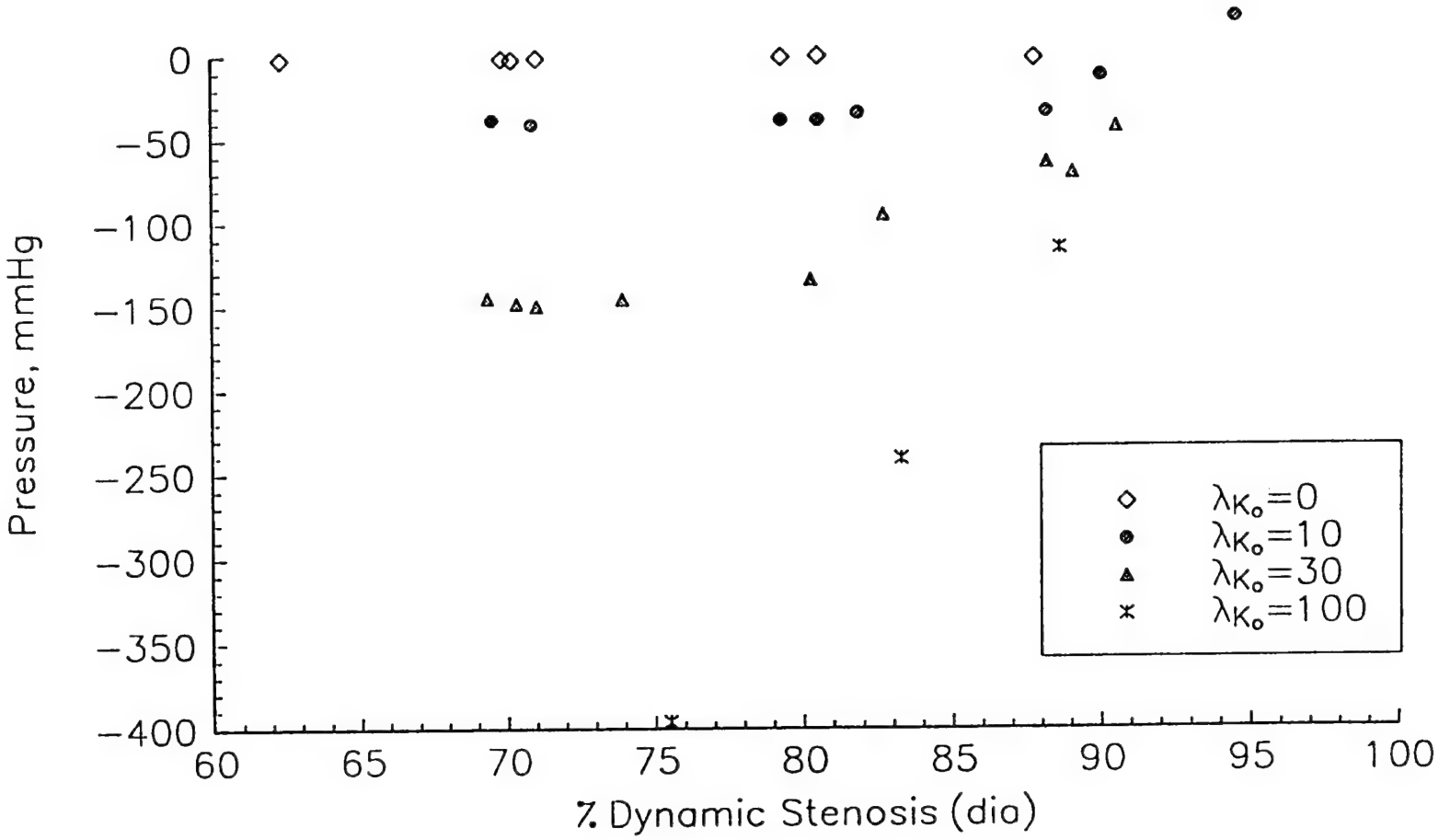

Figure 18b Effect of Stiffness Variations on the Minimum Pressure versus Dynamic Stenosis Relationship.

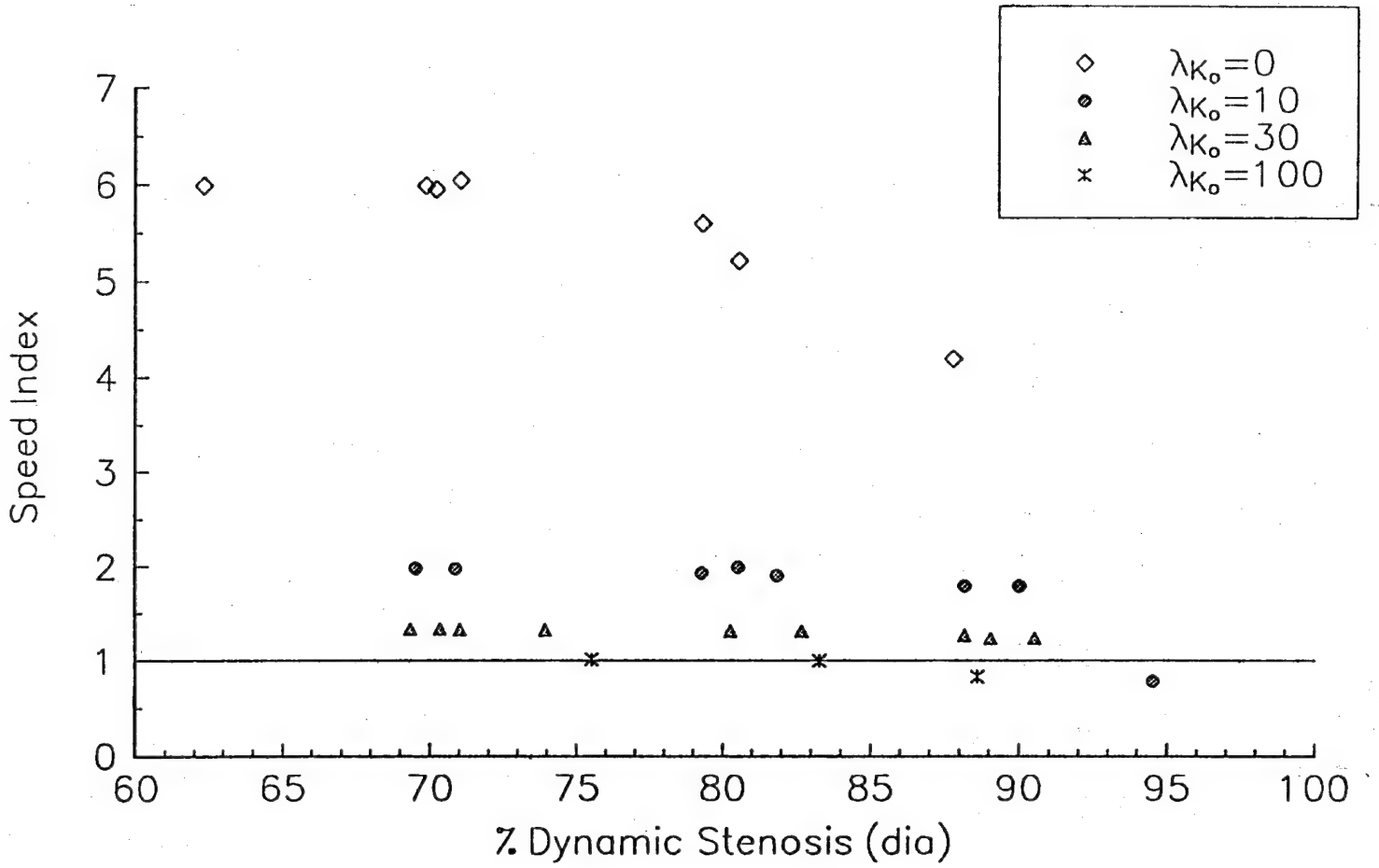

Figure 18c Effect of Stiffness Variations on the Maximum Speed Index versus Dynamic Stenosis Relationship.

Nominal Stiffness: Kp_o. Variations in the nominal tube stiffness, Kp_o, are considered since arteries have a wide variation in physical properties. Kp_o variation was exhibited between the tube stiffness of the bovine and canine carotid arteries, (whose average values differ by a order of magnitude). Thus, to observe the effect that Kp_o had on the flow, a series of solutions were obtained for Kp_o from 12.5 to 625 Pa, (Note that the baseline solutions had Kp=125 Pa). The other parameter were held at their baseline values. The dynamic stenosis ranged from 70% to 90% (dia), and the results are summarized in Table 6. Overall, the changes in the nominal stiffness affected the flow in a similar manner as variation in λ_{K_o}. Since Kp_o variations affected the nominal area, the effect of Kp_o on the flow rates was considered under constant nominal diameter and constant dynamic inlet area conditions. For the constant diameter case, Q_c had a local minimum as Kp_o increased. For a 70% dynamic stenosis the minimum occurred around Kp_o=80 Pa. However, for the constant inlet area case, Q_c increased monotonically with Kp_o, as shown in figure 19a.

P_{min} and S_{max} were reduced by increasing Kp_o similar to the previous findings for changes in λ_{K_o}. The effect on P_{min} is shown in figure 19b. The P_{min} s ranged from 0 to -170 mmHg for changes in Kp_o of 12.5 to 625 Pa. At 90% stenosis, P_{min} for Kp_o=625 was greater than the other values since the flow was no longer critical for this condition. Figure 19c shows S_{max} versus dynamic stenosis for the range of Kp_o values. In this figure, as Kp_o was increased, S_{max} decreased, and for 90% stenosis critical flow was not obtained for the Kp_o=625 Pa case. Therefore, these results demonstrated that as an artery became more stiff, Q_c raised, and the arterial was less likely to collapse. However, if collapse was established, P_{min} was greatly reduced.

In summarizing the effect of compliance, it is important to distinguish between the tube law parameters and the tube stiffness. *n1* and *n2* govern how the tube response to transmural pressure variations, and the stiffness describes the structural characteristics of the tube. Thus, changes in *n1* and *n2* values can be interpreted as changes in the vasoactive response of the artery. As *n1* decreased, the artery expansion was greater which corresponded to a vasodilation, and increases in *n1* would relate to vasoconstriction conditions. The results showed for *n1* values of 4, 7, and 20, the physiologic collapse was enhanced as the tube response stiffened for a given nominal diameter. This trend agreed with the findings of Tulenko et al (62) and Li et al (63) who showed the effects of vasoconstriction were accentuated by the presence of a high grade stenosis. Vasoconstriction within a high grade stenosis reduced the flow rate through an artery compared to normal flow condition. However, the results also showed that for a given dynamic inlet area the *n1* values did not affect the flow. The other effect illustrated by *n1* changes was on the dynamic stenosis. For increasing *n1*, (decreasing compliance), the nominal area reduction has to be increased to generate the same degree of dynamic stenosis. Changing *n1* from 4 to 20, the nominal area reduction had to be increased by 15% to produce a 70% (dia) dynamic stenosis. For an area reduction of 0.88, the *n1*=20 tube solution generated a 70% dynamic stenosis with Q_c=17.2 ml/s whereas the *n1*=4 tube solution generated an 80% dynamic stenosis with a Q_c=19.9 ml/s. Changes in *n2* affected the supercritical regions with only minimal effect on the subcritical region. Increasing *n2* from 1.5 to 4 caused P_{min} to drop 80 mmHg. These changes in *n2* did not affect the occurrence of physiologic collapse, but they showed that a more stiff tube response within the

Table 6. Variations in Nominal Tube Stiffness

Kp_o (Pa)	A_{in} (mm^2)	λ_{A_o}	% Stenosis (dia)	Q_c (D_o=const) (ml/s)	Q_c (A_{in}=const) (ml/s)	P_{min} (mmHg)	S_{max}
12.5	76.5	.800	68.4	40.0	28.8	-2.0	6.22
		.820	70.0	35.9	25.8	-2.5	6.08
		.925	80.8	14.8	10.7	-2.5	5.77
		.985	91.1	2.95	2.12	-1.0	5.00
25	69.3	.820	90.9	32.6	25.9	-5.2	4.30
62.5	60.8	.820	91.2	29.0	26.3	-17.1	2.72
		.915	95.9	13.6	12.3	-18.0	2.63
93.75	57.4	.810	91.1	29.2	28.0	-29.3	2.24
125	55.1	.800	69.5	30.0	30.0	-38.3	1.98
		.915	80.5	12.6	12.6	-38.6	1.92
		.980	90.0	2.91	2.91	-12.8	1.79
250	49.9	.783	91.0	31.6	34.9	-107.	1.49
		.800	92.3	29.1	32.1	-132.	1.49
		.915	96.3	12.2	13.5	-69.4	1.46
625	43.9	.791	70.2	33.0	41.4	-174.	1.14
		.920	80.0	12.5	15.7	-91.8	1.11
		.985	90.0	1.84*	2.31*	13.6	.465

negative pressure region would increase the magnitude of the collapsed pressure. Thus, with the above results, vasoconstriction of a stenotic segment would increase the likelihood of collapse and the collapsed stresses whereas vasodilation of the segment would lessen the chances of collapse occurring in the artery.

The next aspect of compliance involved the structural quality of the artery and the plaque. Increases in the nominal tube stiffness, Kp_o, marginally reduced the chances of physiologic collapse when considering a constant nominal diameter. However, for a constant dynamic inlet area, the likelihood of collapse was enhanced by decreases in Kp_o. The clinical significance of this finding is that arteries with thinner walls would be more susceptible to collapse than an artery with normal wall thickness. The other stiffness effect considered was the variations of stiffness along the stenosis. A series of solutions were obtained for varying local stiffness to estimate a range of plaque structural qualities from completely soft to hard. For a soft plaque, (λ_{K_o}=0), solution, Q_c was reduced by 12.6 % for a 70% stenosis, and by 12.9% for a 80% stenosis from the baseline solution which had a peak local stiffness which was 10 times the nominal stiffness. Also, soft plaques tended to have smaller P_{min} magnitudes ranging from -0.5 to -2.0 mmHg for 70 to 90% stenoses, whereas the

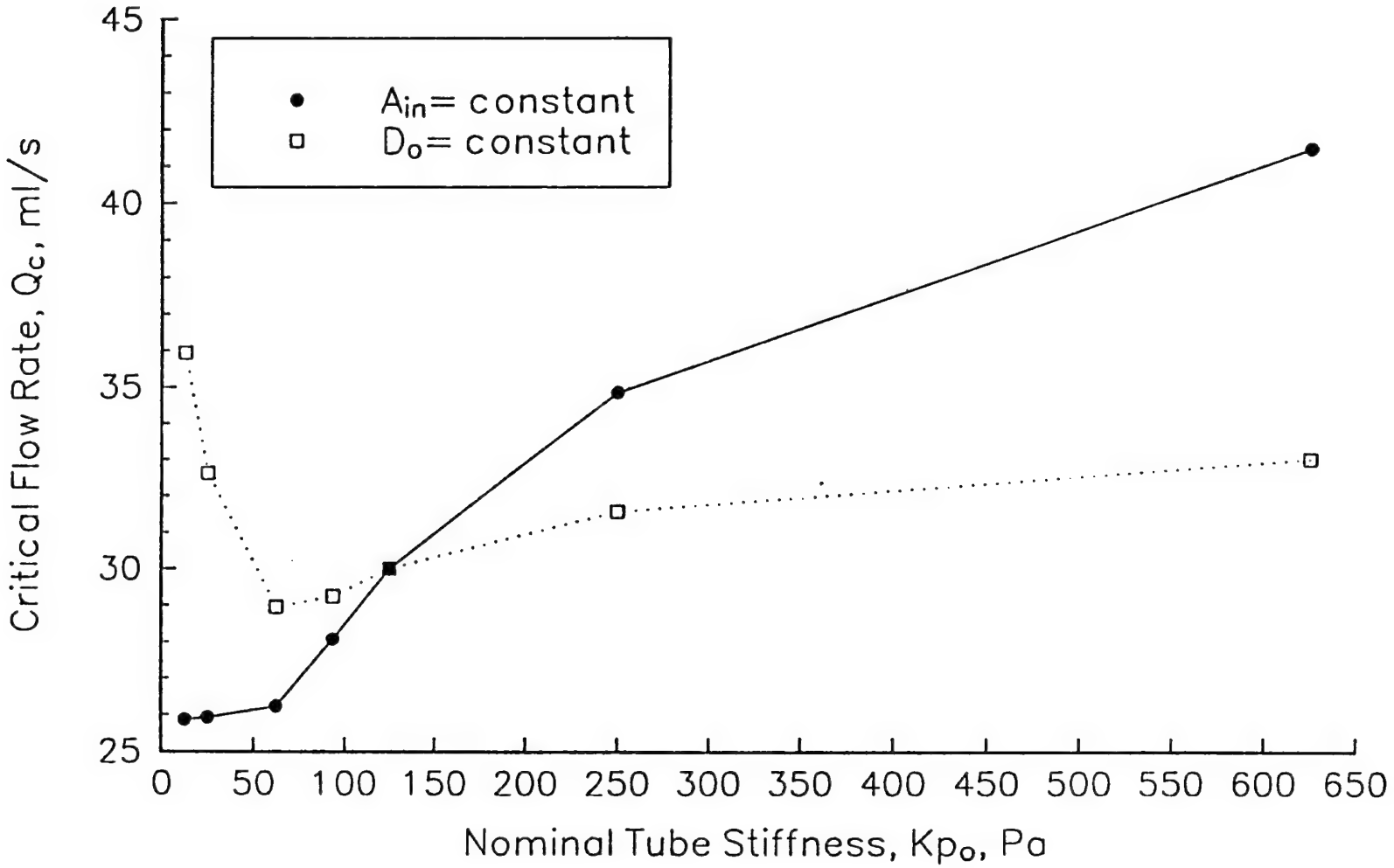

Figure 19a Effect of Nominal Stiffness Variations on the Critical Flow Rate for a 70%(dia) Dynamic Stenosis: Nominal Diameter held Constant (D_o=6.0 mm case) and Dynamic Inlet Area held Constant (A_{in}=55.1 mm^2 case).

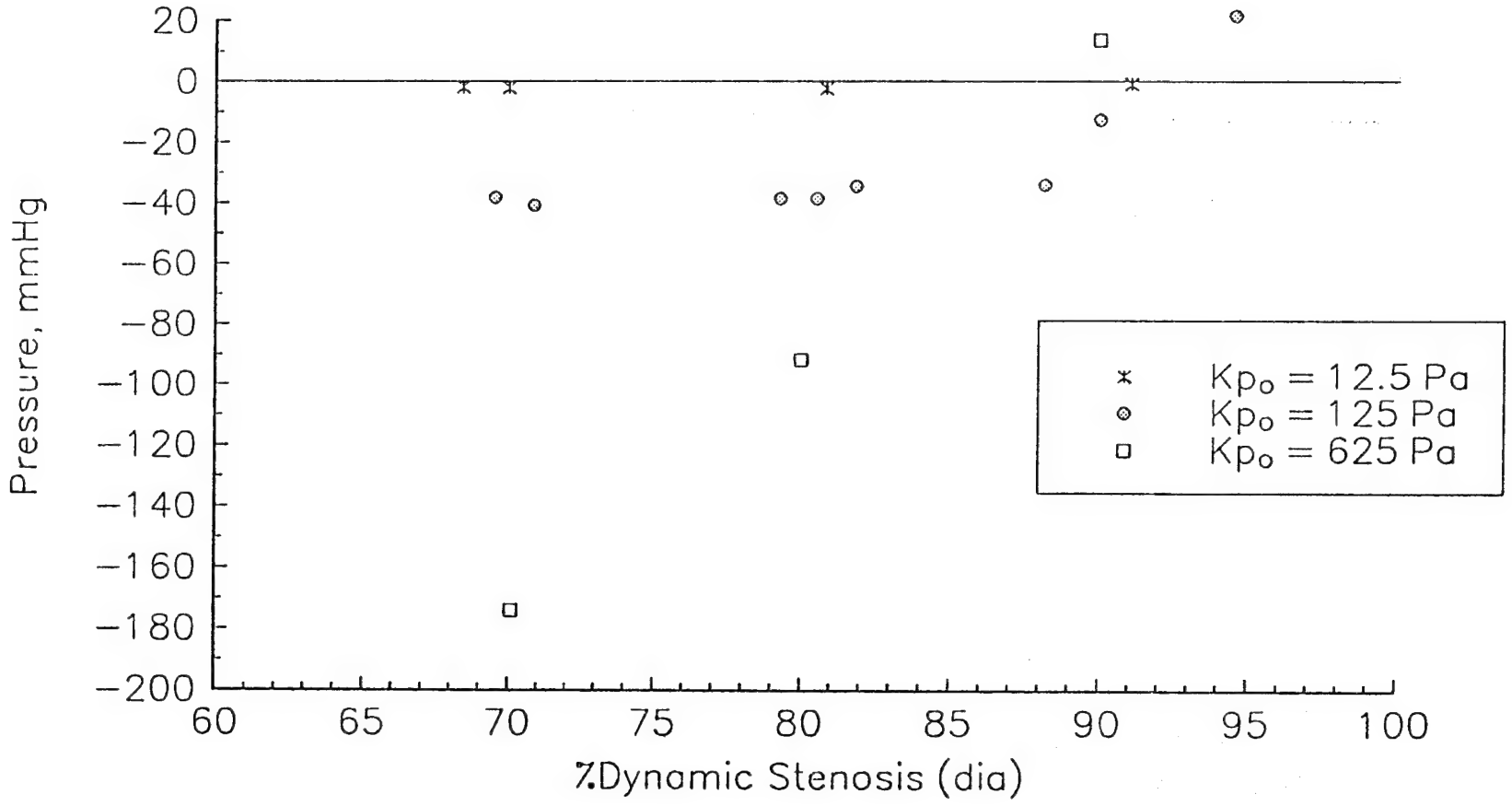

Figure 19b Effect of Nominal Stiffness Variations on the Minimum Pressure versus Dynamic Stenosis Relationship.

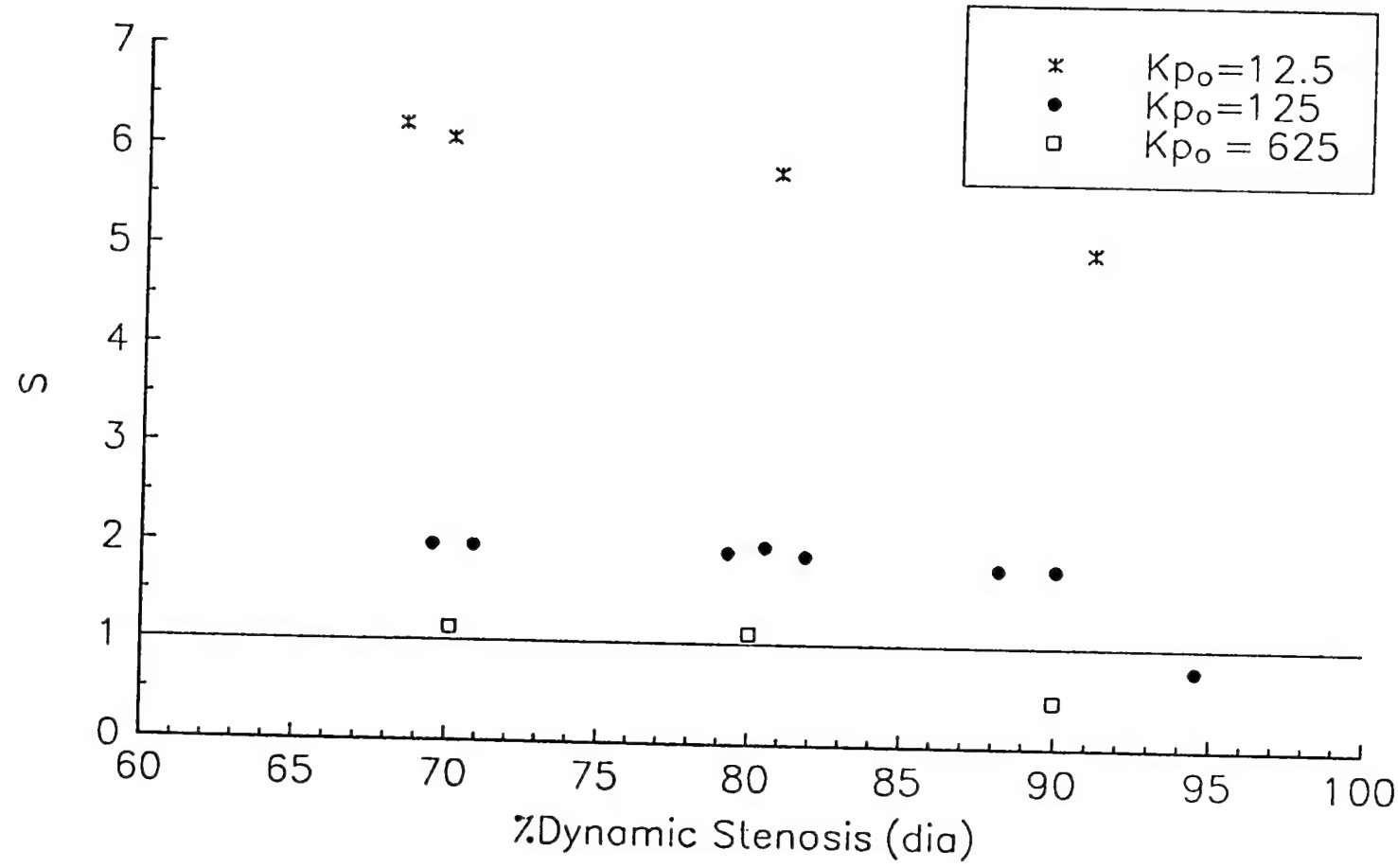

Figure 19c Effect of Nominal Stiffness Variations on the Maximum Speed Index versus Dynamic Stenosis Relationship.

baseline P_{min} values ranged from -12.8 to -38.6 mmHg for the same range of stenoses. This finding reveals that physiologic collapse was enhanced by soft plaques, although the estimated compressive pressure was much smaller for the softer plaques. It should be noted that harder plaques would be able to withstand higher stresses than the soft plaques. Thus, the increased flow rate with increased stiffness points out that calcification within a plaque is a constructive adaptation process, which allows the plaque to withstand greater compressive pressures while increasing the maximum flow rate through the artery. These results agree with the clinical observations that soft plaques are more symptomatic than hard plaques (20). Thus, calcification may be an adaptive mechanism which helps to stent the artery open. This fact is illustrated in the difference in plaques within coronary and carotid arteries compared to those in the iliacs. The iliacs are more susceptible to chronic compression which results in calcification. However, the carotids and coronaries may experience only transient compression resulting in much less calcification within their plaques.

Frictional Losses

Another important factor in stenotic blood flow is the effect of frictional losses. The basic frictional loss incorporated into the model assumed fully developed Poiseuille flow as expressed by equation 16. The basic frictional loss due to fluid viscosity can be determined from the wall shear stress which is estimated from the assumed parabolic velocity profile. However, in the converging section of the stenosis, the velocity profile would be blunted and the velocity radial gradient near the wall would steepen. When this occurs, the assumed parabolic profile underestimates the wall shear stress. Therefore, a series of solutions were obtained for a range of basic friction loss coefficients to examine the effect of increased losses on the flow. Also, the effect of including basic friction loss is shown by a comparison of this model's results with those of a previous inviscid model, which only included losses due to the elastic jump (43).

Since the stenosis had both a converging and diverging sections, flow separation was considered downstream of the throat of the stenosis. This separation term was another source of loss in the flow system in addition to the jump and the basic frictional losses. This additional separation term accounted for possible separation of the flow in the diverging section of the stenosis outside of the jump region. Thus, this additional term used the throat area as a basis for approximating the separation loss arising from an adverse pressure gradient produced by the diverging area of the stenosis.

Effect on f_L on Flow. The basic frictional loss becomes greater as the frictional coefficient, f_L, is increased. Variations in f_L affected the flow system globally since it was applied at every point in the domain. However, the quasisteady analysis showed that the basic loss term becomes most important in the throat region of the stenosis where the area was significantly reduced. Elsewhere, this term was small in magnitude. Moreover, from the analysis of Shapiro (33), friction always drives the flow towards the critical point. To evaluate this effect, a series of runs were calculated for f_L ranging from 5 to 50 with the other parameters held at baseline conditions. The results from these calculation are summarized in Table 7. The effect of f_L on the flow rate versus stenosis relationship is highlighted in figure 20a. This

plot confirms that increasing f_L decreased the critical flow rate, and the plot also reveals that the degree of stenosis required to reach a physiologically choked flow condition was slightly reduced with increasing f_L. It should be noted that for P_2=60 mmHg, the flow was subcritical for f_L=50 and for stenoses >75% (dia) with f_L=35. For both of these cases, critical flow was established by decreasing the distal pressure, P_2, (increase the stenotic pressure drop). The reason for the reduced degree of stenosis can be seen in the effect of f_L on P_{min}, which is displayed in figure 20b. As f_L increased the magnitude of P_{min} was reduced with a correspondingly increased minimum area.

Since friction always drives the flow toward choking, S_{max} was affected by changes in f_L. This effect is provided in figure 20c, which shows that as the frictional loss grew, S_{max} was reduced. Along with reducing S_{max}, frictional losses shortened the supercritical section by driving the supercritical flow back to the critical point and by creating more losses downstream of the jump. Thus, the jump occurred sooner as f_L increased to match the same outlet boundary condition. This shortening of the supercritical section is highlighted in Table 7 and by comparing these results to the inviscid results.

The comparison to the inviscid results involved solutions with the highly compliant tube law ($n1$=4) with f_L=5 and the inviscid model of Ziegler (42). The comparative results are summarized in Table 8 for 70 and 80% (dia) stenoses for a range of distal pressures. For 70% stenosis, basic frictional losses (f_L=5) only reduced the critical flow rate by 3.7% from the inviscid solution, and for 80% stenosis, Q_c was reduced by 8.2%. This comparison shows that basic frictional losses slightly decreased Q_c and these losses increased with the degree of stenosis. The elastic jump location was further downstream for the inviscid case as shown in figures 21a-c. Figure 21a, which displays the pressure along the tube for both cases, shows that the solutions agreed except in the region of the jump. Also, the small effect of friction on S_{max} is evident in Table 8 and figure 21b. From these, S_{max} was only reduced by 3% when the frictional losses were included in the solution. The difference in these results were produced by the explicit modelling of the laminar frictional losses. As expressed in the quasisteady analysis, friction becomes an important factor in the supercritical region because of the reduced areas and the greatly accelerated velocities. Overall, basic frictional losses incorporated in this model conformed to the analysis of Shapiro (33) which stated that friction always forces the flow toward choking. This influence of friction was exhibited in the above results by the shortening of the supercritical region, figure 21c, and the reduction of the flow rate with increased f_L, Table 8.

Table 7 Summary of Results for Variations in f_L

Frict. Coef. f_L	λ_{A_o}	% Stenosis (dia)	Q (ml/s)	P_{min} (mmHg)	S_{max}	Jump Location (ξ)
5	.80	69.5	30.0	-38.3	1.98	1.80
10		69.5	29.6	-34.2	1.94	1.78
25		67.9	28.4	-16.6	1.82	1.70
35		67.4	27.6	-6.0	1.48	1.64
50		64.5	24.1*	36.0	.53 (P_2=60)	--
50		67.0	26.4	0.3	1.21 (P_2=50)	1.62
50		67.1	26.4	-11.9	1.59 (P_2=40)	1.70
5	.920	81.8	11.9	-34.0	1.90	1.66
10		80.5	11.6	-25.0	1.66	1.66
35		77.6	9.67*	33.1	.56	--
50		77.0	7.36*	53.5	.33	--
5	.970	88.2	4.39	-34.0	1.79	1.60
10		87.8	4.26	-10.0	1.70	1.58
35		85.9	2.52*	56.3	.28	--
50		85.9	1.84*	71.0	.19	--
5	.980	90.0	2.91	-12.8	1.79	1.58
10		89.5	2.80	-3.8	1.39	1.56
35		88.2	1.41*	59.7	.23	--
50		88.2	1.03*	73.9	.16	--

Table 8. Comparison to the Inviscid Model of Ziegler

% Stenosis (dia)	P_2 (mmHg)	Q_{Frict} (ml/s)	Q_{INV} (ml/s)	$P_{minFrict}$ (mmHg)	P_{minINV} (mmHg)	$S_{maxFrict}$	S_{maxINV}
70	60	26.9	27.9	-15.6	-17.4	2.79	2.89
70	40	26.9	27.9	-17.5	-18.4	2.82	3.18
80	60	12.1	13.2	-19.5	-24.5	2.54	2.62
80	40	12.1	13.2	-32.5	-43.2	2.54	2.62
80	20	12.1	13.2	-39.6	-61.8	2.54	2.62

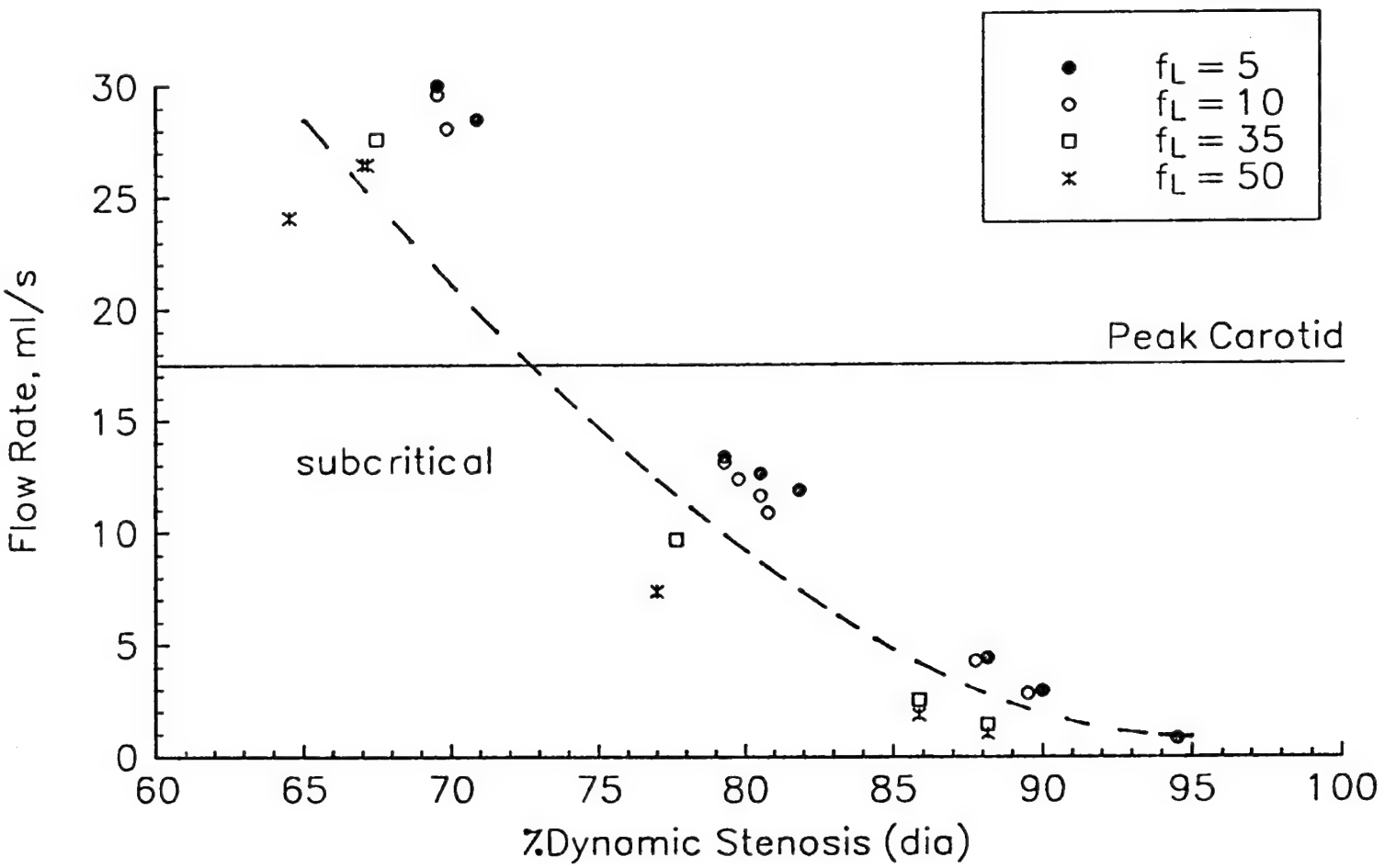

Figure 20 a Effect of Basic Friction Loss in the Critical Flow Rate versus Dynamic Stenosis Relationship.

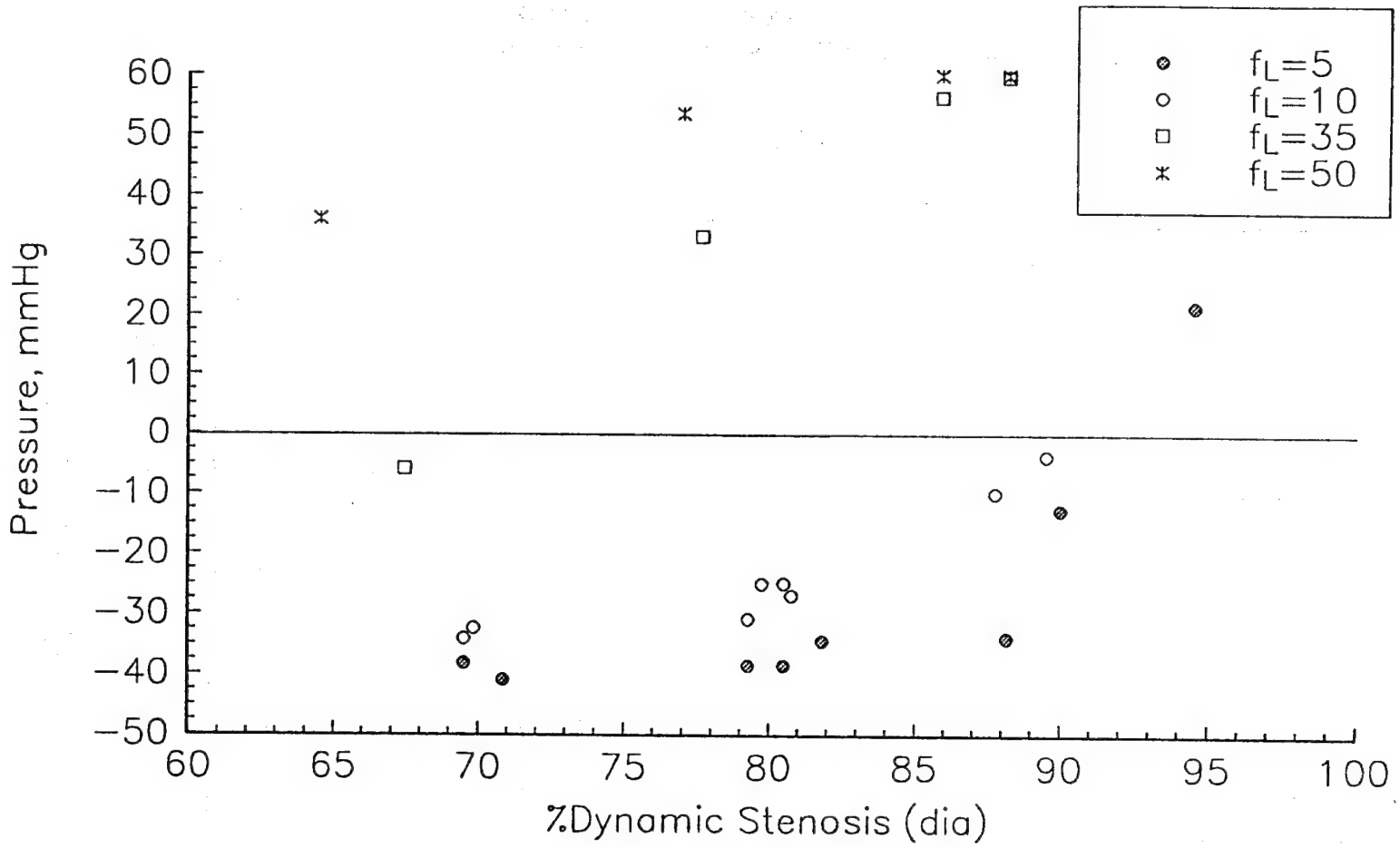

Figure 20 b Effect of Basic Friction Loss on the Minimum Pressure versus Dynamic Stenosis Relationship.

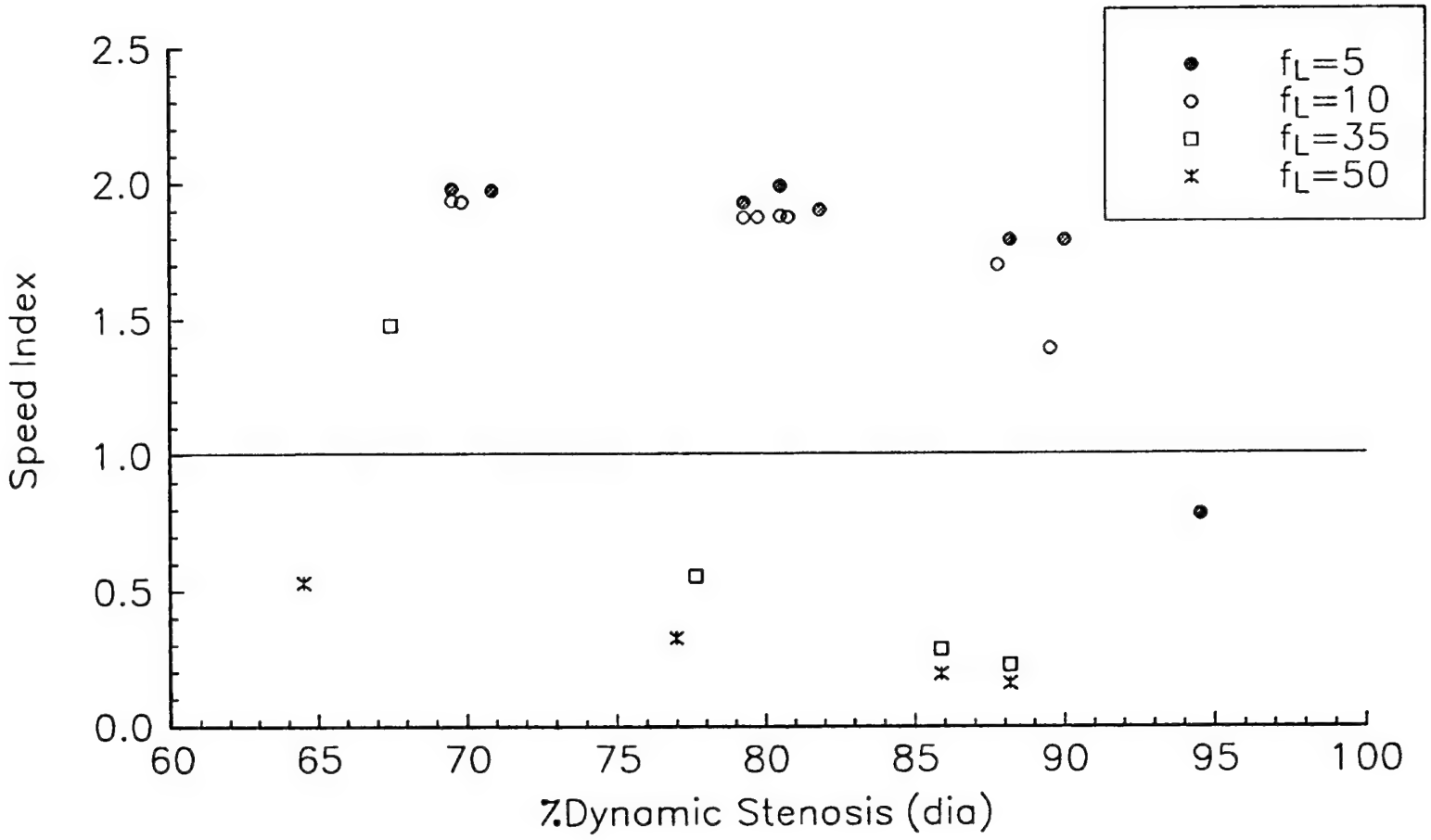

Figure 20c Effect of Basic Friction Loss on the Maximum Speed Index versus Dynamic Stenosis Relationship.

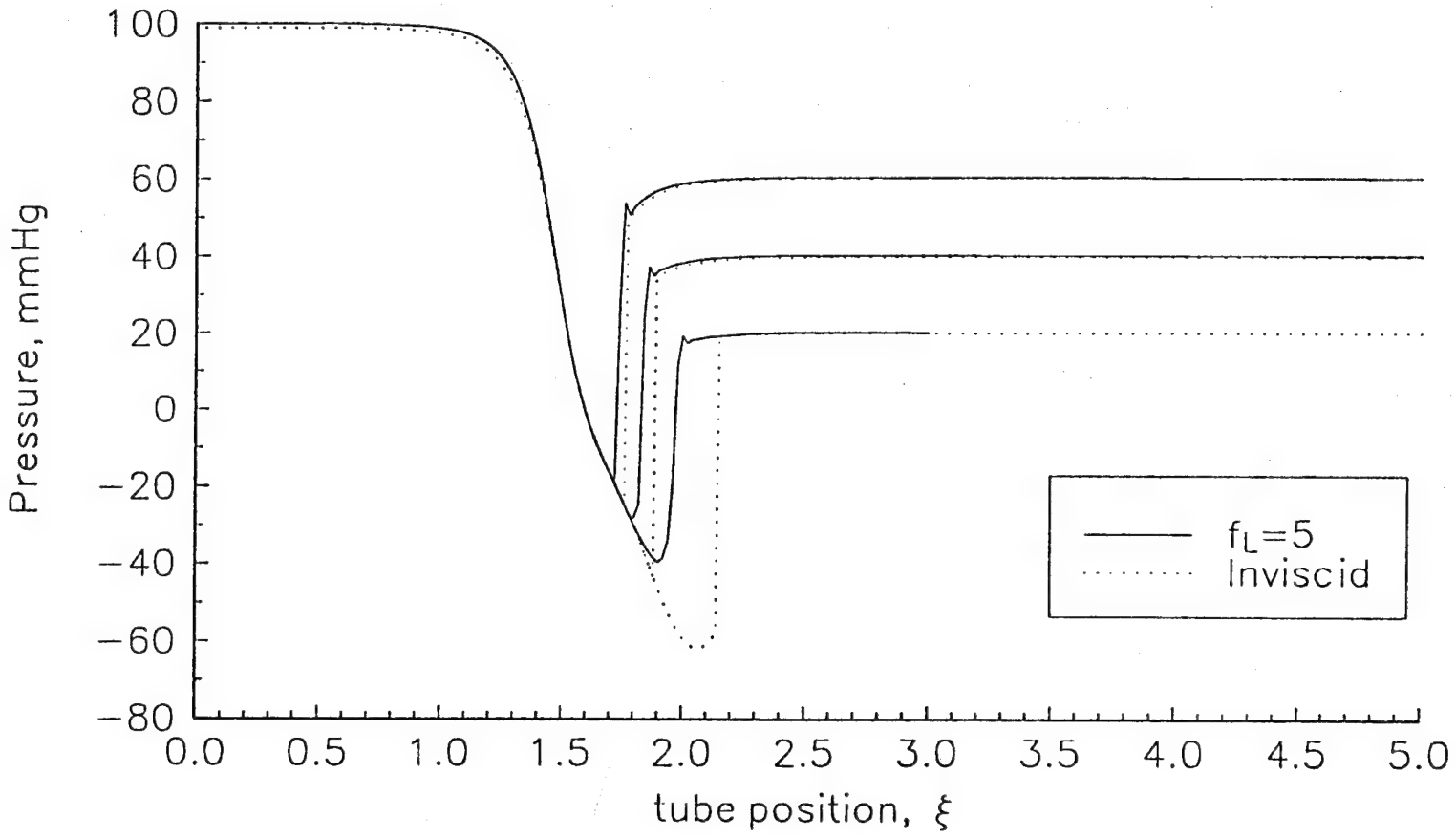

Figure 21a Comparison with Inviscid Model: Pressure Curves for a Range of P_2 settings with $n1$=4, and an 80%(dia) Dynamic Stenosis.

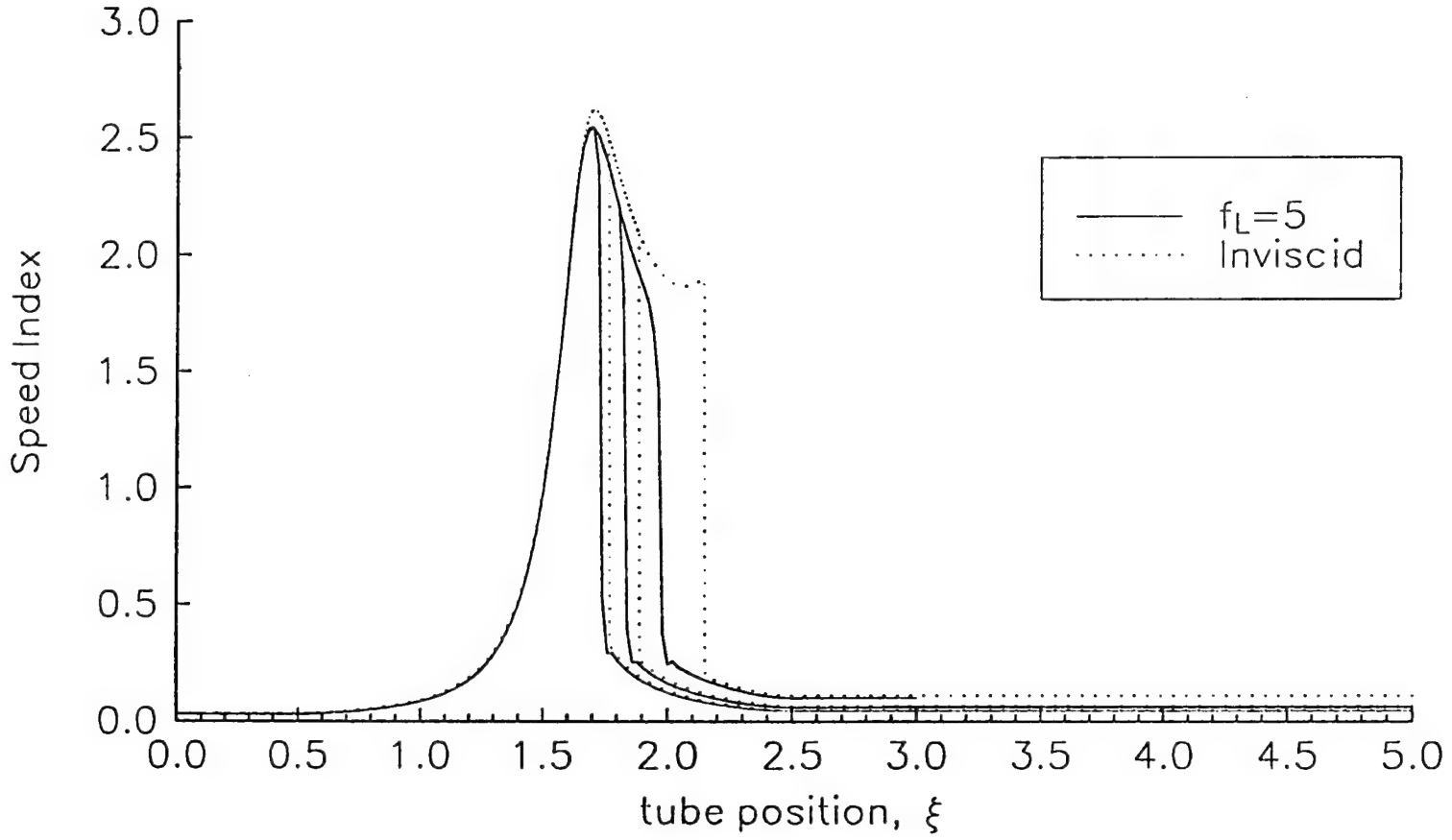

Figure 21 b Comparison with Inviscid Model: Speed Index Curves for Various Distal Pressure Settings

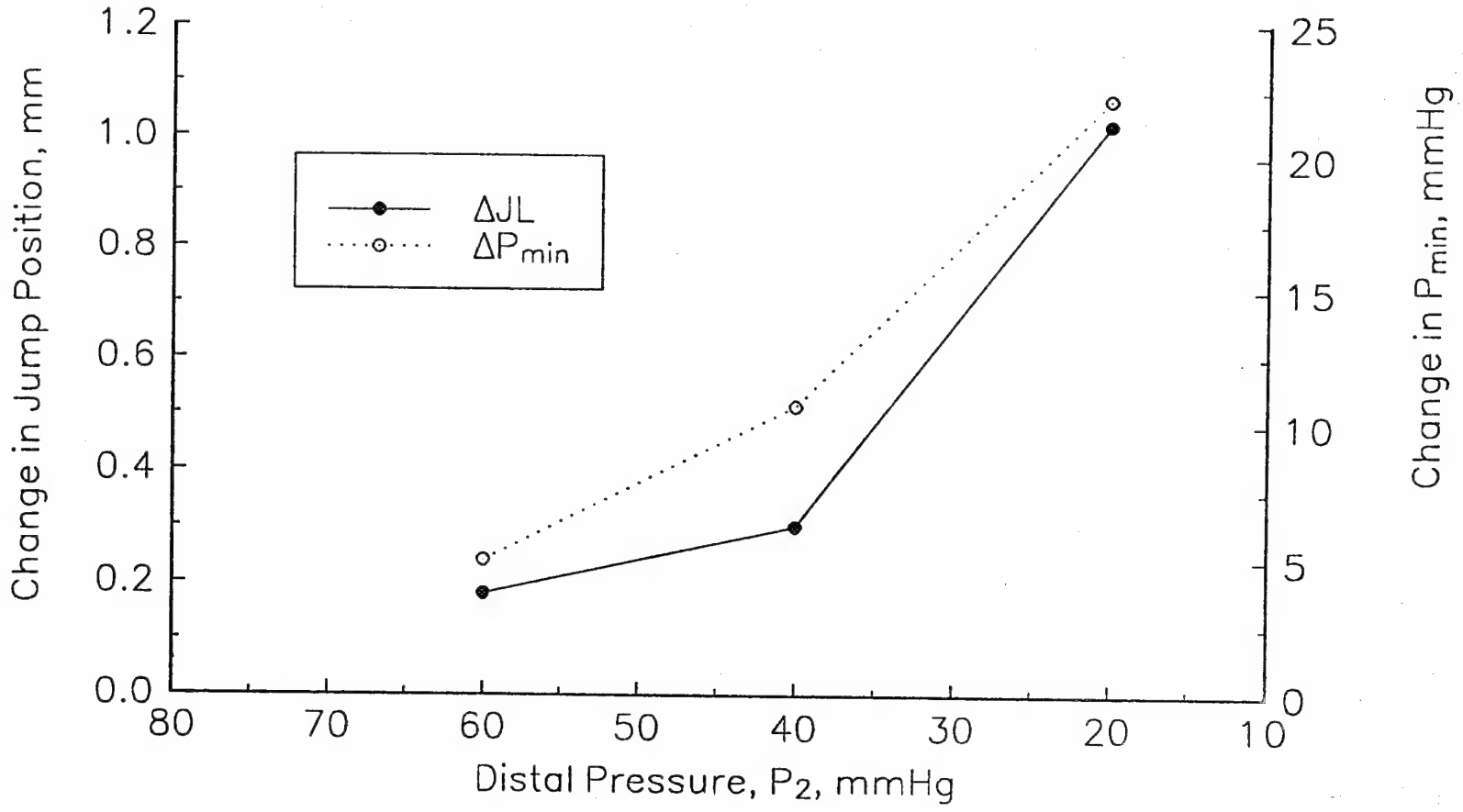

Figure 21c Comparison with Inviscid Model: Difference between Elastic Jump Location and Minimum Pressure (Viscous-Inviscid) versus the Distal Pressure.

Separation Losses. Now, the effect of the additional separation loss is considered. It should be noted that the loss term was applied over a length of two nominal diameters after the jump for critical flow or after an adverse pressure gradient for subcritical flows. This series of solutions was calculated with the additional separation loss term as defined in equation 19b. The coefficient, K_{Sep}, was varied from 0 to 1.0, while the other parameters were set at the baseline conditions. These results are summarized in Table 9. These results show that the additional loss could prevent the establishment of critical flow for the given 40 mmHg pressure drop. For $K_{Sep} > 0.25$, the flows were subcritical throughout the domain for an outlet pressure of 60 mmHg. This impediment to the establishment of critical flow had the effect of increasing P_{min} and reducing S_{max}. This additional separation term generated more loss downstream of the throat which forced the throat pressure to increase so that the distal boundary condition could be met. This effect was clearly exhibited in the pressure curves for the various setting of K_{Sep}, as shown in figure 22. For the two critical solutions (K_{Sep}= 0 and 0.25), the upstream pressures were identical as expected, but P_{min} was increased and the supercritical length was reduced when the additional loss term was added. However, for K_{Sep}=0.5 and 1.0, critical flow was not established with P_2=60mmHg, and the additional loss influenced the upstream conditions. For the K_{Sep}=1.0 case, the throat pressure was greater that the distal pressure.

This series demonstrated that the inclusion of the additional separation loss term impeded the establishment of critical flows although this term did not affect the critical flow rates. This term increased P_{min} and decreased both S_{max} and the degree of dynamic stenosis by shortening the supercritical length. Thus, separation effects are important in determining the stenotic pressure gradient needed to establish critical flow through a stenotic artery.

Table 9. Effect of Additional Separation Loss Term on Flow Solution

Separation Coef. K_{Sep}	% Stenosis Diameter)	λ_A	Q_c (ml/s)	P_{min} (mmHg)	S_{max}
0	69.5	.800	30.0	-38.6	1.98
.25	70.2	.821	26.8	-15.0	1.9
.5	69.8	.854	32.7*	32.7	.67
1.0	70.0	.866	15.1*	63.4	.37
0	80.5	.915	12.6	-38.6	1.92
.25	79.8	.916	12.5	-14.7	1.85
.5	79.8	.935	8.97*	36.3	.62
1.0	79.7	.939	6.65*	64.2	.36
0	90.0	.980	2.91	-12.8	1.79
.25	87.0	.980	2.89*	15.1	.89
.5	90.0	.985	1.85*	48.3	.48
1.0	89.3	.983	1.71*	67.1	.32

The inclusion of frictional losses distributed throughout the flow domain was an important improvement of this model. This improvement incorporated two types of losses into the model: basic viscous losses and separation losses, in addition to the losses incorporated into the elastic jump relationships. The basic friction factor was increased to approximate the effects of the converging wall and possible increases in the fluid viscosity. As f_L was increased from 5 to 50, the larger frictional loss drove the flow towards the critical point faster. For an area reduction of .92, doubling f_L decreased the flow rate slightly from 11.86 to 11.63 ml/s, but for a ten fold increase in f_L the flow decreased from 11.86 to 7.36 ml/s. For this case the dynamic stenosis was reduced from 81.8% to 77.0%. Also, the tenfold increase delayed the onset of the critical point and lessened the magnitude of P_{min} from -34.0 to 53.5 for an outlet P_2 of 60 mmHg. For the doubling of f_L, P_{min} was increased from -34.0 to -25.0 mmHg. Thus, the effect of the basic loss term was twofold. The increased losses enhanced collapse by decreasing the flow required to induce collapse. However, the increased losses required lower distal pressures for collapsed flow to become established. Clinically, it is important to note that a trade off exists when considering viscous frictional loss in that decreasing blood viscosity (i. e. hemodilution) requires higher critical flow rates, but a higher distal pressure can establish collapsed flow and its resultant compressive stresses on the plaque.

The additional separation term included possible losses arising from separation from the diverging section of the stenosis outside of the elastic jump. The results showed that additional separation losses could delay the onset of critical flow and lessen the magnitude of P_{min}, but it would not effect the critical flow rate since it can only influence the downstream section during critical flow. This study considered a range of K_{Sep} from 0 (baseline) to 1.0. This term is important in establishing the exact onset of critical flow since it can delay the onset by a substantial margin. Also, this term becomes the dominate loss term in the case of sub-critical flow since no elastic jump will be present in the flow. The clinical significance of separation losses lessen the chances of physiologic collapse because lower distal resistances or pressures are required to establish collapsed flow.

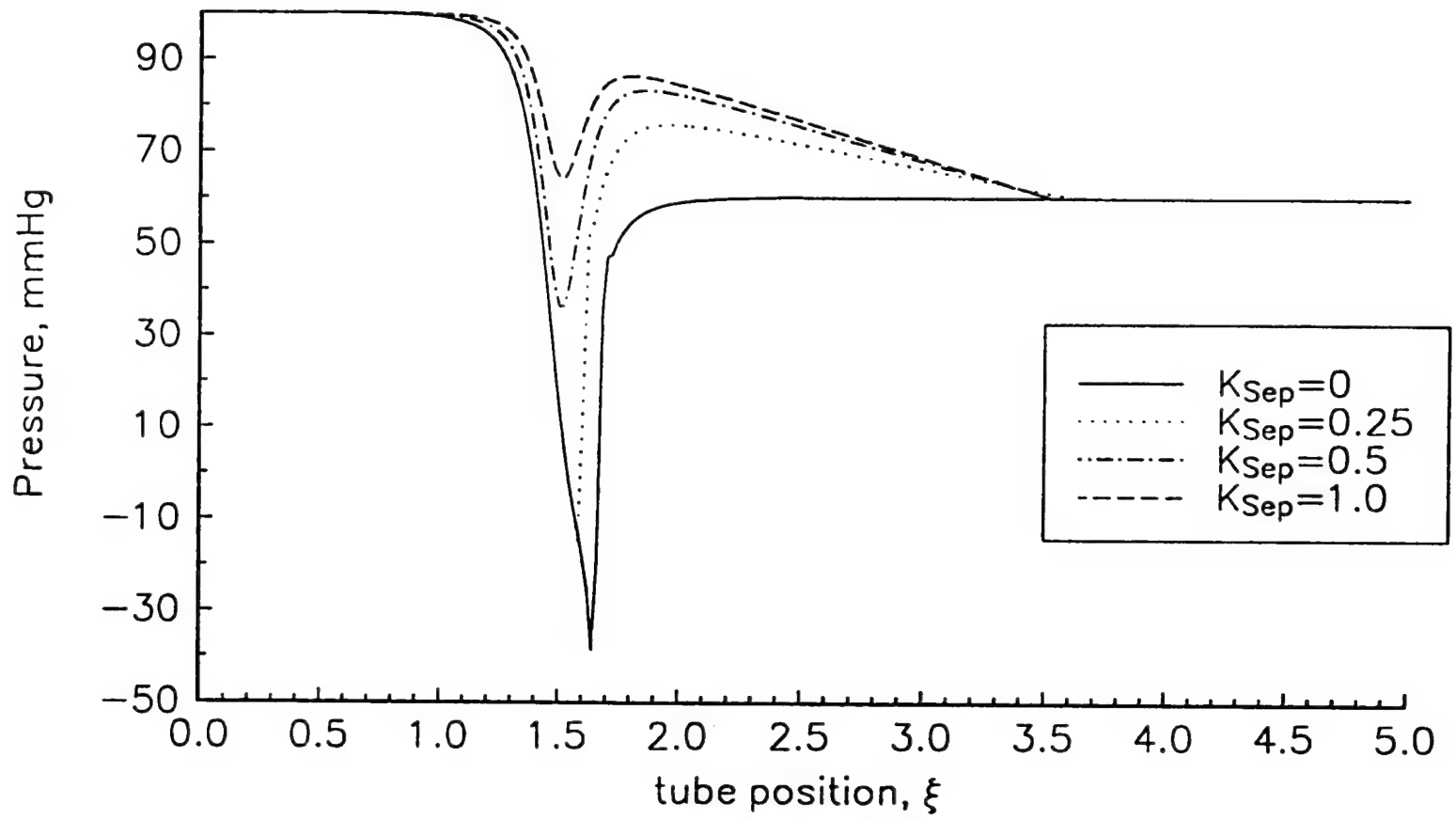

Figure 22 **Effect of Additional Separation Loss on Pressure Curves for an 80%(dia) Dynamic Stenosis with P_1=100 mmHg, and P_2=60 mmHg.**

Perfusion Pressure, P_1

The inlet, or perfusion, pressure is another parameter which affects the flow through a stenotic artery. Increases in P_1 have been shown to increase the flow rate in excised arteries (57). This effect is expected since increasing P_1 expands the lumen. To demonstrate the influence of P_1 on the flow, a series of solutions for 80 and 90% (dia) dynamic stenoses with the three simplified tube laws were calculated with P_1 ranging from 50 to 200 mmHg with a constant P_1-P_2 of 40 mmHg. Results from this series are listed in Tables 10.a-c, which provide the critical flow rates, P_{min} and S_{max}, respectively. The critical flow rate increased with P_1, as shown in figure 23a which plots the critical flow rate versus P_1. Compared to the baseline P_1 of 100 mmHg with an 80% stenosis, the flow rate increased by 33 to 64% for an increase in P_1 to 200 mmHg with the nominal diameter held constant. Holding the inlet area constant resulted in flow rate increases of 43 to 53%. For a decrease in P_1 to 50 mmHg, the flow rate decreased by 29 to 37% for D_o held constant and 32 to 36% for a constant inlet area. Thus, physiologic collapse will occur at lower degrees of stenoses as P_1 is lowered, as displayed in figure 23b which plots the critical flow rate versus the degree of stenosis for the different P_1 settings..

P_1 also influenced P_{min} and S_{max}. P_{min} increased with the perfusion pressure, and the rate of this increase varied between the *n1*=4 and 20 and the *n1*=7 solutions because of the differences in the *n2* values. S_{max} also increased with P_1 for all of the cases except when *n1*=20 with a 90% stenosis. In this case, S_{max} decreased when P_1 increased, and the flow was subcritical when P_1=200 mmHg. This unique result arises from the influence of the tube law coupled with the high grade stenosis. As P_1 increased, the pressure moved into the stiff region of the tube law and, for this case, never reached the flattened, or compliant, regime of the curve. Thus, larger pressure drops were required to reach the compliant regime of the tube law where the wave speed becomes reduced. The result appeared first in the stiff tube law (*n1*=20) case since it has the most steep pressure/area relationship with correspondingly high wave speeds. This situation will appear with the other tube laws with further increases in P_1. Therefore, the combination of the more stiff tube law with increasing P_1 can impede critical flow, but when critical flow is established, increasing P_1 results in increasing S_{max} and P_{min}. Overall, increasing P_1 always increases the flow rate and can prevent collapse.

Table 10a. Inlet Pressure Effects on the Flow Rate

% Stenosis (dia)	Q_{50} (ml/s)	Q_{100} (ml/s)	Q_{200} (ml/s)	Tube Law *n1*
80	12.6	19.9	32.8	4
	11.1	12.6	18.1	7
	5.34	7.48	10.8	20
90	2.67	4.98	8.15	4
	1.92	2.91	4.48	7
	0.95	1.38	1.67*	20

Table 10b. Inlet Pressure Effects on the Minimum Pressure				
% Stenosis (dia)	P_{min} (50) (mmHg)	P_{min} (100) (mmHg)	P_{min} (200) (mmHg)	Tube Law *n1*
80	-36.6	-19.5	-5.0	4
	-80.0	-38.6	-15.0	7
	-30.5	-22.5	-13.8	20
90	-27.4	-19.6	0.2	4
	-34.3	-12.8	3.6	7
	-16.2	-4.3	80.2	20

Table 10c. Inlet Pressure Effects on the Maximum Speed Index				
% Stenosis (dia)	S_{max} (50)	S_{max} (100)	S_{max} (200)	Tube Law *n1*
80	1.87	2.54	2.90	4
	1.46	1.92	2.40	7
	2.17	2.98	4.10	20
90	1.75	2.38	2.67	4
	1.37	1.79	1.84	7
	1.73	1.06	0.34	20

Also, since vasodilation or vasoconstriction should make the artery more or less compliant, this series also highlighted the same trends shown by Higgins et al (57). Their data showed that vasoconstriction combined with a reduction in P_1 reduced the flow by 87% for changes in P_1 from 150 to 75 mmHg. A similar reduction of 77% was interpolated from the model results between *n1*=4 and *n1*=20 for an 80% (dia) stenosis. Thus, the effect of perfusion pressure demonstrated that if P_1 was reduced either by lowering the blood pressure or by increasing the external pressure, the chances of physiologic collapse was enhanced. This is important for the carotid artery since a Valsalva maneuver can create sufficiently high external pressures to reduce P_1 to critical levels.

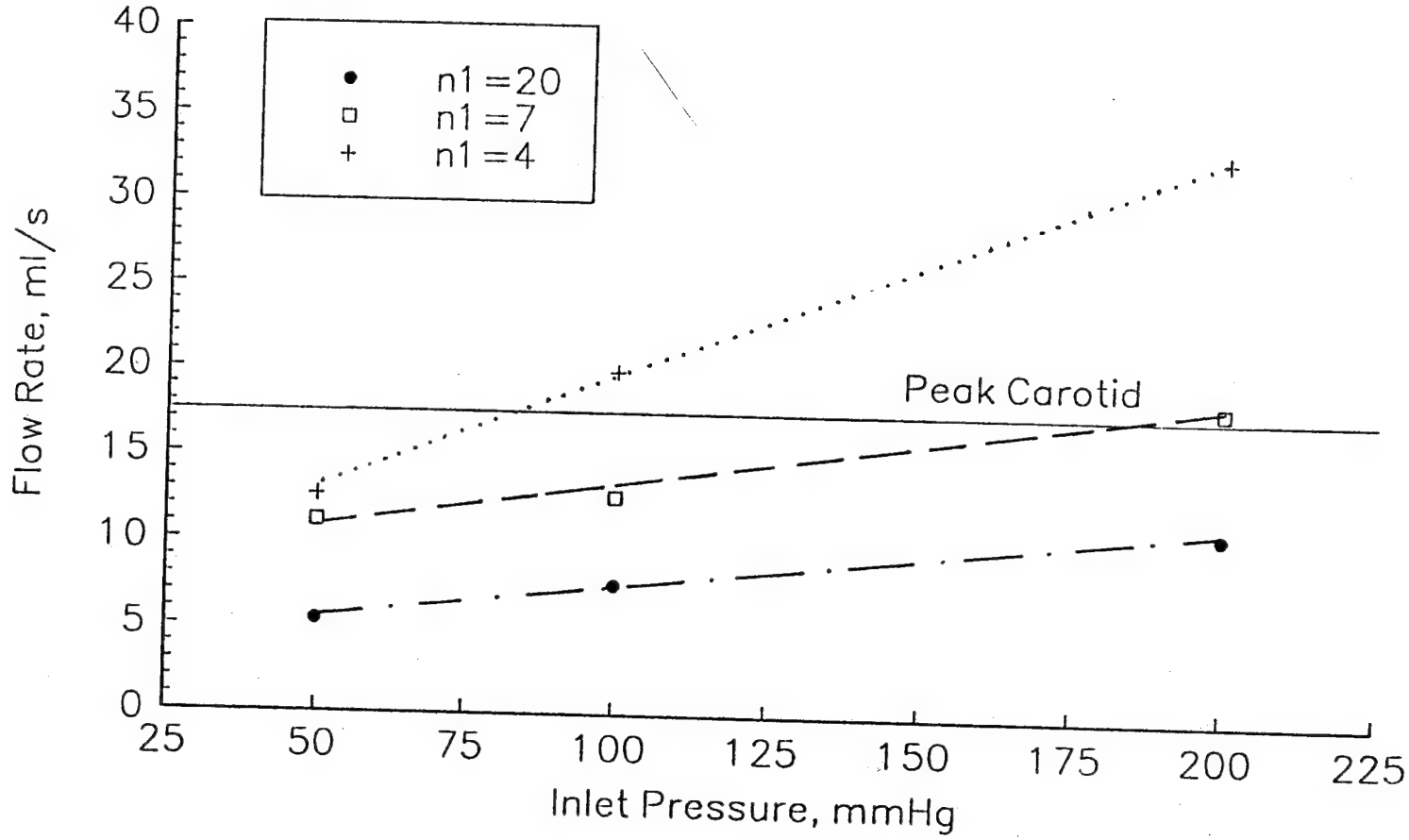

Figure 23a Effect of Inlet Pressure Variation on the Critical Flow Rate for an 80%(dia) Dynamic Stenosis with Stenotic Pressure Gradient of 40 mmHg.

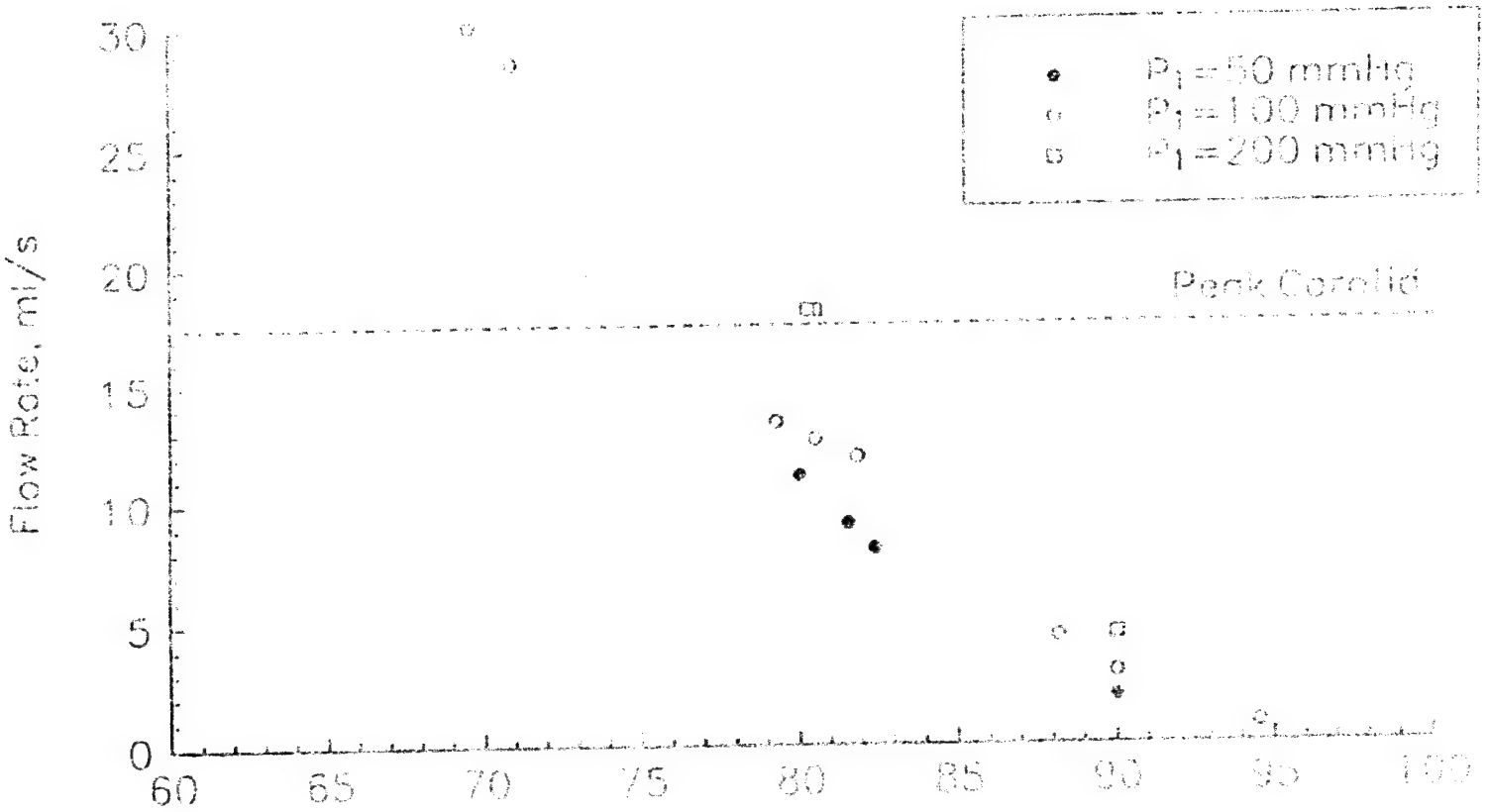
Flow Rate, ml/s
30
25
20
15
10
5
0
60
65
70
75
80
85
90
95
100
P_1=50 mmHg
P_1=100 mmHg
P_1=200 mmHg
Peak Coronary

Figure 15b

Unsteady Solutions

The final series of results considers unsteady effects on the flow. The dimensional analysis has shown that the unsteady term is small in magnitude when compared to the convective acceleration and friction terms. Several unsteady solutions were obtained to illustrate unsteady effects and the conditions under which cyclic collapse could occur. For this series, deterministic variations were applied to the inlet pressure with the downstream boundary condition set by imposing a constant distal resistance as described in Chapter 2. Solutions were calculated for f=1, 5, and 10 Hz with low, moderate, and high distal resistance settings. The other parameters defining the system were set at baseline values. A nominal area reduction of λ_{A_o} =.915 was used and corresponds to an 80% dynamic stenosis for the steady flow solution with P_1=100 mmHg. The pressure pulse of 120/80 resulted in an area change of 3.0 mm^2 or 5% of the average inlet area. The three distal resistance settings were 1.26, 5.05, and 6.10 mmHg/(ml/s).

The averaged flow rates versus the phase of the cycle is provided in figure 24a, for each distal resistance setting. Unsteady effects generated very small changes in the variables with the most pronounced occurring for the case where the flow was subcritical throughout the cycle, (R_{dis}=6.10 mmHg/(ml/s)). The effect was almost negligible for the case where the flow was supercritical throughout the cycle, (R_{dis}=1.26 mmHg/(ml/s)). For the high distal resistance setting of 6.10 mmHg/(ml/s), the flow varied from 8.52 to 12.6 ml/s. The flow varied from 10.4 to 13.3 ml/s for the low distal resistance setting of 1.26 mmHg/(ml/s). For the moderate distal resistance setting of 5.05 mmHg/(ml/s), the flow varied from 9.45 to 13.3 ml/s, and it transition between subcritical (65% of cycle) and supercritical (35% of cycle) states during the systolic cycle.

The transition of the flow is highlighted by the variation in S_{max} along the cycle, as shown in figure 24b. For the moderate distal resistance setting, S_{max} varied from an initially subcritical value to supercritical values during the systolic portion of the cycle. During the deceleration phase and into the diastolic cycle, S_{max} returned to subcritical values. S_{max} varied approximately from 0.54 to 1.60 for this case. For the other cases, the variation in S_{max} was 0.42 to 0.65 and 1.56 to 1.90 which were much smaller than the transition case. Moreover, the distortion of this curve suggests that non-linear effects were occurring within the transitioning flow. This distortion did not appear in the other curves since they retained their sinusoidal shape. Also, in the transitioning and subcritical cases, phase lags of approximating 35° can be observed for increases in the frequency.

Correspondingly, the transition of the flow created larger variations in P_{min} as shown in figure 24c. For this case, P_{min} varied 34 mmHg (from -4.5 to 29.5 mmHg) whereas for the other cases P_{min} varied only 6 mmHg (from 36.6 to 42.4 mmHg) for the high distal resistance case and 16 mmHg (from -45.3 to -29.2) for the low distal resistance case. These transition pressure variations resulted in a large cyclic collapse of the stenotic section of the artery. For the other cases, the pressure remained either positive or negative throughout the cycle, and the artery was not being transition between expanded and collapsed states. This transition was also highlighted in the changes of the minimum area as shown in figure 24d. A_{min} varied by 0.36 mm^2, or 13% of the average A_{min}, for this transitioning flow, whereas A_{min} varied by 0.03, or 1% of the average, and 0.14 mm^2, or 6% of the average for the subcritical and supercritical cases,

respectively. The corresponding minimum diameter changes for the transitioning case were 0.12 mm or 7%. Also, the phase response was reversed for the transition flow since the minimum occurs during systole. This response of the flow agreed with the experimental observations of Binns and Ku (29) who noted that collapse first occurred during systole. This cyclic nature can produce large stresses on the stenosis and set up conditions for fatigue of the underlying plaque, which has been suggested by McCord (68) as a possible mechanism leading to disruption of the plaque.

Overall, the unsteady effects resulted in some minor variations in the flow variables for a given distal resistance. The major effect demonstrated by this series of unsteady solutions is the sensitivity of the flow in relation to the boundary conditions. Only small reductions in the distal resistance between the high and moderate settings produced this transition of the flow during the systolic portion of the cycle. Also, when cyclic collapse occurred, large variations were generated in P_{min}, S_{max}, and A_{min}.

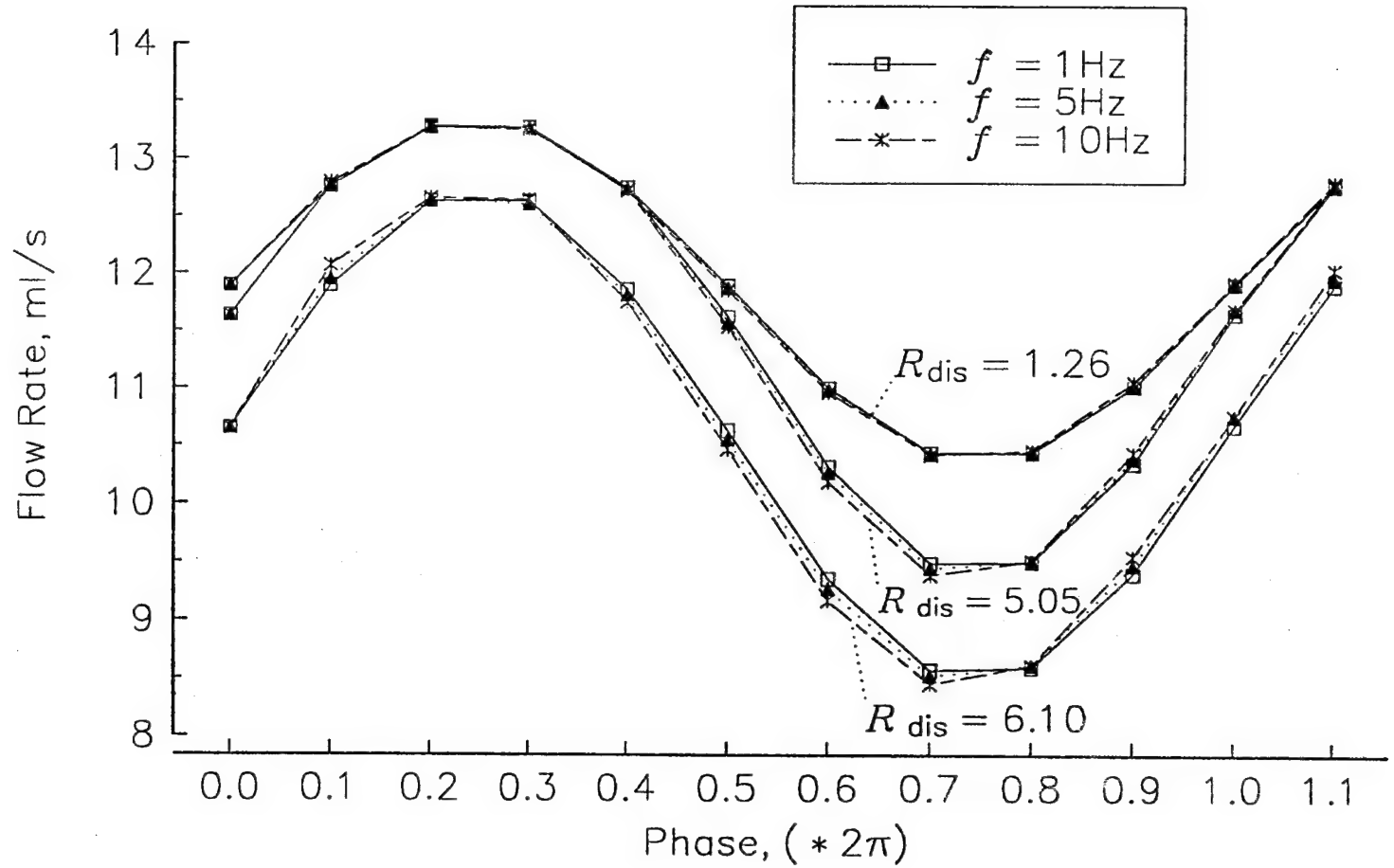

Figure 24 a Unsteady Solutions with Sine Wave Variation in P_1: Flow Rate versus Phase with the baseline parametric values: except for f_L=20, K_{Sep}=.2

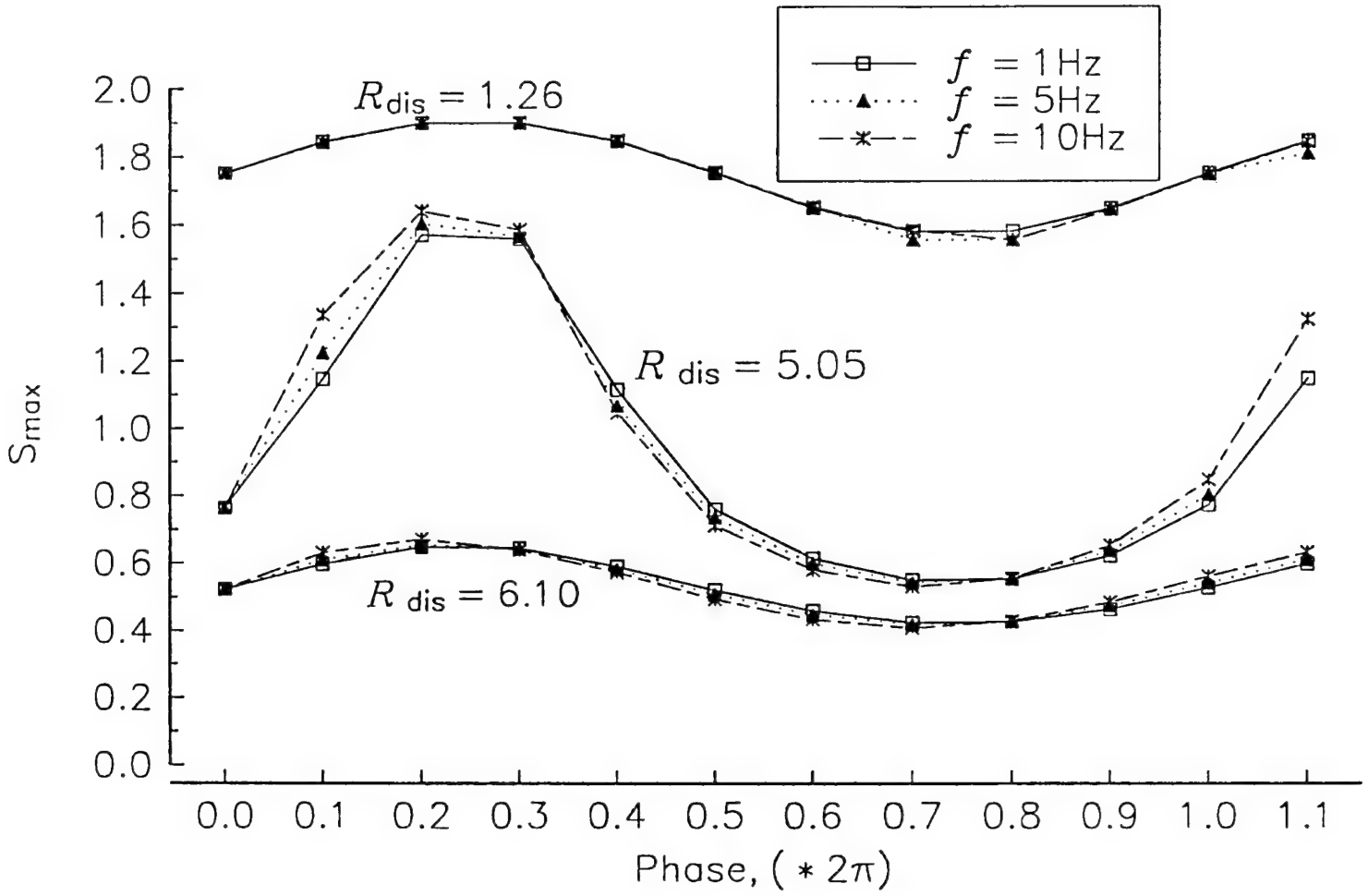

Figure 24 b Unsteady Solutions with Sine Wave Variation in P_1: S_{max} versus Phase with the baseline parametric values: except for f_L=20, K_{Sep}=.2

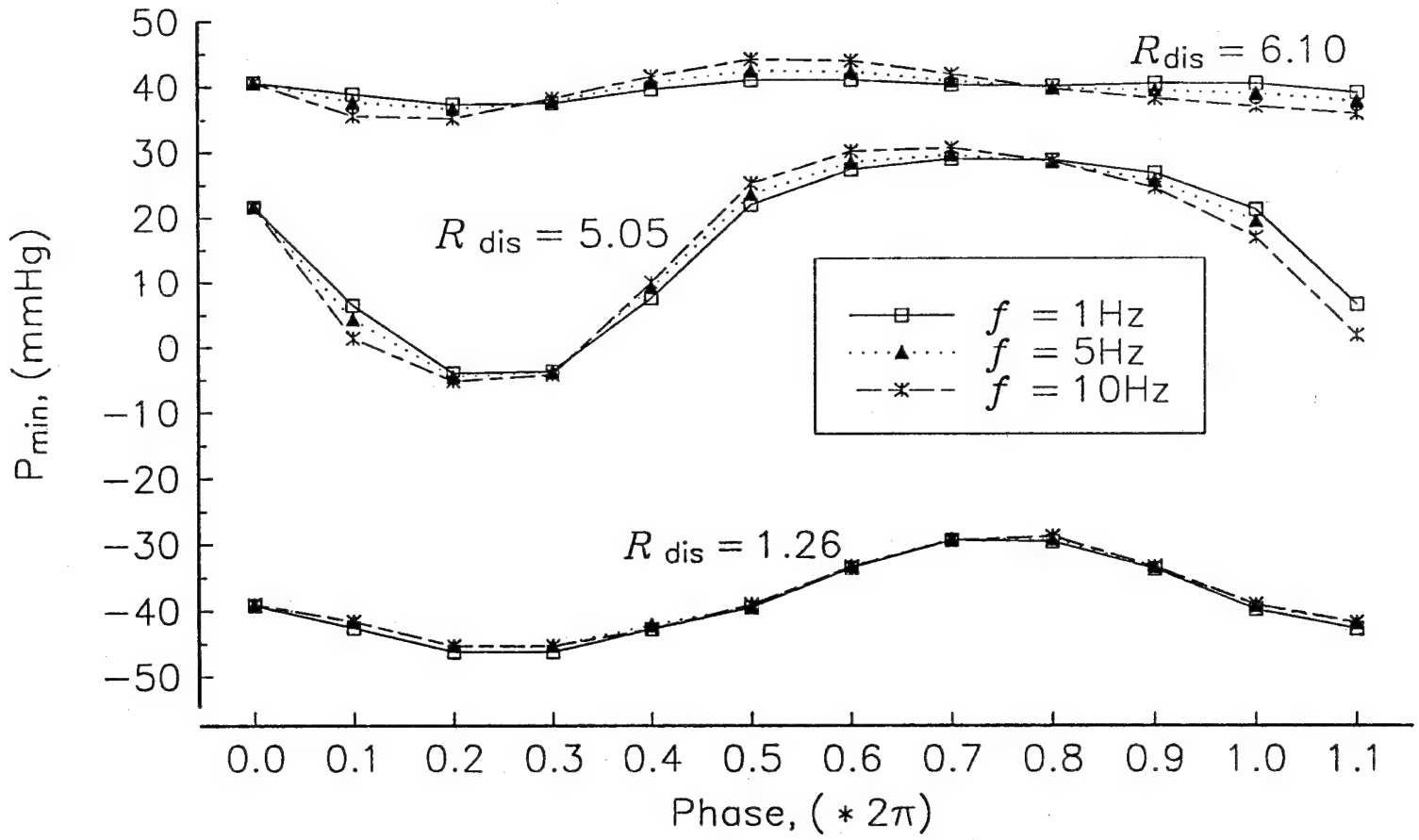

Figure 24 c Unsteady Solutions with Sine Wave Variation in P_1: P_{min} versus Phase with the baseline parametric values: except for f_L=20, K_{Sep}=.2

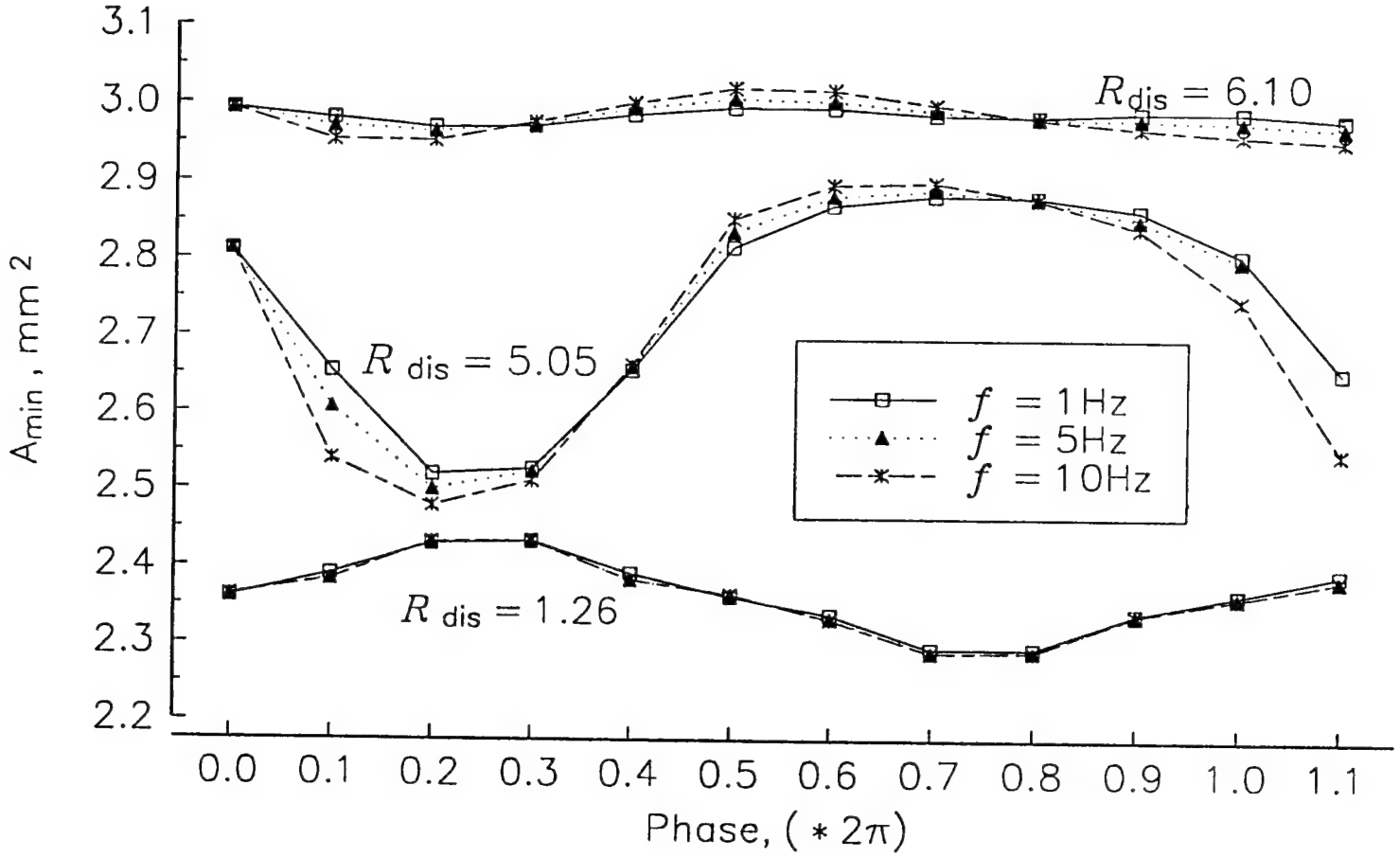

Figure 24d Unsteady Solutions with Sine Wave Variation in P_1: A_{min} versus Phase with the baseline parametric values: except for f_L=20, K_{Sep}=.2

DISCUSSION

This new model has extended the study of collapsible tube flow to unsteady flows with separation losses for high grade stenoses. The model can be used to describe the interaction of the hemodynamics with a compliant stenotic artery. Comparison of the effects of these parameters on the critical flow rate is shown in figure 25. From this it can be seen that the degree of stenosis is the dominant mechanism influencing the establishment of critical flow. Variations in the tube stiffness, frictional losses, and mean pressure are secondary and only modify the critical flow rate value established by the degree of stenosis. An increased stenosis generated larger accelerations in the velocity. Thus, as the degree of stenosis increased, the inlet velocity required for critical flow is lowered, which, in turn lowers the critical flow rate. Increases in tube stiffness tend to impeded the establishment of critical flow by increasing the wave speed as the throat is approached. This action required the inlet flow to be increased for the critical condition to be reached. The other factors of frictional losses, decreasing tube stiffness, and increasing external pressure reduce the critical flow rate by lowering the wave speed within the stenosis. Thus, smaller accelerations in the velocity are required to establish critical flow within the stenosis.

This evaluation has shown that the degree of stenosis is the most important parameter governing physiologic collapse of a stenotic artery. The distal pressure (P_2) also influences the attainment of critical flow, since it determines the arterial pressure gradient. The other parameters, frictional losses, the external pressure (P_e), and the plaque stiffness, were shown not to be as important. For the baseline conditions, a critical stenosis of 77% (dia) would initiate localized physiologic collapse in a carotid artery, and a critical stenosis 76% (dia) would produce localized collapse in a coronary artery under high demand conditions. Collapse was normally established for P_2 values less than 60 mmHg. However, when large viscous and separation losses were included, P_2 had to be lowered to approximately 30 mmHg before the stenosis would collapse. Increased viscous losses were shown to decrease the critical stenosis by 4%, but the extent of the collapse would be lessened. A 50 mmHg increase in P_e reduced the critical stenosis by 2%. Finally, a stiff plaque increased the critical stenosis by 5% and decreased the critical P_2 value by 28 mmHg, and a soft plaque decreased the critical stenosis by 2%. The relative size of these effects on the critical stenosis and the critical value of P_2 are displayed in figure 26 and listed in Table 11. Thus, the occurrence of physiologic collapse would be enhanced in a soft stenosis of greater than 80% (dia) with a low distal resistance and/or elevated external pressure. The chances of collapse would be reduced in a stiff stenosis of less than 80% (dia) with a high distal resistance and low external pressure. However, collapse is predicted for all stenoses between 80 and 90% so long as the distal pressure is less than 30 mmHg.

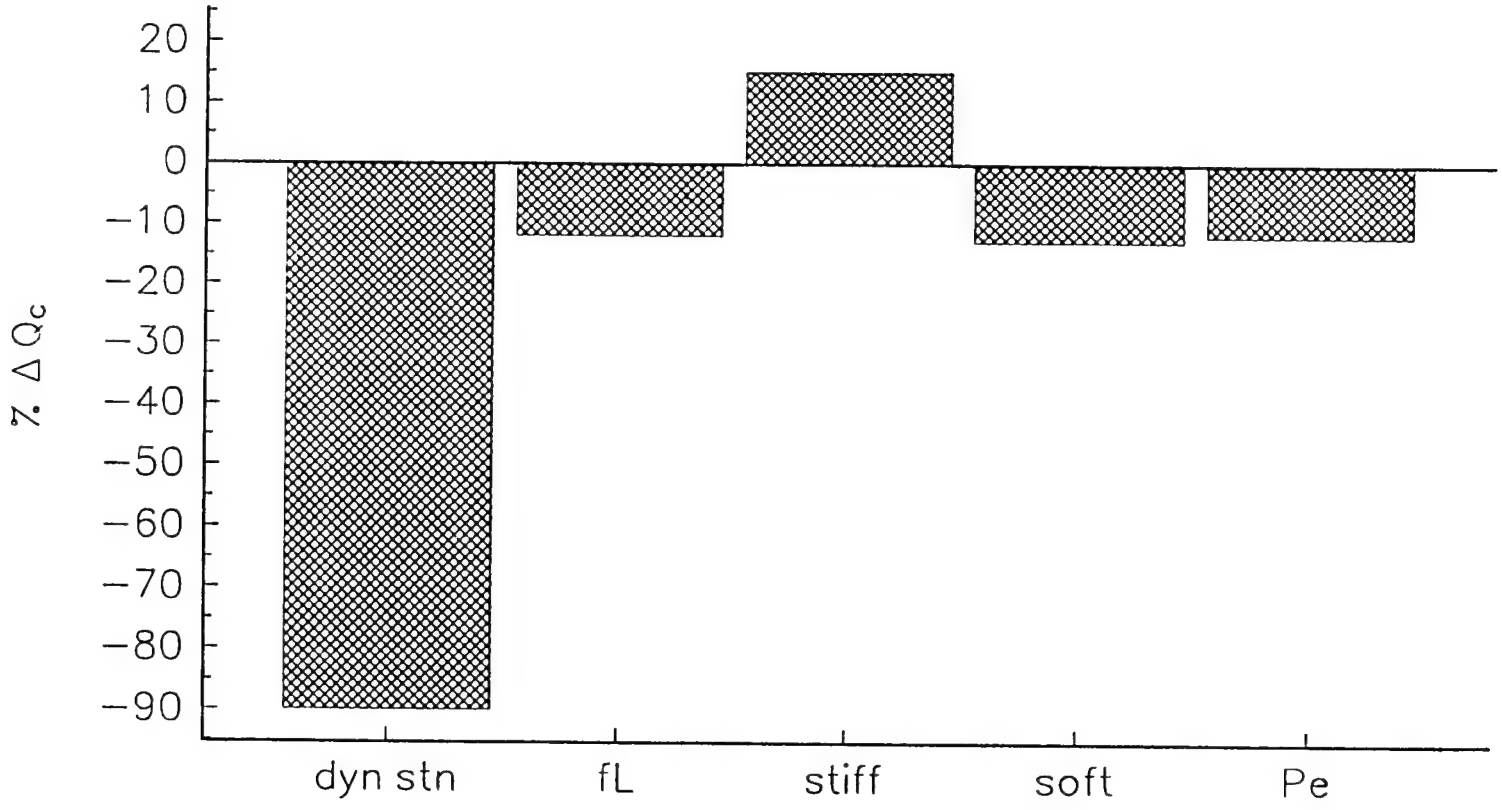

Figure 25 Parameter Changes Effect on Critical Flow Rate. 'dyn stn' represents an increase in the degree of dynamic stenosis from 70 to 90% (dia); f_L represents a tenfold increase in f_L; 'stiff' represent a plaque stiffness variation of $\lambda_{K_e} = 100$; 'soft' represents a plaque stiffness of $\lambda_{K_e} = 0$; P_e represents a 50 mmHg increase in P_e.

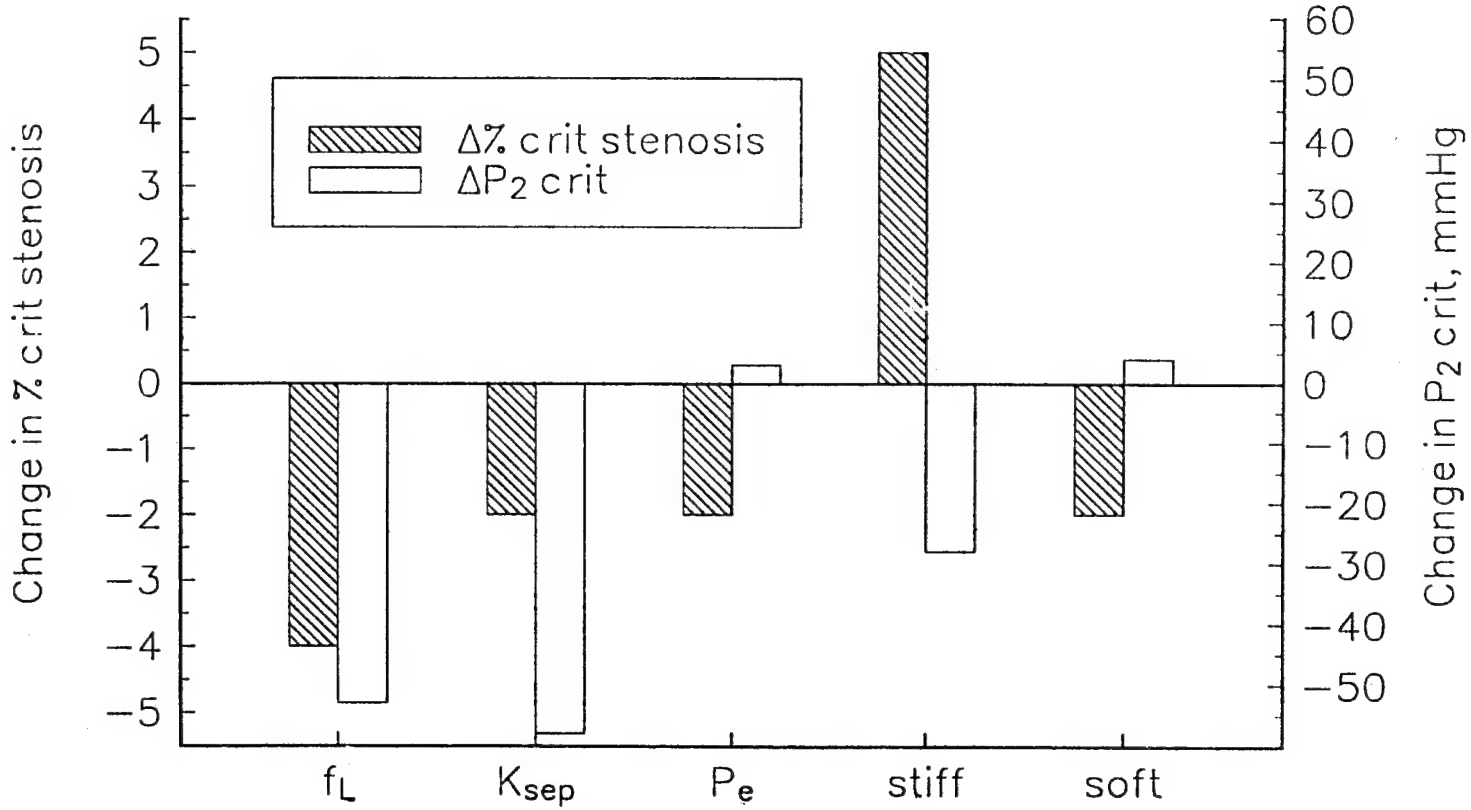

Figure 26 Parameter Changes Effect on Critical Stenosis and P_2 Critical. f_L represents a tenfold increase in f_L, K_{sep} represents the inclusion of separation, P_e represents a 50 mmHg increase in P_e, 'stiff' represent a plaque stiffness variation of $\lambda_{K_e} = 100$, and 'soft' represents a plaque stiffness of $\lambda_{K_e} = 0$. (For baseline conditions the critical stenosis was 78% (dia) and P_2 critical was 88 mmHg)

Table 11 Parameter Changes Effect on Critical Stenosis and P_2 Critical.
(Baseline Conditions: Critical Stenoses = 78%(dia) and P_2 Critical = 88 mmHg)

Parameter	Δ% Critical Stenosis	ΔP_2 critical (mmHg)
f_L (tenfold increase)	-4%	-53
K_{Sep} (inclusion of separation)	-2%	-58
P_e (50 mmHg increase)	-2%	+3
stiff ($\lambda_{K_o} = 100$)	+5%	-28
soft ($\lambda_{K_o} = 0$)	-2%	+4

Comparison to Analytical Models

The results presented above can be compared to a number of previously published studies of flow through a compliant stenosis. Santamore and Bove (53) developed a mathematical model of flow which included viscous losses which were dependent on the minimum area of the stenosis. Their model predicted a critical nominal stenosis of 55% (dia) for high demand coronary flow rates of 5 ml/s and a 70% for low demand flows of 1 ml/s. In contrast, our model predicts slightly greater critical nominal stenoses of 63% and 76% for similar flow conditions. Our model differs from theirs by solving the full 1-D fluid equations over the entire tube length which allows pressure recovery downstream of the stenosis. Also, our model has a much finer spatial grid which allows a better resolution of the extent of viscous losses. These improvements are expected to yield a baseline critical stenosis which is greater than those predicted by Santamore and Bove. Both models show that the critical stenosis is increased by vasodilation or increases in the perfusion pressure (P_1), and the opposite was found for vasoconstriction and lowering of P_1.

The comparison between my computational results and the simulations of Siebes et al (60, 61) is restricted to qualitative effects since they only considered stenoses that were less than 70% (dia). First, both models showed that the minimum area of the stenosis is the dominant factor influencing the flow through a stenotic artery. Second, significant area reductions were estimated by both models to occur during the high flow segment of the pulsatile flow cycle. The model of Siebes et al estimated temporal variations in the diameter of a 55% (dia) stenosis to be approximately 0.5 mm for a coronary artery. Our model predicted variations of only 0.06 mm in the diameter of an 80% (dia) stenosis during a sinusoidal waveform. Sources of this inconsistency may be because of differences in the degree of stenosis, the tube laws, the grid spacing and stenotic shape, and the boundary conditions. A smaller degree of stenosis restricts the stenotic diameter less than a larger stenosis. Their tube law stated that the diameter goes to zero as the transmural pressure goes to zero, whereas our tube law states that the diameter approaches its nominal value as the transmural pressure goes to zero. Thus, their tube law would predict much larger reductions in the diameter for the lower

pressures predicted within the stenosis. Also, their larger spatial grid and stenotic shape would accentuate the viscous losses occurring within the stenotic throat since their minimum area was present for 50% of the stenotic length. Finally, the difference in boundary conditions between the models would create different variations in the diameter over the pulsatile cycle.

Ziegler (42) developed a compliant stenosis model which solved the inviscid steady collapsible tube equations developed by Shapiro (33). For an 80% (dia) dynamic stenosis with P_2=20 mmHg, our model predicted a critical flow rate of 12.1 ml/s with a minimum pressure of -40 mmHg for f_L=5, but the inviscid solution predicted a critical flow rate of 13.2 ml/s with a minimum pressure of -62 mmHg. These differences resulted directly from the inclusion of viscous effects. For an 80% (dia) stenosis, viscous losses impacted the flow by decreasing the critical flow rate by 8% and by forcing the elastic jump earlier in the stenosis compared to the inviscid solution, as shown in Table 8 and figure 21c. This comparison reveals that the effect of viscous losses reduced the % critical stenosis since they decrease the critical flow rate, but minimizes also the extent and magnitude of the collapsing pressure.

Comparison to Experimental Research

The behavior of the compliant stenotic tube demonstrated in the computational results can be compared to the experiments of Conrad (27). Conrad (27) first observed these characteristics in a normal compliant tube mounted between to rigid pipes. He observed collapse to appear first at the distal end of the collapsible tube. This point of collapse corresponded to the point of lowest transmural pressure for his experimental arrangement. Our model showed that the inclusion of compliant effects led to the collapse of the tube at the throat of the stenosis, and that this collapse corresponded to the choking of flow. For stenoses the minimum pressure was located at the throat of the stenosis.

Next, results are compared to three experimental studies which modelled a stenotic artery with latex tubing. In the experiments by Judd and Mates (48), the effect on the flow was measured for eccentric stenoses of 61, 78 and 86% (dia), as defined by a static pressure of 165 mmHg. Their experimental conditions correspond to the solution series with f_L=35 since their test fluid had a viscosity seven times that of blood. For a 78% stenosis with P_1=100 and P_2=60 mmHg, they found that the flow rate produced a Re of 60 and our model predicted a Re of 83. For an 86% stenosis at the same above conditions, they measured a Re of 2.0, and our model predicted a Re of 23. It should be noted that the measured and predicted flows were subcritical for these conditions. For the 86% stenosis with P_2=20 yielding choked conditions, the measured Re was 2.3 and the predicted Re was 36. These slight differences in the Re may be the result of the uncertainty in the experimental degree of dynamic stenosis. Judd and Mates observed collapse to occur at P_2=60 mmHg, when water was used, compared to P_2=50 mmHg for the original fluid. Our model predicted a similar trend due to the reduction of viscosity. A reduction in f_L from 50 to 5 resulted in the critical P_2 value to increase from 30 to about 80 mmHg. This difference in critical P_2 values may be due to separation losses that were not included in the predictions.

In the experimental series by Powell (22), a rigid funnel shaped stenosis was utilized to create a stenosis within the latex tubing. For a 70% (dia) stenosis, he observed a critical flow rate of 22.0 ml/s with a critical P_2 value of -1.0 mmHg. The model predicted a critical flow of 25.4 ml/s with a critical P_2 value of 2.5 mmHg when it was modified to match the effect of the rigid stenosis. For an 80% (dia) stenosis, the measured critical flow rate was 9.0 with a critical P_2 of 2.5 mmHg, and the predicted values were 10.6 ml/s with a critical P_2 of 4 mmHg. Moreover, our model showed good agreement for the subcritical flow rates at various values of P_2, which are listed in Table 12 and displayed in figure 14a. This table shows that the predicted flow rates were within 25% over the range of P_2 settings. The main differences between the experimental model and our numerical model were longitudinal tension and the dynamic versus rigid stenoses. Since the tube was mounted horizontally between two rigid pipes, some tension was applied to the tube. This would decrease the critical P_2 value compare to the predicted condition. Also, the numerical stenosis was allowed to vary dynamically with the changes in P_2, whereas the experimental stenosis was rigid and remained constant, as illustrated in figure 14b.

Table 12 Comparison between the Experimental Flow Rates of Powell (22) and the Model Predictions. (P_1=70 mmHg)

	Experimental Q (ml/s)		Model Q (ml/s)	
P_2 (mmHg)	70% (dia)	80% (dia)	70% (dia)	80% (dia)
30	15.1	7.1	20.3	8.0
20	17.0	8.0	23.0	9.4
10	19.3	8.6	24.6	10.1
5	20.7	8.9	25.2	10.5
0	21.9	9.0	25.4	10.6
-1	22.0	9.0	25.4	10.6

In a third latex tube experiment, the effect of pulsatile flows through a stenosis were observed (29). The experiment used a pressure pulse of 100/60 mmHg compared to the computational solutions pulse of 120/80 mmHg. Although the exact flow conditions were different between these experiments and the unsteady solutions of our model, good agreement exists in the nature of the flow. Three regimes were observed in both the experiments and our model. In the first regime, the tube remained expanded during the entire cycle with increased expansion during systole. Thus, the flow remained subcritical throughout the cycle. In the second regime, distal collapse was observed only during systole with expansion occurring during diastole. The authors referred to this paradoxical motion as "systolic wall collapse" (29) which is displayed in figure 24d. In the third regime, distal collapse was established throughout the entire cycle. Thus, the flow remained supercritical throughout the cycle. For an 81% stenosis with P_2=25 mmHg, the systolic wall collapse was initiated by a P_e=38 mmHg in the experiment. For the computational solution, the systolic wall collapse was initiated by a P_e=0 mmHg for a mean distal pressure of 55 mmHg. The difference in the collapse condition may be ascribed to longitudinal tension and the rigid stenosis. The tube was mounted between two rigid pipes which applied some tension to the tube, but the major tension effect was due to the stenting open of the tube by the rigid stenosis. These factors would require larger external pressures to collapse the vessel compared to a

compliant stenotic artery with no externally applied tension. However, the important part of this comparison was the accurate prediction of the systolic wall collapse along with the other two flow regimes for physiological conditions. Thus, the unsteady solutions illustrate that physiological conditions exist for cyclic collapse within a stenotic artery and their sensitivity to the distal pressure.

Comparison to Physiological Studies

The major influence of the degree of stenosis on physiological collapse are consistent with the findings of Logan (1) who studied the flow characteristics through excised human coronary arteries which contained high grade stenoses. He showed that the stenotic resistance and the flow depended on the minimum area. He also showed that the length of the stenosis and/or the arterial segment had no effect on the flow and the stenotic resistance, as also shown by the model. For a 76% (dia) static eccentric stenosis with P_2=20 mmHg, the stenotic resistance at the onset of choked flow was 180 mmHg/(ml/s). For these conditions, our model predicted a stenotic resistance of only 44 mmHg/(ml/s). Even if the viscous losses were increased by a factor of ten, the predicted stenotic resistance was 61 mmHg/(ml/s). This difference may be explained by the large frictional losses observed in Logan's experimental arteries. These large roughness ratios would lead to more losses than those modelled. However, the effect of increased losses have been illustrated to increase the stenotic resistance at choking by decreasing both the critical flow rate and distal pressure.

The next comparison involves the discrepancy between the observations of Gould and Kelley (59) and those of Schwartz and Bache (56). Our model predictions can be used to reconcile these opposing findings. The computational solutions demonstrating the effects of decreases in P_2, (figures 11a-e), show that the stenotic and distal luminal areas narrowed with decreasing distal pressures. However, this narrowing was very small in magnitude. For *n1*=7 and a 80% dynamic stenosis with P_2=60 mmHg, the actual magnitude of the stenotic area narrowing was on the order of 2% of the inlet area or 35% of the static throat area (P=100 mmHg), which would correspond to experimental area changes on the order of 0.1 mm^2. This magnitude of collapse would be very hard to measure *in vivo*. Thus, in the experiments of Gould and Kelly (59), the minimum area changes would have been obscured by the lack of control on the size of the experimental stenoses. Therefore, these computational results affirm with the observations of Schwartz and Bache (56).

The final comparison involves an *in vitro* study performed with canine carotid arteries with an implanted stenosis. This study examined the pressure/flow relationship for three perfusion pressures of 149, 97, and 72 mmHg and two distal resistance settings (58). Eccentric stenoses were produced by 4 mm long silicone plugs which allowed a section of the normal artery to remain compliant. The different perfusion pressures generated dynamic stenoses of 65, 68, and 70% (dia). The distal and stenotic pressure were measured along with the flow rate for the above conditions. No passive collapse was observed in the arteries for any of the above conditions, and the stenotic pressure was always greater than the distal pressure. However, their analysis showed that the minimum area was inversely related to the stenotic resistance. These findings led Higgins et al (58) to state that the dynamic changes in the stenotic severity results from reduced stenotic pressure and luminal area, but that flow choking due to collapse of the stenotic artery could not explain critical stenoses.

These findings appear to conflict with the computational results of this study and experimental observations (22, 29, 48), yet this conflict can be explained by lack of overlap between their experimental flow rates and the expected collapsed flow rates. The critical flow versus the degree of stenosis relationship for the experimental condition can be modelled by using the $n1$=4 baseline solutions. The highest measured flow rate was only 1.3 ml/s, which corresponded to a scaled model flow rate of 17.8 ml/s. For this flow rate, it would take a 81% (dia) stenosis to produce collapse. Thus, the experimental conditions were outside the predicted collapsible flow regime as illustrated in figure 27. From this graph, it is clear that the experimental findings of Higgins et al (58) do not discount choking due to collapse since the experimental stenoses were not severe enough to produce collapse for the experimental distal resistance settings.

Limitations

This computational model provided qualitative results on how the different parametric variations influence the flow through a stenotic artery. However, these results were limited since the flow was modelled as 1D. The 1D assumption forced the inclusion of empirical friction loss terms which have not been accurately measured for compliant stenoses. Thus, a more detailed description of the separation losses is needed to account for the accurate impact of separation losses on the solution.

Also, the model assumed elastic jumps to occur over very short distances, but in non-stenotic tubes Kececioglu et al (34) observed elastic jumps which were one to two diameters in length. The effect of this difference is unknown. Elastic jumps in a stenotic artery could lengthen the collapse section, or it could lessen the collapsing pressure. Thus, more work is needed to resolve this discrepancy in the amount and the effect of the spread in the elastic jump region.

The tube laws employed in this investigation accurately account for the positive pressure response, but they are lacking in matching the negative pressure response of an artery. As shown in the analysis, the negative response control the magnitude of the compressive pressures which would be applied to the plaque. Therefore, some error in the P_{min} prediction could exist if the negative pressure of the tube law did not accurately predict the response.

Another limitation is the neglecting of longitudinal tension and viscoelastic properties of the arterial wall. The tube law incorporated into the model assumes no hysteresis, although hysteresis occurs in biological tissues.

Further, this model only considered idealized stenotic shapes and stiffness variations. Variant shapes and multiple stenosis are not included in this investigation.

Although the range of parameters included in this were large, there may have been some physiological conditions that were not contained in these variations. Even if some conditions are outside of the parameter range studied, the effects may be extrapolated from the trends demonstrated in the results of this study as an estimate to the magnitude of their effect. The flow conditions appear to cover the range of physiological flows except for very low flow conditions.

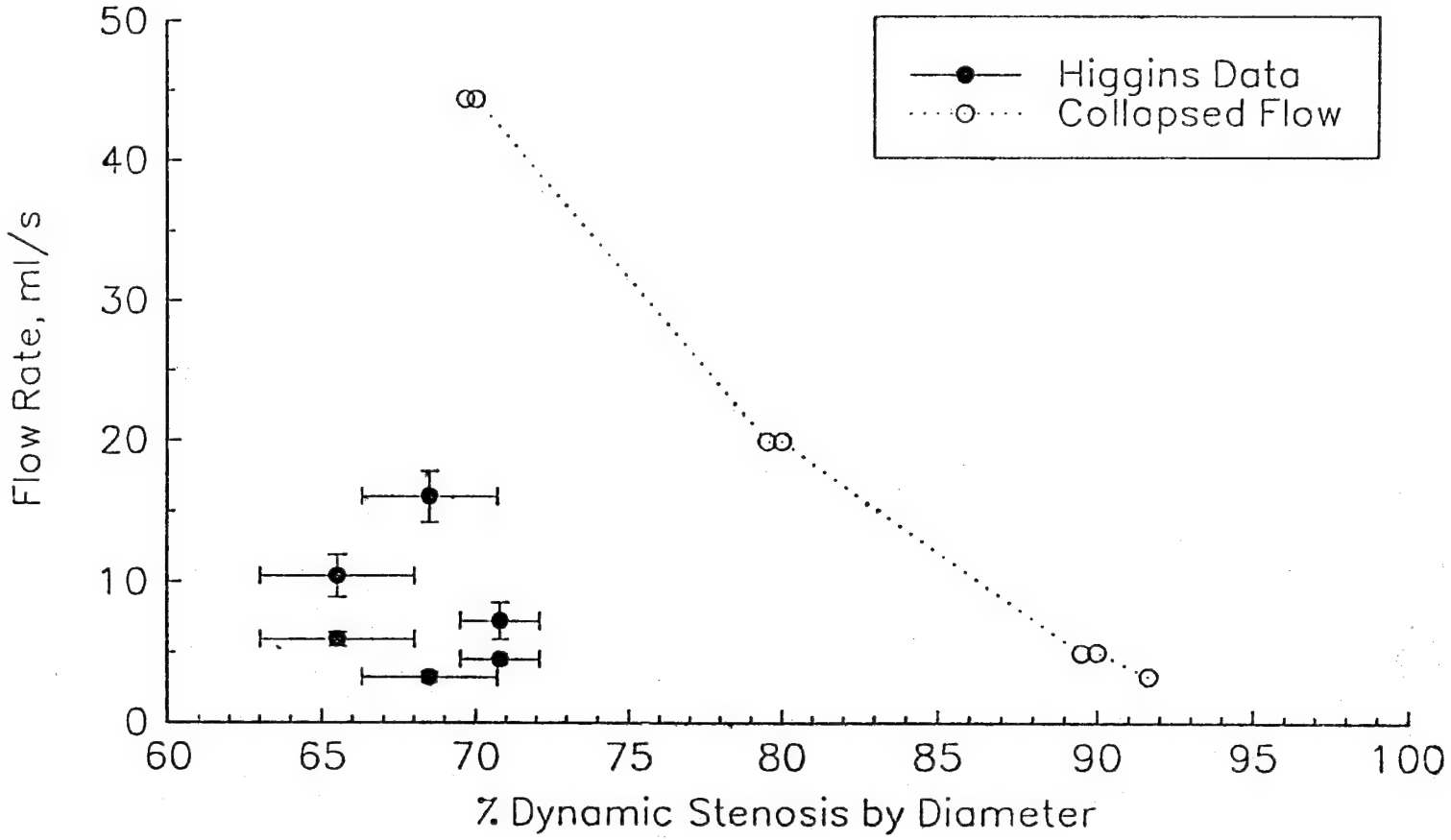

Figure 27 Comparison of Critical Flow Rate to Higgins Data

Other limitations include the second order accuracy of the computational algorithm and the convergence of the solutions. The second order accuracy limitation is minor and more than likely obscured by the oscillation introduced by the Gibb's phenomena in the discontinuous elastic jump region. Artificial viscosity had to be used to prevent the Gibb's oscillation from causing unrecoverable floating point errors in the computation, but it is an accepted method in CFD modelling. However, this action affects the variables, A_{min}, P_{min}, S_{max}, since they are estimated mainly at the elastic jump location.

Clinical Significance

For compliant arteries, the quantification of percent stenosis is problematic. The luminal area is highly dependent on the intraluminal pressure, especially near zero pressure. For high grade stenoses, the intraluminal pressure may vary over 50 mmHg depending on the blood flow rate. Thus, the stenosis is highly dynamic and the notion of fixed stenosis is not likely under physiologic conditions.

The dynamic nature of the stenosis can lead to conditions which may induce flow "choking" from a local "collapse" of the arterial wall. *In vivo*, arteries which have stenoses between 80 and 95% (dia) and have a distal pressure of 40 mmHg are likely to collapse during a systolic flow rate of 10 ml/s. These flow conditions are common for the human carotid artery (69). Collapse is likely to occur for lower degrees of stenosis if plaques are highly compliant, the distal resistance falls, or the external pressure around the artery is elevated as with increases in internal jugular pressure during coughing. The chances of collapse are reduced if the plaque is very stiff, the distal resistance is high, or the external pressure is negligible. Flow through many diseased arteries may create borderline conditions for the occurrence of collapse. Slight flow variations may produce transient oscillations between collapse and no collapse throughout the day. Since a compliant stenosis gradually chokes the flow, the net effect of collapse on blood flow would be to limit the maximum capacity during high demands beyond that of viscous losses.

A more significant impact of stenotic collapse may be from fatigue of the atheromatous plaque cap. Most clinical symptoms of carotid and coronary disease result from rupture of the plaque cap (5). Repeated bending loads of an artery have been shown to induce a fatigue failure of the plaque cap (61). The results presented here strongly suggest that some form of compression or collapse can be produced by the physiologic hemodynamics in arteries with high-grade stenoses.

A common response of animal tissue to compression is calcification (70). It may be that the widely observed calcification of the atheroma is a direct response to the compressive loading conditions generated by stenotic collapse. Since collapse is subsequently less likely with increasing stiffness, the calcification may actually be a beneficial adaptive mechanism. In one study, very few calcified high grade stenoses led to strokes and TIAs in contrast to fatty high grade stenoses which had a high incidence of strokes and TIAs (20).

Future Work

Future research involving the collapse of a stenotic artery should concentrate on the validation of the computer model. A compliant stenotic model needs to be fabricated so that choked flow and collapse can be demonstrated *in vitro*. This experimental model should be compliant throughout the flow region, so that compliant effects are included both upstream and downstream of the stenosis. The validation would check the one-dimensional assumption and would serve to quantify the characteristics of the elastic jump region. Visualization of the elastic jump region in a stenosis is needed to understanding better its structure and impact on flow through a stenosis.

Also, such an experiment will aid in establishing the values of the friction coefficients along with the length of any flow separation. The validation of the friction coefficients could also involve a distributed friction coefficient which varies with the area gradient to include the effects of the converging and diverging sections of the stenosis on basic frictional losses.

Some improvements can be implemented into the model to enhance its physical representation. Such improvements include the incorporation of tension and validation of the friction coefficients. Longitudinal tension can be incorporated into the equations, but this will introduce higher order derivatives into the system. Also, tension will more than likely impact the effectiveness of the artificial viscosity and the numerical smoothing. Thus, the incorporation of tension is expected to increase the instability of the numerical solution especially in the region of the jump.

CONCLUSION

A computer model was developed to simulate flow through a compliant stenotic artery. The model solved the governing one-dimensional, unsteady, partial differential system of equations by utilizing the MacCormack's method, which is an established computational fluid dynamics technique. This simulation illustrated that hemodynamic forces may produce vessel collapse and flow choking within a high grade arterial stenosis of greater than 80% (dia). Moreover, the collapse of the stenotic artery induced by hemodynamics may generate sufficient stresses on the plaque to result in plaque disruption by either fracture or fatigue (68). The critical flows needed to produce collapse were shown to occur under physiological conditions. Also, the effect of variations in the physical parameters of the system were investigated to understand how they influence the flow. The degree of stenosis was the main factor influencing collapse. Other important parameters were the distal pressure, frictional losses, the external pressure, and variations in the plaque stiffness. Also, pulsatile conditions resulted in the cycling of the flow between supercritical during systole and subcritical during diastole.

The model results agree with both experimental and clinical observations which provides a good indication that stenotic arteries may generate conditions favorable for plaque collapse and flow limitation. The chances of physiologic collapse were reduced in a stiff plaque which indicates that calcification of the plaque may be a beneficial adaptive response by the artery. Conversely, collapse would be augmented in a lipid-laden plaque. Frictional losses could hinder collapse by decreasing the critical distal pressure. Sufficiently large increases in frictional losses delayed the establishment of critical flows. Increased external pressure would enhance collapse by lowering the critical flow. Thus, the results from this model indicate that the coupling of the blood flow with the structural response of the artery plays an important role in flow limitation through a high grade stenosis, and this interaction may lead to plaque disruption and clinical complications such as myocardial infarction, strokes, and transient ischemic attacks.

REFERENCES

1. Logan, S.E, "On the Fluid Mechanics of Human Coronary Artery Stenosis," *IEEE Trans. on Biomedical Eng*, Vol. BME-22, No. 4, July 1975, pp. 327-334.

2. Glagov,S., Zarins, C.K., Giddens, D.P., and Ku, D.N., "Hemodynamics and Atherosclerosis, Insights and Perspectives Gained from Studies of Human Arteries," *Arch. Path. Lab. Med.*, 1988, Vol. 112, pp. 1018-1031.

3. Strandness, D.E. and Summer, D.S., *Hemodynamics for Surgeons*, Grune and Stratton, 1975.

4. Alpert, D.H., Hirsh, P.D., Cowley, M.J., et al, "Angiographic demonstration of plaque fissure associated with acutecoronary occlusion," *Am Heart J*, Vol. 117, Part 1, pp 185-186, 1989.

5. Davies, M.J., Thomas, A.C., "Plaque Fissuring - the Cause of Acute Myocardial Infarction, Sudden Ischemic Death, and Crescendo Angina," *Br Heart J*, 53:363-73, 1985.

6. Falk, E., "Plaque Rupture with Severe Pre-existing Stenosis Precipitating Coronary Thrombosis (Characteristics of Coronary Atherosclerotic Plaques Underlying Fatal Occlusive Thrombi)," *Br Heart J*, 50, 1983, pp 127-134.

7. Born, G.V.R., and Richardson, P.D., "Mechanical Properties of Human Atherosclerotic Lesions," *Pathobiology of the Human Atherosclerotic Plaque*, Springer-Verlag, New York, NY, 1990, pp 413-423.

8. Constantinides, P., "Plaque Hemorrhages, Their Genesis and Their Role in Supra-Plaque Thrombosis and Atherogenesis," *Pathobiology of the Human Atherosclerotic Plaque*, Springer-Verlag, New York, NY, 1990, pp 393-411.

9. Ridolfi, R.L., and Hutchins, G.M., "The Relationship Between Coronary Artery Lesions and Myocardial Infarcts: Ulceration of Atherosclerotic Plaques Precipitation Coronary Thrombosis," *Am Heart J.*, Vol. 93, No. 4, April 1977, pp 468-486.

10. Horie, T., Sekiguchi, and Hirosawa, K., "Coronary Thrombosis in Pathogensis of Acute Myocardial Infarction," *Br Heart J*, Vol. 40, 1978, pp 153-161.

11. Chapman, I., "Morphogenesis of Occluding Coronary Artery Thrombosis," *Arch Path*, Vol. 80, Sept 1965.

12. Oliva, P.B., "Pathophysiology of Acute Myocardial Infarction, 1981," *Annals of Internal Medicine*, Vol. 94, 1981, pp 236-250.

13. Lambert, C.R., and Pepine, C.J., "The Role of Vasospasm in Acute Myocardial Infarction," *Acute Myocardial Infarction: Emerging Concepts of Pathogenesis and Treatment*, Praeger Publishers, New York, NY. 1989.

14. Imparato, A.M., Riles, T.S., and Gorstein, F., "The Carotid Bifurcation Plaque: Pathological Findings Associated with Cerebral Ischemia," *Stroke*, Vol. 10, No. 3, 1979, pp. 238-244.

15. Santamore, W.P., Yelton, B., and Ogilby, D., "Dynamics of Coronary Occlusion in the Pathogenesis of Myocardial Infarction," *J. Am Coll Cardiol.* in press, 1992.

16. Fuster, V., Badimon, L., Cohen, M., et al, "Insights into the Pathogenesis of Acute Ischemic Syndromes," *Circulation*, Vol. 77, No. 6, June 1988.

17. Schwartz, S.I., *Principles of Surgery*, McGraw-Hill, New York, NY, 1984, p. 918

18. Eisenberg, R.L., Nemzek, W.R., Moore, W.S., and Mani, R.L., "Relationship of Transient Ischemic Attacks and Angiographically Demonstrable Lesions of Carotid Artery," *Stroke*, Vol. 8, No. 4, July-August 1977, pp 483-486.

19. Ricotta, J.J., Schenk, E.A., Ekholm, S.E., et al, "Angiographic and Pathologic Correlates in Carotid Artery Disease," *Surgery*, p 284.

20. Johnson, J.M., Kennelly, M.M., Decesare,D., et al., "Natural History of Asymptomatic Carotid Plaque," *Arch. of Surgery*, 1985, Vol. 120, pp. 1010-1012.

21. Kamm, R.D., and Pedley, T.J., "Flow in Collapsible Tubes: A Brief Review," ASME, *J. of Biomechanical Engineering*, Vol. 111, 1989, pp. 177-9.

22. Powell, B.E., "Experimental Measurements of Flow through Stenotic Collapsible Tubes," Master's Thesis, ME, Ga Tech, 1991.

23. Fry, D.L., "Theoretical Considerations of the Bronchial Pressure-Flow-Volume Relationship with Particular Reference to the Maximum Expiratory Flow Volume Curve," *Phys. Med. Biol.*, Vol. 3, 1958, pp. 174-194.

24. Brower, R.W., and Noordergraaf, A., "Pressure Flow Characteristics of Collapsible Tubes: A Reconciliation of Seemingly Contradictory Results," *Ann. Biomed. Eng.*, Vol. 1, 1973, pp.333-335.

25. Bonis, M., and Ribreau, C., "Etude de quelques proprietes de l'ecoulement dans une conduite collabable," *La Houille Blanche*, Vol. 3/4, 1978, pp.165-173.

26. Bertram, C.D., "Unstable Equilibrium Behavior in Collapsible Tubes," *J. Biomech.*, Vol. 19, 1986, pp. 61-69.

27. Conrad, W.A., "Pressure-Flow Relationships in Collapsible Tubes," *IEEE Trans Biomedical Eng.* Vol. BME-16, No. 4, October 1969, pp. 284-295.

28. Bertram, C.D., "Control-Space Diagrams For Flow through Collapsible Tubes," *Phys. Med. Biol.*, Vol. 33, Suppl. I, 1988, p. 259.

29. Binns, R.L. and Ku, D.N., "Effect of Stenosis on Wall Motion; A Possible Mechanism of Stroke and Transient Ischemic Attack," *Arteriosclerosis*, Nov/Dec 1989.

30. Katz, A.I., Chen, Y., and Moreno, A.H., "Flow Through a Collapsible Tube. Experimental Analysis and Mathematical Model," *Biophysical J.*, Vol. 9, 1969, pp. 1261-1279.

31. Griffiths, D.J., "Hydrodynamics of Male Micturition I. Theory of Steady Flow Through Elasti-Walled Tubes," *Med. Biol. Eng.*, Vol.9, 1971, pp. 581-588.

32. Oates, G.C., "Fluid Flow in Soft-Walled Tubes: I. Steady Flow," *Med. Biol. Eng.*, Vol. 18, pp. 773-778.

33. Shapiro, A.H., "Steady Flow in Collapsible Tubes," ASME, *J. of Biomechanical Engineering*, 1977, Vol. 99, pp. 126-127.

34. Kececioglu, I., McClurken, M.E., Kamm, R.D., and Shapiro, A.H., "Steady, Supercritical Flow in Collapsible Tubes. Part 1. Experimental Observations," *J. Fluid Mech*, Vol. 109, 1981, pp. 367-389.

35. McClurken, M.E., Kececioglu, I., Kamm, R.D., and Shapiro, A.H., "Steady, Supercritical Flow in Collapsible Tubes. Part 2. Theoretical Studies," *J. Fluid Mech*, Vol. 109, 1981, pp. 367-389.

36. Kamm, R.D., and Shapiro, A.H., Unsteady Flow in a Collapsible Tube Sujected to External Pressure or Body Forces," *J. Fluid Mech.*, Vol. 95, 1979, pp. 1-78.

37. Elad, D., and Kamm, R.D., "Parametric Evaluation of Forced Expiration Using A Numerical Model," ASME, *J. Biomechanical Engineering*, Vol. 111, August 1989, pp. 192-199.

38. Kimmel, E., Kamm, R.D., and Shapiro, A.H., "Numerical Solutions for Steady and Unsteady Flow in a Model of the Pulmonary Airways," ASME, *J. Biomechanical Engineering*, Vol. 110, November 1988, pp. 292-299.

39. Jensen, O.E., and Pedley, T.J., "The Existence of Steady Flow in a Collapsed Tube," *J. Fluid Mechanics* (in press).

40. Grotberg, J.B., and Shee, T.R., "Compressible-Flow Channel Flutter," *J. Fluid Mech.*, Vol. 159, 1985, pp.175-193.

41. Grotberg, J.B. Gavriely, N., Shee, T.R., and Cugell, D.W., "Flow Limitation and Flutter Phenomena in Collapsible Tubes," *Phys. Med. Biol.*, Vol. 33, Suppl. I, 260, 1988.

42. Zeigler, M.N., "One Dimensional Inviscid Flow Through A Stenotic Collapsible Tube," Master Thesis, ME, Ga Tech, 1989.

43. Ku, D.N., Zeigler, M.N., and Downing, J.M., "One-Dimensional Steady Inviscid Flow Through a Stenotic Collapsible Tube," ASME, *J. Biomechanical Engineering*, Vol. 112, November 1990, pp. 444-450.

44. Fung, Y.C., *Biomechanics Mechanical Properties of Living Tissues*, Springer-Verlad, New York, NY, 1981.

45. Flaherty, J.E., Keller, J.B., and Rubinow, S.I., "Post Buckling Behavior of Elastic Tubes and Rings with Opposite Sides in Contact," SIAM, *J. Applied Mathematics*, 23(4), 1972, pp. 446-455.

46. Cowley, S.J., "Elastic Jumps on Fluid-Filled Elastic Tubes," *J. Fluid Mech.*, Vol. 116, 1982, pp. 459-473.

47. White, F.M., *Fluid Mechanics*, McGraw-HIll, Inc., New York, NY, 1986.

48. Judd and Mates, "Flow Through a Stenosis in a Compliant Tube," *Proc of the 2nd Intl Symp on Biofluid Mechanics and Bioreheology*, Munich, Germany, 1989.

49. Young, D.F., and Stergiopulos, N., "Pulsatile Flow Through Models of Compliant Stenoses," *World Congress on Medical Physics and Biomedical Engineering*, San Antonio, TX, 1988.

50. Gould, K.L., Lipscomb, K., and Hamilton, G.W., "Physiologic Basis for Assessing Critical Coronary Stenosis. Instantaneous Flow Response and Regional Distribution During Coronary Hyperemia as Measures of Coronary Flow Reserve," *Am J. Cardiology*, January 1974, pp. 87-94.

51. Gould, K.L., "Pressure-Flow Characteristics of Coronary Stenoses in Unsedated Dogs at Rest and during Coronary Vasodilation," *Circulation Research*, Vol. 43, No. 2, August 1978, pp. 242-253.

52. Santamore, W.P., Bove, A.A., and Carey, R.A., "Tachycardia induced reduction in coronary blood flow distal to a stenosis," *International J Cardiology*, Vol. 2, 1982, pp. 23-37.

53. Santamore, W.P., and Bove, A.A., "A Theoretical Model of a Compliant Arterial Stenosis," *Am. J. Pysiol.* 248 (Heart Circ. Phyiol. 17), 1982, pp. H274-H285.

54. Schwartz, J.S., Carlyle, P.F., and Cohn, J.N., "Effect of Dilation of the Distal Coronary Bed On Flow and Resistance in Severely Stenotic Coronary Arteries in the Dog," *Am. J. Cardiology*, Vol. 43, February 1979, pp. 219-224.

55. Schwartz, J.S., Tockman, B., Cohn, J.N., and Bache, R.J., "Exercise-Induced Decrease in Flow Through Stenotic Coronary Arteries in the Dog," *Am. J. Cardiology*, Vol. 50, December 1982, pp. 1409-1413.

56. Schwartz, J.S., and Bache, R.J., "Effect of Arteriolar Dilation on Coronary Artery Diameter Distal to Coronary Stenoses," *Am. J. Physiol.* 249 (Heart Circ. Physiol. 18), 1985, pp. H981-H988.

57. Higgins, D., Santamore, W.P., Walinsky, P., and Nemir, Jr., P., "Hemodynamics of human arterial stenoses," *Int J Cardiol*, Vol. 8, 1985, pp. 177-192.

58. Higgins, D., Santamore, W.P., Bove, A.A., and Nemir,Jr.,P., "Mechanism for dynamic changes in stenotic severity," *Am. J. Physiol.* 249 (Heart Circ. Physiol. 18), 1985, pp. H293-H299.

59. Gould, K.L. and Kelley, K.O., "Physiological Significance of Coronary Flow Velocity and Changing Stenosis Geometry during Coronary Vasodilation in Awake Dogs," *Circ Res*, Vol. 50, 1982, pp 695-704.

60. Siebes, M. and D'Argenio, D.Z., "Mathematical Model of Flow Through a Partially Collapsible Coronary Stenosis," *Advances in Bioengineering*, ASME, BED-Vol. 17, 1990, pp. 139-142.

61. Siebes, M., "Effect of Nonlinear Wall Mechanics on Compliant Coronary Stenoses: A Flow Simulation Study," *Advances in Bioengineering*, ASME, BED-Vol. 20, 1991, pp. 345-348.

62. Tulenko, T.N., Constantinescu, D., Kikuchi, T., Cox, R.H., and Santamore, W.P., "Mutual interaction of vasoconstriction and endothelial damage in stenotic arteries," *Am. J. Physiol.* 256 (Heart Circ. Physiol. 25), 1989, pp. H881-H889.

63. Li, K., Santamore, W.P., Morley, D.L., and Tulenko, T.N., "Stenotic amplification of vasoconstriction responses," *Am. J. Physiol.* 256 (Heart Circ. Physiol. 25), 1989, pp. H1044-H1051.

64. Aoki, T. and Ku, D.N., "Collapse of Diseased Arteries with Eccentric Cross Section," *J Biomech*, Vol. 26, 1993, pp. 133-142.

65. Cox, R.H., "Anisotropic Properties of the Canine Carotid Artery In Vitro," *J. Biomechanics*, Vol. 8, 1975, pp. 293-300.

66. Cancelli, C., and Pedley, T.J., "A Separated Flow Model for Collapsible-Tube Oscillations," *J. Fluid Mech.*, Vol. 157, 1985, pp. 375-404.

67. Anderson, D.A., Tannehill, J.C., and Pletcher, R.H., *Computational Fluid Mechanics and Heat Transfer*, Hemishpere Publishing Corporation, New York, NY, 1984.

68. McCord, B.N., "Fatigue of Atherosclerotic Plaque," PhD Thesis, ME, Geogria Institute of Technology, Atlanta GA, 1992.

69. Archie, J.P., "Technique and Clinical Results of Carotid Stump Back-Pressure to Determine Selective Shunting During Carotid Endarterectomy," *J. Vascular Surgery*, Vol. 13, No. 2, February 1991, pp. 319-327.

70. Rodbard, S., "Negative Feedback Mechanisms in the Architecture and Function of the Connective and Cardiovascular Tissues," *Perspect Biol Med*, vol. 13, 1970, pp. 507-527.

APPENDIX A: Hyperbolic System of Equations

The system of equations as given in equation 9:

$$\begin{Bmatrix} A \\ U \end{Bmatrix}_t + \begin{Bmatrix} AU \\ \frac{1}{2}U^2 + \frac{P - P_e}{\rho} \end{Bmatrix}_x = \begin{Bmatrix} 0 \\ 0 \end{Bmatrix} \qquad 9$$

with

$$A = f^{-1}(P - P_e),$$

can be rewritten in the following form to find its eigenvalues:

$$\begin{Bmatrix} A \\ U \end{Bmatrix}_t + \begin{bmatrix} U & A \\ \frac{c^2}{A} & U \end{bmatrix} \begin{Bmatrix} A \\ U \end{Bmatrix}_x = \begin{Bmatrix} 0 \\ 0 \end{Bmatrix}.$$

The eigenvalues of the matrix are determined in the following steps:

$$det \begin{bmatrix} U - \lambda & A \\ \frac{c^2}{A} & U - \lambda \end{bmatrix} = 0.$$

$$(U - \lambda)^2 - c^2 = 0$$

$$\lambda^2 - 2U\lambda + (U^2 - c^2) = 0$$

Solving for λ gives the eigenvalues:

$$\lambda = U \pm c.$$

Since both of the egienvalues are real, the system is hyperbolic with information propagating through the domain at speeds of U+c and U-c. When U is less than c, information will propagated upstream and downstream. When U is greater than c, information only propagates downstream.

APPENDIX B: Compatability Condition

Since the boundary conditions were applied on α at the inlet and outlet, the velocity at the boundaries had to be evaluated by a compatability condition. This condition allows the boundary velocity to remain compatable with the governing system of equation while not over-specifying the boundary conditions. For this model, the compatability condition utilized the modified momentum equation:

$$\frac{\partial}{\partial\tau}(\lambda_A\alpha u) + \frac{\partial}{\partial\xi}\{\lambda_A[\alpha u^2+\lambda_K(\alpha\Pi-\Gamma)]\} + \Gamma\lambda_A\frac{\partial\lambda_K}{\partial\xi}$$

$$- \lambda_K(\alpha\Pi-\Gamma)\frac{\partial\lambda_A}{\partial\xi} + \frac{32\rho}{\mu c_o De}\frac{D_o}{De}f_L'\lambda_A\alpha u = 0$$

At the boundaries, both $\frac{\partial\lambda_A}{\partial\xi}$ and $\frac{\partial\lambda_K}{\partial\xi}$ were zero. Thus, α was defined at a boundary, the boundary velocity was determined by the following steps:

Let

$$du_i = \lambda_{A_i}\left(\alpha_i^n(u_i^n)^2 + \lambda_{K_i}(\alpha_i^n\Pi_i^n-\Gamma_i^n)\right).$$

Then the inlet u is evaluated by:

$$u_1^{n+1} = \frac{1}{\lambda_{A_1}\alpha_1^{n+1}}\left\{\lambda_{A_1}\alpha_1^n u_1^n - \frac{\Delta\tau}{\Delta\xi}\left[\frac{1}{2}(-3du_1+4du_2-du_3)\right] - \Delta\tau\frac{32\mu}{\rho c_o D_e}\frac{D_o}{D_e}f_L'\lambda_{A_1}\alpha_1^n u_1^n\right\},$$

and the outlet u is evaluated by:

$$u_{out}^{n+1} = \frac{1}{\lambda_{A_{out}}\alpha_{out}^{n+1}}\left\{\lambda_{A_{out}}\alpha_{out}^n u_{out}^n - \frac{\Delta\tau}{\Delta\xi}\left[\frac{1}{2}(-3du_{out}+4du_{out-1}-du_{out-2})\right] - \Delta\tau\frac{32\mu}{\rho c_o D_e}\frac{D_o}{D_e}f_L'\lambda_{A_{out}}\alpha_{out}^n u_{out}^n\right\}.$$

This compatability condition used second order forward (inlet) and backward (outlet) differencing to maintain the numerical accuracy at the boundaries. These conditions allowed the boundary velocities to remain compatable to the governing equations, and no numerical oscillations were present at the boundaries of the solutions.

APPENDIX C: Computer Code

```
      Program CLTUB12
c     This program solves for unsteady flow through a compliant stenotic artery
c     Using MacCormack predictor-corrector method
c     This program does include elastic jump relationship of Oates and Cowley as
incorporated by Kamm
c     numerical dissipation-- normal stress dampening and high order smoothing
c     corrects the friction term term to include the tube length and
c     dynamic diameter, De, includes an additional separation term
c     Friction array is laminar--jump--turb(2D)--laminar
c     Unsteady bc:  P1=Po+20 sin(wt) with L =3Do

cccc Identification of Variables
c     in = # of points in arrays
c     ii = error count for convergence
c     ifile = output file counter
c     nlim = iteration limit for subroutine ALINET
c     ll = counter
c     status = status check flag
c     imax = jth point where (u+c)max occurs
c     ijump = jth point where elastic jump occurs
c     iflag = flag for determing separation point
c     xx(j) = tube position array
c     u(j) = nondimensional velocity
c     al(j) = area ratio, alpha (area/ao)
c     c(j) = wave speed
c     Kp(j) = tube stiffness
c     Ao(j) = nominal area curve
c     pin = prescribed inlet pressure
c     pout = prescribed outlet pressure
c     Kpo = nominal tube stiffness
c     time = nondimensional time
c     dia = nominal tube diameter
c     co = nominal wave speed
c     lamk(j) = stiffness variation array
c     lama(j) = area variation array
c     p(j) = nondimensional pressure
c     frict(j) = frictional loss array
c     ft = separation loss coefficient, Ksep
c     fl = laminar loss coefficient
c     gam = high order smoothing coefficient
c     xn1 = n1, tube law coefficient
c     b1 = tube law coefficient, physiological
c     n2 = tube law coefficient
c     b2 = tube law coefficient, physiological
c     delx = spatial grid size
c     Aoo = nominal area
c     nu = artifical viscosity coefficient
c     eta = time step saftey factor
c     resist = distal resistance setting
c     pb11, pb12, pb21, pb22, pc2 = intermediate predictor terms
```

```
c     cb11, cb10, cb20, cb21, cc2 = intermediate corrector terms
c     w1, w2 = intermediate numerical terms
c     du = [B] array gradient at boundary
c     sb(j) = high order smoothing variable
c     De(j) = hydraulic diameter
c     den = density
c     g = Gamma variable, integral of p(j) wrt al
c     bc1, bc2, bc3 = intermediate boundary terms for du
c     delk(j) = stiffness gradient wrt xx
c     dela(j) = nominal area gradient wrt xx
c     s(j) = speed index
c     delt = time step
c     err = error tolerance for convergence check
c     max = (u+c)max term for time step determination
c     alin = prescribed inlet alpha
c     alout = prescribed outlet alpha
c     q = initial flow rate for initial u(j,1)
c     ep = error term for convergence check
c     pi = 3.141592654
c     xtol, ftol = tolerance coefficients for subroutine ALINET
c     upc = (u+c)
c     to = initial time interval for transient reduction
c     len = length of stenosis
c     xstrt = position of stenosis starting point
c     xstp = position of stenosis stopping point
c     tlmt = time limit for steady solution (comvergence not reached)
c     beta(j) = high order smoothing term
c     tout = time for output of solution (unsteady)
c     tend = time for output of solution (steady)
c     delout = outlet spatial step to determine qout
c     qout = flow rate at outlet (constant distal resistance bc)
c     eta1 = intermediate time step saftey factor
c     outfile = output file names
c
cccc  Initialization
      integer*2 in,ii
      integer*2 ifile
      integer*2 nlim,ll,status,imax
      integer*2 ijump,iflag,isep
      real*4 xx(1002),u(1001,3),al(1001,3),c(1001),kp(1001),ao(1001)
      real*4 pin,pout,kpo,time,dia,co,lamk,lama,p(1001,2),frict(1001)
      real*4 ft,fl,gam,xn1,b1,n2,b2,delx,aoo,nu,eta,resist
      real*4 pb11,pb12,pb21,pb22,cb11,cb10,cb20,cb21,w1,w2,du,sb(1001)
      real*4 de(1001),den,g(1001,2),bc1,bc2,bc3
      real*4 delk(1001),dela(1001),s(1001)
      real*4 delt,err,max,alin,alout,q,ep,pi
      real*4 xtol,ftol,upc,to,len,xstrt,xstp
      real*4 pc2,cc2,tlmt,BETA(1001)
      real*4 tout,delout,qout,eta1
      character*12 outfile(12)
      common/outi/in
      common/out1/xx,u,al,c,kp,ao
```

```
      common/out2/pin,pout,kpo,time,dia,co,lamk,lama,p,frict
      common/out3/ft,fl,gam,xn1,b1,n2,b2,delx,aoo,NU,eta,resist
50    data den,pi /995.0,3.141592654/
      data nlim,xtol,ftol/500,0.001,0.001/
      data ep/0.01/

cccc Input values
      print*,'Pin & Pout (mmHg)'
      read*, pin,pout
      pin =pin*133.32/kpo
      pout=pout*133.32/kpo
      dia=0.006
      aoo=pi/4*dia**2
      print*,'lambda A, lambda K'
      read*, lama,lamk
      print*,' Kpo (Pa), q'
      read*, kpo,q
      print*,'N1, B1, N2, B2'
      read*,xn1,b1,n2,b2
      xstrt=0.5
      xstp=2.5
      len=xstp-xstrt
      print*,len
      print*,' input distal resistance in mmHg/(ml/s):'
      read*,resist
      resist=resist*133.32*100**3
      print*,'friction factor: fl & ft'
      read*,fl,ft
      PRINT*,'GAMMA NU'
      READ*,gam,NU
      print*,'status check yes=1'
      read*,status
      print*,'time out, time end & eta'
      read*,tout,tend,eta
c     print*,'enter output file '
c     read*,outfile
      outfile(1)='out1.prn'
      outfile(2)='out2.prn'
      outfile(3)='out3.prn'
      outfile(4)='out4.prn'
      outfile(5)='out5.prn'
      outfile(6)='out6.prn'
      outfile(7)='out7.prn'
      outfile(8)='out8.prn'
      outfile(9)='out9.prn'
      outfile(10)='out10.prn'
      outfile(11)='out11.prn'
      outfile(12)='out12.prn'
      print*,pin,pout,xn1,n2
c
c     determine alpha in and alpha out
      alin=2.0
```

```
      call alinet(alin,xn1,b1,n2,b2,xtol,ftol,nlim,pin)
      alout=2.0
      call alinet(alout,xn1,b1,n2,b2,xtol,ftol,nlim,pout)
      print*,alin, 'inlet area ratio'
      print*,alout,'outlet area ratio'
cccc Index
      in=151

ccccc  initial values (cont')
      co=sqrt(kpo/den)
c      co=sqrt((kpo/den)*(b1*xn1*alin**xn1+b2*n2*alin**(-n2)))
      cf=kpo/den/co**2
      delx=0.02
      to=1.0
      tlmt=50.0
      delt=0.01*delx
      xx(1)=0.0
      time=0.0
      max=0.0
      ifile=1

      do 100 j=1,in
        If(xx(j).lt.xstrt-0.005)then
          ao(j)=1.00
          kp(j)=1.0
          dela(j)=0.0
          delk(j)=0.0
          xx(j+1)=xx(j)+delx
        elseif(xx(j).ge.xstp-0.005)then
          ao(j)=1.00
          kp(j)=1.0
          dela(j)=0.0
          delk(j)=0.0
          xx(j+1)=xx(j)+delx
        else
          ao(j)=(1.0-lama*(sin(pi*(xx(j)-xstrt)/len))**2)
          kp(j)=(1.0+lamk*(sin(pi*(xx(j)-xstrt)/len))**2)
         dela(j)=-pi*lama*(sin(2*pi*(xx(j)-xstrt)/len))/len
         delk(j)=pi*lamk*(sin(2*pi*(xx(j)-xstrt)/len))/len
          xx(j+1)=xx(j)+delx
        endif
c
cccc Initial BC
c
c         al(j,1)=alin-(alin-alout)*xx(j)/5
c         al(j,1)=1.00
c         p(j,1)=b1*al(j,1)**xn1-b2*al(j,1)**(-n2)
c
          p(j,1)=(pin+(pout-pin)*xx(j)/3)/kp(j)
          al(j,1)=2.0
          call alinet(al(j,1),xn1,b1,n2,b2,xtol,ftol,nlim,p(j,1))
          de(j)=(4*aoo*ao(j)*al(j,1)/pi)**0.5
```

```
          u(j,1)=q/(co*ao(j)*al(j,1)*aoo)
        g(j,1)=b1*al(j,1)**(1+xn1)/(1+xn1)-b2*al(j,1)**(1-n2)/(1-n2)
          frict(j)=8.45186e-5*dia*fl*ao(j)*al(j,1)*u(j,1)/de(j)**2/co
  100   continue

        ll=1

      ccccccccccccccccccccccccccc
      c     start Computation of Predictor/Corrector
      c

  210   if(ll.eq.32700)then
          ll=0
        endif
        ll=ll+1
      c
      ccc Inlet Boundary Condition
      c
        if(time.lt.to)then
          al(1,2)=alin+0.002*sin(pi*time/to)
      c     al(1,2)=alin-(alin-1)*cos(pi*time/to)
        elseif(time.lt.9.0)then
          al(1,2)=alin
        else
          p(1,2)=pin+2666.4*sin(2*PI*5*(TIME-9.0)*DIA/CO)/kpo
          al(1,2)=2.0
          call alinet(al(1,2),xn1,b1,n2,b2,xtol,ftol,nlim,p(1,2))
        endif
        al(1,3)=al(1,2)
      ccc Compatability Condition
      c
        bc1=ao(1)*(al(1,1)*u(1,1)**2+cf*kp(1)*(al(1,1)*p(1,1)-g(1,1)))
        bc2=ao(2)*(al(2,1)*u(2,1)**2+cf*kp(2)*(al(2,1)*p(2,1)-g(2,1)))
        bc3=ao(3)*(al(3,1)*u(3,1)**2+cf*kp(3)*(al(3,1)*p(3,1)-g(3,1)))


        du=(-3*bc1+4*bc2-bc3)/2
        w2=ao(1)*al(1,1)*u(1,1)-delt/delx*du-delt*frict(1)
        u(1,2)=w2/al(1,2)/ao(1)
        u(1,3)=u(1,2)
        p(1,2)=b1*al(1,2)**xn1-b2*al(1,2)**(-n2)
        g(1,2)=b1*al(1,2)**(1+xn1)/(1+xn1)-b2*al(1,2)**(1-n2)/(1-n2)

      cccc Predictor
      c
        do 200 j=2,in-1
          n=(-1)**ll
          pb12=ao(j+n)*al(j+n,1)*u(j+n,1)
          pb11=ao(j)*al(j,1)*u(j,1)
          pb22=ao(j+n)*(al(j+n,1)*u(j+n,1)**2+cf*kp(j+n)*(al(j+n,1)*
       + p(j+n,1)-g(j+n,1))-N*NU*(U(J+N,1)-U(J,1))/DELX)
          pb21=ao(j)*(al(j,1)*u(j,1)**2+cf*kp(j)*(al(j,1)*
```

```
     + p(j,1)-g(j,1))-N*NU*(U(J,1)-U(J-N,1))/DELX)
        pc2=cf*g(j,1)*ao(j)*delk(j)-cf*kp(j)*(p(j,1)*al(j,1)-
     +g(j,1))*dela(j)+frict(j)
       w1=al(j,1)*ao(j)-n*delt/delx*(pb12-pb11)
        al(j,2)=w1/ao(j)
        w2=ao(j)*al(j,1)*u(j,1)-n*delt/delx*(pb22-pb21)-delt*pc2
        u(j,2)=w2/al(j,2)/ao(j)

       if(al(j,2).lt.0.0)then
         print*,j,'  stopped because alpha lt 0.0'
         call output(2,outfile)
       endif

        p(j,2)=b1*al(j,2)**xn1-b2*al(j,2)**(-n2)
       g(j,2)=b1*al(j,2)**(1+xn1)/(1+xn1)-b2*al(j,2)**(1-n2)/(1-n2)
200    continue

ccc  OUTLET Boundary Condition
c
       if(time.lt.to)then
         al(in,2)=alout+0.02*sin(pi*time/to)
c         al(in,2)=alout-(alout-1)*cos(pi*time/to)
       elseif(time.lt.9.0)then
         al(in,2)=alout
       else
c         al(in,2)=alout

         delout=(u(in,1)+u(in-1,1))*delt/2
         qout=aoo*co*((u(in,1)*al(in,1)-u(in-1,1)*al(in-1,1))*delout/
      +delx+u(in-1,1)*al(in-1,1))
         p(in,2)=qout*resist/kpo+666.6/kpo
         al(in,2)=1.5
         call alinet(al(in,2),xn1,b1,n2,b2,xtol,ftol,nlim,p(in,2))
       endif
       al(in,3)=al(in,2)

ccc Compatability Condition
c
        bc1=ao(in)*(al(in,1)*u(in,1)**2+cf*kp(in)*(al(in,1)*p(in,1)-
      +g(in,1)))
       bc2=ao(in-1)*(al(in-1,1)*u(in-1,1)**2+cf*kp(in-1)*(al(in-1,1)*
      + p(in-1,1)-g(in-1,1)))
       bc3=ao(in-2)*(al(in-2,1)*u(in-2,1)**2+cf*kp(in-2)*(al(in-2,1)*
      + p(in-2,1)-g(in-2,1)))

        du=(3*bc1-4*bc2+bc3)/2
        w2=ao(in)*al(in,1)*u(in,1)-delt/delx*du-delt*frict(in)
        u(in,2)=w2/al(in,2)/ao(in)
        u(in,3)=u(in,2)
c        p(in,2)=b1*al(in,2)**xn1-b2*al(in,2)**(-n2)
       g(in,2)=b1*al(in,2)**(1+xn1)/(1+xn1)-b2*al(in,2)**(1-n2)/(1-n2)
```

```
ccc  Corrector step
c
      do 201 j=2,in-1
        cb11=al(j,2)*u(j,2)*ao(j)
        cb10=al(j-n,2)*u(j-n,2)*ao(j-n)
        cb20=ao(j-n)*(al(j-n,2)*u(j-n,2)**2+cf*kp(j-n)*(al(j-n,2)*
     + p(j-n,2)-g(j-n,2))-N*NU*(U(J,2)-U(J-N,2))/DELX)
        cb21=ao(j)*(al(j,2)*u(j,2)**2+cf*kp(j)*(al(j,2)*
     + p(j,2)-g(j,2))-N*NU*(U(J+N,2)-U(J,2))/DELX)
        cc2=cf*g(j,2)*ao(j)*delk(j)-cf*kp(j)*(p(j,2)*al(j,2)-
     +g(j,2))*dela(j)+frict(j)


        w1=0.5*(ao(j)*(al(j,1)+al(j,2))-n*delt/delx*
     +(cb11-cb10))
        al(j,3)=w1/ao(j)
        w2=0.5*(ao(j)*(al(j,1)*u(j,1)+al(j,2)*u(j,2))-n*delt/delx*
     +(cb21-cb20)-delt*cc2)
        u(j,3)=w2/al(j,3)/ao(j)

       if(al(j,3).lt.0.0)then
        print*,j,'stopped because alpha lt 0 (corrector)'
        call output(2,outfile)
       endif
 201   continue
c
cccc Wave speed cal & '(u+c)max' cal
c
      do 250 j=1,in
      c(j)=sqrt(cf*kp(j)*(b1*xn1*al(j,3)**xn1+b2*n2*al(j,3)**(-n2)))
 250   continue

      max=0.0
      do 260 j=1,in
        upc=abs(u(j,3))+c(j)
        if(upc.gt.max)then
           max=upc
           imax=j
        endif
 260   continue
c
ccccc CONVERGENCE Check
      ii=0
      do 300 l=1,in
        err=abs(al(l,3)-al(l,1))/abs(al(l,1))
        if(err.gt.ep)then
           ii=ii+1
        endif
 300   continue
c
cccc  Check for critical flow and jump location
c
```

```
301   ijump=0
      do 270 j=1,in
       s(j)=u(j,3)/c(j)
270   continue
      do 280 j=74,in
       if(s(j).ge.1.00)then
        iflag=1
       elseif(s(j).lt.1.00.and.iflag.eq.1)then
        ijump=j
        iflag=0
       else
        iflag=0
       endif
280   continue
c
ccc Adjust Array & high order smoothing
c
      do 306 j=3,in-2
         beta(j)=abs(u(j-1,2)-2*u(j,2)+u(j+1,2))/
     +abs(u(j-1,2)+2*u(j,2)+u(j+1,2))
          sb(j)=beta(j)
         if(sb(j).gt.gam)then
          sb(j)=gam
         endif
       al(j,1)=al(j,3)-sb(j)*(al(j+2,3)+al(j-2,3)-4*(al(j-1,3)+
     +al(j+1,3))+6*al(j,3))
        u(j,1)=u(j,3)-sb(j)*(u(j+2,3)+u(j-2,3)-4*(u(j+1,3)+u(j-1,3))+
     +6*u(j,3))
306   continue
      al(1,1)=al(1,3)
      al(2,1)=al(2,3)
      u(1,1)=u(1,3)
      u(2,1)=u(2,3)
      al(in,1)=al(in,3)
      al(in-1,1)=al(in-1,3)
      u(in,1)=u(in,3)
      u(in-1,1)=u(in-1,3)

      do 314 j=1,in
         p(j,1)=b1*al(j,1)**xn1-b2*al(j,1)**(-n2)
         g(j,1)=b1*al(j,1)**(1+xn1)/(1+xn1)-b2*al(j,1)**(1-n2)/(1-n2)
         if(al(j,1).ge.1.00)then
          de(j)=(4*aoo*ao(j)*al(j,1)/pi)**0.5
         else
          de(j)=al(j,1)*(4*aoo*ao(j)*al(j,1)/pi)**0.5
         endif
         al(j,2)=al(j,1)
         u(j,2)=u(j,1)
         p(j,2)=p(j,1)
         g(j,2)=g(j,1)
314   continue
```

```
ccc Output time check
c      if(time.gt.tend.and.ii.lt.10)then
c         call output(2,outfile)
c      endif
       if(time.gt.tout)then
        print*,outfile(ifile)
        call output(1,outfile(ifile))
        ifile=ifile+1
        tout=tout+0.02*co/dia
       endif
       if(ifile.gt.12)then
        stop
       endif
c      if(ll.eq.ink) goto 500
c
ccc separation point and friction array
c
       isep =0
       do 304 j=74, in-1
        delp=kpo*(kp(j+1)*p(j+1,1)-kp(j-1)*p(j-1,1))/
     +(2*delx*dia)
       if(delp.gt.0.1)then
        isep=j
        goto 305
       endif
304     continue

305    if(ijump.eq.0)then
       call friction(in,delx,isep,dia,fl,ft,ao,al,u,de,co,frict)
       else
       call friction(in,delx,ijump,dia,fl,ft,ao,al,u,de,co,frict)
       endif
c
cc status check:  Prints values to screen
303    if(status.eq.1)then
       write(5,302)ii,time,ll,u(76,3)/c(76),max,imax,
     +u(imax,3),c(imax),ijump,isep
302    format(1x,i3,2x,f7.4,2x,i6,2x,f6.3,2x,f7.3,2x,i3,2x,
     +f7.3,2x,f8.3,2x,i3,2x,i4)
       endif

cccccccc determine time step
666    if(time.lt.8.9)then
       eta1=eta
c      elseif(time.lt.10.0)then
c       eta1=eta/2
       else
        eta1=eta/2
       endif
       delt=eta1*delx/max
c         print*,'delt',delt
       time=time+delt
```

```
      goto 210
c      if(time.lt.tlmt) goto 210
c      print*,'time limit reached without convergence'
c      print*,ii,time,ll,u(76,3)/c(76)
c      call output(2,outfile)
c      stop
      end
ccccccccccccccccccccccccccccccccccccc
c
c     OUTPUT
      subroutine output(iout,datafile)
      character*12 datafile
      integer*2 in,iout
      real*4 xx(1002),u(1001,3),al(1001,3),c(1001),kp(1001),ao(1001)
      real*4 pin,pout,kpo,time,dia,co,lamk,lama,p(1001,2),frict(1001)
      real*4 ft,fl,gam,xn1,b1,n2,b2,delx,aoo,nu,eta,resist
      real*4 vel(1001),press(1001),s(1001),area(1001),qx,dt
      real*4 pinx,poutx
      common/outi/in
      common/out1/xx,u,al,c,kp,ao
      common/out2/pin,pout,kpo,time,dia,co,lamk,lama,p,frict
      common/out3/ft,fl,gam,xn1,b1,n2,b2,delx,aoo,NU,eta,resist
      pinx=pin*kpo/133.32
      poutx=pout*kpo/133.32
      dt=time*dia/co

      do 499 j=1,in
       vel(j)=u(j,1)*co*100
      if(al(j,3).lt.0.0)then
       press(j)=999
      else
       press(j)=p(j,1)*kpo*kp(j)/133.32
      endif
       s(j)=u(j,1)/c(j)
       area(j)=aoo*ao(j)*1000000
499   continue

     open(3,file=datafile,status='new',carriagecontrol='list')
     write(3,515)datafile
515  format(/,'**  ',a15,'  **')
     write(3,501)
501  Format(/,' .  Input data  (CGS units) CLTUB11a unsteady')
     write(3,502) 'friction factor:  Ft = ',ft,' &  Flam = ',fl
502  format(1x,'.',a24,f6.3,a10,f6.3)
     write(3,512) 'Smooth. GAMMA = ',gam,'  ART. VIS. = ',NU
512  format(1x,'.',a20,1x,f6.3,a16,1x,f6.4)
     write(3,503) pinx, poutx
503  format(1x,'.','inlet pressure (mmHg) = ',f9.3,/,'outlet pressure
    + mmHg = ',f9.3)
     write(3,504) dia*100,aoo*1000000
504  format(1x,'.','inlet diameter (cm) = ',f10.4,'inlet area (mm^2) =
    +',f9.5)
```

```
      write(3,505) kpo, lamk
  505 format(1x,'.','Nominal stiffness, Kp, = ',f9.3,/,'  (stiffness
     + amplitude lambda Kp = ',f9.3)
      write(3,506) lama
  506 format(1x,'.','Area reduction lambda A = ',f9.3)
      write(3,514)resist/100**3/133.32
  514 format(1x,'.',' Distal Resistance, mmHg/ml/s, = ',f9.5)
      write(3,513)
  513 format(1x,'.',' Tube Law Parameters:')
      write(3,507)xn1,b1,n2,b2
  507 format(1x,'.','N1 = ',f6.2,'  B1 = ',f6.3,'   N2 = ',f6.2,
     +'   B2 = ',f6.3)
      write(3,508)delx,eta
  508 format(1x,'.','spatial step size = ',f5.3,' ETA =  ',f4.2)
      write(3,509) time, dt
  509 format(1x,'time (nd)= ',f9.6,'  time (s)=',f10.8,///)

      write(3,510)
  510 format(1x,' x  ',' Area (mm^2)  ','vel   ',' press  ','alpha',
     +  '   c   ','    s  q   Kp')
      do 525 j=1,in
      qx=area(j)*al(j,1)*vel(j)/100
      write(3,511)xx(j),area(j)*al(j,1),vel(j),press(j),al(j,1),c(j)*
     +100*co,s(j),qx,kp(j)*kpo
  511 format(1x,f5.2,4(2x,f8.3),2x,f8.2,2x,f6.3,2x,f7.2,2x,e10.4)
  525 continue
      close(unit=3)
c     if(iout.ne.2)then
      return
c     else
c      stop
c     endif
      end



ccccccccccccccccccccccccccccccccccccccccccccccccccccccccccccccccccccccccccccc
      subroutine alinet(x,xn1,b1,n2,b2,xtol,ftol,nlim,p)
      real*4 x,fx,del,xtol,ftol,xn1,n2,p,b1,b2
      integer*2 j,nlim
       fx=b1*x**xn1-b2*x**(-n2)-p
      do 20 j=1,nlim
       del=fx/(b1*xn1*x**(xn1-1)+b2*N2*x**(-n2-1))
       x=x-del
       if(x.lt.0.0)then
        print*, 'Crash & Burn'
        call output(2,'crash')
       endif
       fx=b1*x**xn1-b2*x**(-n2)-p
       if(abs(del).le.xtol)then
            return
       endif
```

```
      if(abs(fx).le.ftol)then
           return
      endif
20    continue
      write(*,205)nlim
205   format(/' value of alpha at ends not found after',i4,'
     +iterations')
      print*,'program aborted'
      stop
      end
ccccccccccccccccccccccccccccccccccccccccccccccccccccccccccccccccccccccccccc
      subroutine friction(in,delx,ipt,dia,fl,ft,ao,al,u,de,co,frict)
      integer*2 ipt,in,iat
      real*4 dia,fl,ft,co,de(1001),frict(1001),ao(1001)
      real*4 al(1001,3),u(1001,3),delx
C       iat=ifix(2/delx)
C       if(ipt+iat+5.gt.in)then
C        iat=in-ipt-6
C       endif
      if(ipt.eq.0.or.ipt.gt.125)then
       do 10 j=1,in
      frict(j)=abs(8.45186e-5*dia*fl*ao(j)*al(j,1)*u(j,1)/de(j)**2/co)
 10     continue
       else
        do 20 j=1,ipt-1
      frict(j)=abs(8.45186e-5*dia*fl*ao(j)*al(j,1)*u(j,1)/de(j)**2/co)
 20     continue

 C       do 40 j=ipt,ipt+iat
        do 40 j=ipt,in
 ccc Separation Loss Coefficient
      frict(j)=abs(ft*u(j,1)**2*(al(j,1)*ao(j))**3/(4*(al(76,1)*
     +ao(76))**2)+8.45186e-5*dia*fl*ao(j)*al(j,1)*u(j,1)/de(j)**2/co)

 ccc Borda-Carnot pressure loss w/u1 ref Kececioglu et al
 c     frict(j)=abs(ft*(1-2*ao(76)*al(76,1)/(ao(j)*al(j,1)))*AL(76,1)*
 c    +AO(76)*u(76,1)**2/4)+abs(8.45186e-5*dia*fl*ao(j)*al(j,1)*u(j,1)
 c    +/de(j)**2/co)
 c
 ccc Borda-Carnot pressure loss w/u2 ref Kececioglu et al
 c     frict(j)=abs(ft*((ao(j)*al(j,1)/(ao(76)*al(76,1)))**2-2*(ao(j)*
 c    +al(j,1)/(ao(76)*al(76,1)))*AL(j,1)*AO(j)*u(j,1)**2/4)+
 c    +abs(8.45186e-5*dia*fl*ao(j)*al(j,1)*u(j,1)/de(j)**2/co)
 ccc Separation losses ref. Santamore & Gould Models
 c     frict(j)=abs(ft*(ao(j)*al(j,1)/(ao(76)*al(76,1))-1)**2*AL(j,1)*
 c    +AO(j)*u(j,1)**2/4)+abs(8.45186e-5*dia*fl*ao(j)*al(j,1)*u(j,1)/
 c    +de(j)**2/co)
  40     continue
```

```
C       do 50  j=ipt+iat+1,in
C     frict(j)=abs(8.45186e-5*dia*fl*ao(j)*al(j,1)*u(j,1)/de(j)**2/co)
C 50    continue
      endif
      return
      end
```